

SUPERVISORY CONTROL ON MICRO-GRID COMPRISING OF PV FARM AND  
HYBRID ENERGY STORAGE SYSTEM

by

Aniket Mohan Joshi

A thesis submitted to the faculty of  
The University of North Carolina at Charlotte  
in partial fulfillment of the requirements  
for the degree of Master of Science in  
Electrical Engineering

Charlotte

2016

Approved by:

---

Dr. Sukumar Kamalasan

---

Dr. Yogendra Kakad

---

Dr. Valentina Cecchi



## ABSTRACT

ANIKET MOHAN JOSHI. Supervisory control on Micro-grid comprising of PV Farm and Hybrid Energy Storage System. (Under the direction of DR. SUKUMAR KAMALASADAN).

Renewable Energy has gained high level of attraction as people have understood its significance in the world and the potential it shows for being the prime source of energy of the future. Its eco-friendliness also means sustainable future of the eco-system without any sort of side-effects. These advantages also come with intermittence and reduced density of energy available to harness as far as renewables are considered. In this thesis the problem of PV energy source in terms of intermittence is taken and an approach of sustainable and dispatch-able PV farm using Hybrid Energy Storage System is proposed based on a derived power sharing algorithm. To start with the PV system, the battery and the ultra-capacitor systems are designed with dedicated controllers for each of them. Then the three sub-systems are integrated at common DC link voltage and validated with cascaded controllers to interact with each other as far as power sharing is concerned. In this process the effect of intermittence in terms of irradiance and various loading characteristics are considered as perturbation to the system and the response is recorded and used for system level validation. A similar process is carried out on the AC side in off-grid mode by using a d-q architecture based inverter. Finally a supervisory control structure is proposed, implemented and validated on the micro-inverter system in off-grid

mode which enables the PV system to supply dispatch-able and sustainable power as commanded from the inverter.

## ACKNOWLEDGEMENTS

I would like to express my gratitude towards my family for believing in me and supporting me financially and mentally to follow my dream of pursuing higher education in the USA. They have been with me throughout this process and never let me feel away from home. I would also like to thank the people who are no longer in my life but had supported my ambitions and had faith in me.

I thank my adviser, Dr. Sukumar Kamalasadana, for his guidance and motivation. His ideas instilled in me a clear approach towards solving my problems and his mentorship kept my desire to positively work towards my goals and achieve them in time. I would also like to thank all professors who have taught me.

My friends and colleagues have been my family away from home and I cannot thank them enough for the support they have given me to see through this journey.

## TABLE OF CONTENTS

CHAPTER 1 : INTRODUCTION	1
1.1. Literature Review	3
1.2. Organization	4
CHAPTER 2 : PV SYSTEM, DESIGN AND VALIDATION	6
2.1. Overview of PV Technologies	7
2.2. Operation of a PV Cell	8
2.3. PV Array Design in PSCAD	9
2.4. PV Array with Variable Irradiance	15
2.5. Design and Modeling of DC-DC Boost Converter	16
2.5.1. Mathematical Modeling of DC-DC Boost Converter	16
2.5.2. PI Controllers for the DC-DC Boost Converter	18
2.5.3. Design, Modeling and Validation of DC-DC Boost Converter	22
CHAPTER 3 : DESIGN AND MODELLING OF HYBRID ENERGY STORAGE SYSTEM	27
3.1. Long Term Storage Device – Battery	28
3.1.1. Mathematical Model of Li-Ion Battery	29
3.1.2. The Charge and Discharge Model of the Battery	31
3.1.2.1. The Discharge Model	31
3.1.2.2. The Charge Model	32
3.1.3. Battery Model in PSCAD	33

3.1.4 Power Conditioning for Battery System in PSCAD	37
3.1.5. DC-DC Boost Converter for Battery	39
3.2. Short Term Storage Device – Ultra-capacitor	47
3.2.1. Ultra-capacitor Modelling	47
3.2.2. Ultra-capacitor Modelling in PSCAD	52
3.2.3. Design and Modelling of a DC-DC Boost Converter for Ultra-capacitor	54
3.3. Cascade Control on HESS	58
3.3.1. Zeigler-Nichols Tuning	60
3.3.2. HESS in Standalone Mode of Operation	66
CHAPTER 4 : PV Farm And HESS Connected to DC Load	75
4.1. Slow Varying Load	76
4.2. Fast Varying Load	82
CHAPTER 5: PV SYSTEM AND 3 PHASE D-Q COUPLED INVERTER	88
5.1. Real and Reactive Power Control on Inverter	89
5.2. PV Farm and HESS Integration with Inverter in Off-grid Mode	95
CHAPTER 6: SUPERVISORY CONTROL ON PV FARM AND HESS	105
CHAPTER 7: CONCLUSION AND FUTURE WORKS	111
REFERENCES	113
APPENDIX: MATLAB CODE	117

## CHAPTER 1: INTRODUCTION

The world is turning towards Renewable energy sources for its energy needs. People have understood that at this time of ever-increasing energy demand fossil fuel based energy resources are a bane for the eco-system in general. The huge emissions from conventional energy plants like coal, diesel and petroleum products are increasing the CO<sub>2</sub> level in the atmosphere which has a chain reaction on the environment. The day is not far when the depletion of ozone layer would become irreversible, leading to harmful solar radiation entering and destroying the earth within a decade. The renewable energy sources, though abundantly available has a low power harnessing density. Even though it is freely available, the way it is synthesized into useable energy is very costly. The most important problem in generating from renewable sources is intermittence in the generating output. Be it a solar source or a wind there is intermittence. In case of solar source intermittence in the form of variable irradiance and temperature is observed. The characteristic of a good generating source is that it supplies all the demanded power constantly. One way of mitigating this intermittence problem is to provide PV farm with storage support. The stored power could be used whenever PV is experiencing intermittence and also when the load demand is more than what the PV farm can generate.

In this thesis a hybrid energy storage system will be designed which will be controlled to supply scheduled power during intermittence. A cascade control structure will be employed which will command the power from the HESS. The hybrid energy storage system will consist of battery and ultra-capacitor system

Load demands can be classified slow changing and fast changing loads. The battery will be made responsible to supply for the slow changing power demand whereas the ultra-capacitor will take up the fast changing loads. This is because batteries are classified as short term storage devices which are capable of supplying power for a longer period of time. On the other hand, ultra-capacitors are capable of supplying transient changes in power, occurring for a short period of time, since they have higher power density.

The main goal of thesis is to demonstrate the effects of having a power sharing scheme scheduled based on high frequency and low frequency power change in the system. By successfully implementing a power sharing algorithm between PV farm and hybrid energy storage system, system characteristics like load following and voltage support would be validated in the view of intermittent PV generation. Finally, a supervisory control would be implemented on the AC side of the inverter which will aim at maintaining the AC voltage looking at the reactive power demand. On the DC side of the system, the power references for the hybrid energy storage system will be optimized by deriving the DC equivalent of power from the AC demand at the inverter side.

## 1.1 Literature Review

Majority of research in the field PV farm and the grid-integration has been focused on power enhancement, efficiency of battery life based on charge and discharge cycles, optimization on battery output power using various charging and discharging methodologies and analysis of power and energy efficiency for a pulsed load profile [6, 8, 11, 16]. A good amount of research has gone into energy storage system for wind farms [9-11, 17]. Multilevel power management and control schemes based on minimum variance, dead beat, cascade control and PI compensators have been implemented as well [11-15]. De-coupled d-q architecture based inverters have also been researched which enable a good controllability between the active and the reactive power of inverters. In case of ESS the most common topologies are the DC coupled structure and the cascade structure.

Among all the research, very less emphasis is given to component design of Energy Storage System comprising of battery and ultra-capacitor. Most of the analysis is carried out in steady state analysis software like MATLAB<sup>®</sup> and SIMULINK<sup>®</sup>.

This thesis details the design and validation of the battery and the ultra-capacitor system from a single cell unit to a scaled up version using the static and dynamic characteristics of both systems in Power System Computer Aided Design (PSCAD<sup>®</sup>) - EMTC software. This work presents a detail energy control structure with HESS and PV farm by including the PV intermittence and the ancillary capabilities of the HESS like load following and

voltage support. The advantages of implementing supervisory control has been discussed by comparing the optimized result on the power sharing feature and the system response.

## 1.2 Organization

This thesis is organized as follows:

Chapter 2 describes the design and validation of PV farm and the DC-DC boost converter design along with its analysis. The controller and the logic behind the control is also discussed for the PV farm.

Chapter 3 deals with the design and validation of Hybrid Energy Storage System (HESS) from a single cell unit to a series and parallel combination of cells forming a system pack of higher rating. The controllers on HESS based on bode analysis and Zeigler Nichols method is discussed. The standalone HESS is validated for a DC load demand by scheduling for high and low frequency power.

Chapter 4 describes the integration of HESS with the PV farm on the DC side with variable DC loads and intermittence conditions. The PV farm and HESS is validated as a whole on the DC level.

Chapter 5 includes the implementation and validation of d-q based inverter connected to the PV farm. The PV and HESS is integrated together with the inverter and analyzed in off-grid mode.

Chapter 6 presents the proposed supervisory control on the inverter and validation for off-grid mode with commanded load and PV intermittence cases.

Chapter 7 concludes the thesis with possible future work that can be performed related to the topic discussed.

## CHAPTER 2 : PV SYSTEM MODEL, DESIGN AND VALIDATION

Photovoltaic technologies (PV) and their applications are one of the fastest growing developments in the energy sector today. The amount of research and success in the field of photovoltaics is a promising aspect forecasting solar energy as a potentially primary source of energy for humanity in the future. Unlike conventional energy sources, PV being a direct current generating source, faces the challenge of integration into the alternating current-based power grid. Interconnection of PV with the grid thus typically involve an inverter which outputs an alternating current at the fundamental grid frequency. Also, the PV source generates power at a particular voltage and current which is governed by the series and parallel arrangement of the arrays. The inverter requires a specific voltage at its input for it to process and convert the power from DC to AC. To achieve this specific voltage, we use a DC-DC converter. This type of inverter topology, known as DC-link topology, will be implemented in the proposed design as shown in Figure 2.1 [21].

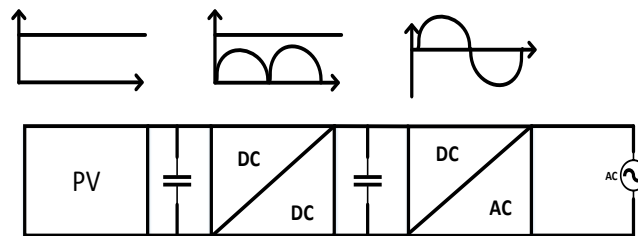


Figure 2.1 DC-link topology

In this chapter, the design dynamic modelling and analysis of PV system is discussed. Some tests are used to evaluate the performance of the PV system during standard operating conditions. The goal is to develop a system that can be used as an intermittent energy source which can imitate the real time dynamics like that of an installed PV system in the field.

### 2.1. Overview of PV Technologies

Edmund Becquerel discovered the photovoltaic effect in 1830s during an experiment with wet-cell batteries. Willoughby Smith discovered the photoconductivity of selenium in 1837 and William Adams and Richard Day discovered the photovoltaic effect in solid selenium. These discoveries set a road map for the modern PV cell. The modern cell was invented by Charles Fritts in 1883. The light-to-electrical power transfer efficiency was between 15% and 2%. With the advent of semi-conductors, PV junction made from single-crystal grown germanium and silicon gave way to the development of first silicon PV cell. The first PV cell was developed in 1954 by Chapin, Fuller and Pearson with an efficiency of 4.5% which improved to 6% within a few months. In the 1970s PV found its way to commercial applications, such as lights, horns, lighthouses, railroad crossings [22].

Eventually, there was a rapid growth in PV production, which decreased the high cost of associated with the PV cells. Today, silicon-mono crystalline, multi crystalline, thin film amorphous; and thin film-cadmium telluride and CIS are the most commonly used PV technologies.

	Silicon			Thin Film	
Efficiency	Mono Crystalline	Multi Crystalline	Thin Film Crystalline	CIS	CdTe
Typical	12-15%	11-14%	5-7%	-	-
Maximum	22.7%	15.3%	-	10.5%	12.1%
Laboratory	24.75	19.8%	12.7%	16%	18.2%

Figure 2.2 Efficiency survey covering typical and maximum efficiency for commercially available PV module.

## 2.2. Operation of a PV Cell

Photovoltaic is the process of converting sunlight directly into electricity using solar cells. This process requires a material in which the absorption of light raise an electron to a higher energy state. This excited electron travels through the external circuits.

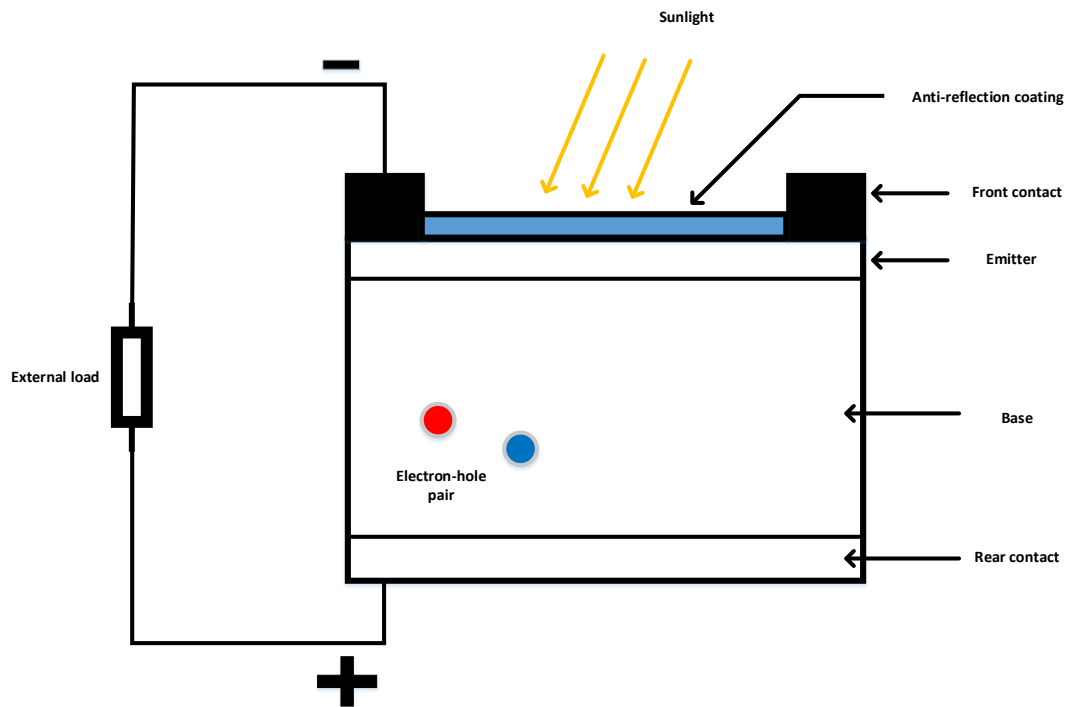


Figure 2.3 Operation of PV cell [23]

A variety of materials and processes can potentially satisfy the requirement for photovoltaic energy conversion, but in practice nearly all the photovoltaic energy conversion uses semiconductor materials in the form of p-n junction. An electric current is result of a large potential developed across the terminals of the solar cell due to the generation and collection of the light generated carriers.

### 2.3. PV Array Design in PSCAD<sup>®</sup>

The mathematical model of solar cell in PSCAD<sup>®</sup> is an equivalent circuit that contains a current source anti-parallel with a diode, a shunt and a series resistance. The DC current generated as a result of exposure to light vary linearly with irradiance The current through the anti-parallel diode ( $I_d$ ) is responsible for producing the non-linear I-V characteristics of the PV cell. The equation that determines the I-V characteristics of the PV cell can be derived from the equivalent circuit shown in Figure 2.4.

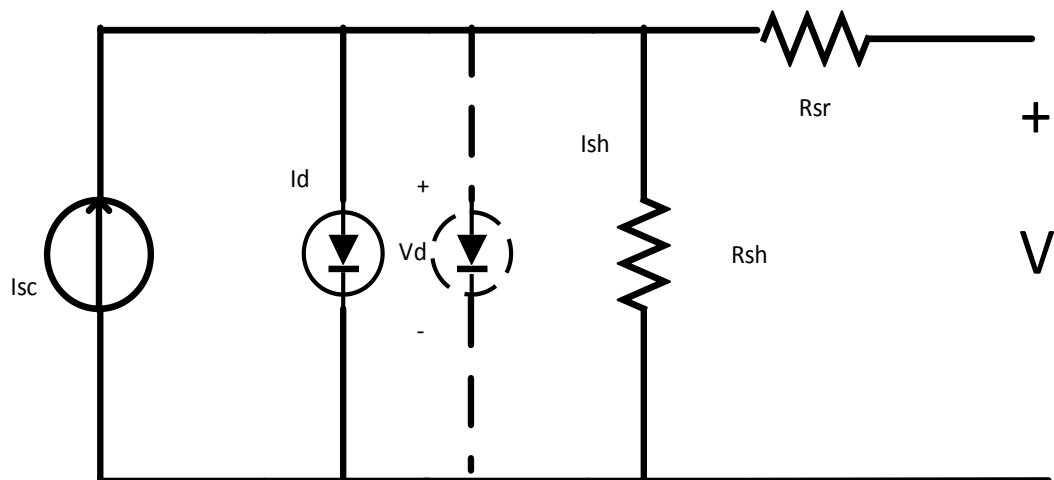


Figure 2.4 Equivalent circuit model of PV cell [24]

Kirchhoff's current law can be written here as,

$$I = I_{sc} - I_d - I_{sh}$$

Where

$$I_{sc} = I_{scr} \frac{G}{G_R} [1 + \alpha_T (T_c - T_R)]$$

$$I_{sh} = \left( \frac{V + IR_{sr}}{R_{sh}} \right)$$

$$I_d = I_0 \left( e^{\frac{V + IR_{sr}}{nkT_c/q}} - 1 \right)$$

$$I_0 = I_{0R} \left( \frac{T_c^3}{T_{CR}^3} \right) \exp \left[ \left( \frac{1}{T_{CR}} - \frac{1}{T_c} \right) \frac{qe_g}{nk} \right]$$

$I_{sc}$  is the short circuit current and is a function of solar radiation on the plan of solar cell  $G$  and the cell temperature  $T_c$ .

$I_{scr}$  is the short circuit current at the reference solar radiation  $G_R$  and the reference cell temperature  $T_{CR}$ .

$\alpha_T$  is the temperature coefficient of photo current.

$I_0$  is called the dark current which is a function of cell temperature.

$I_{0R}$  is the dark current at the reference temperature.

$q$  Is the electron charge.

$k$  is the Boltzmann constant.

$e_g$  is the band gap energy.

$n$  is the diode ideality factor which is between 1 and 2 (1.3 for silicon cells).

All the constants in the above equations can be examined based on manufacturer's specification sheet of PV module. They can also be measured from I-V curves of PV cell or array based on whether a single cell is used or a series and parallel combination of cells forming a PV array is used [24,25].

The PV array is designed for approximately 2 MW of DC power. Figures 2.5 and 2.6 details the parameters of PV cell and array respectively. These parameters are used to design the 2MW PV array.

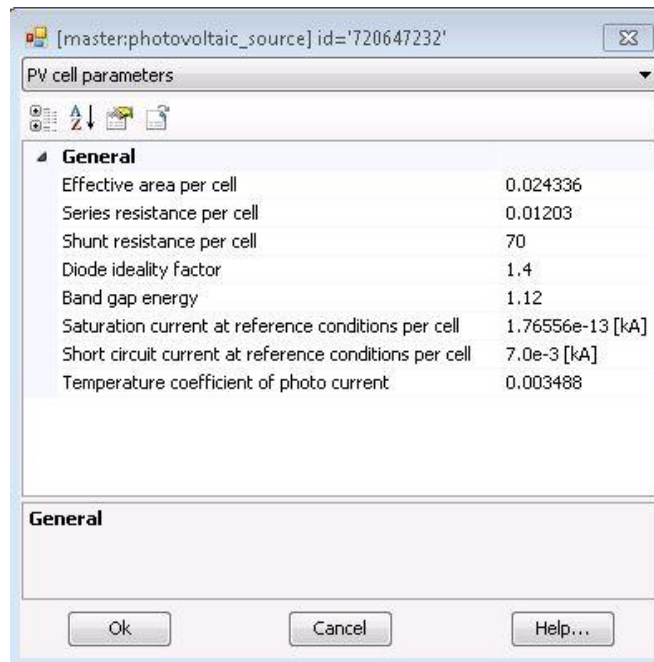


Figure 2.5 PV cell parameters in PSCAD

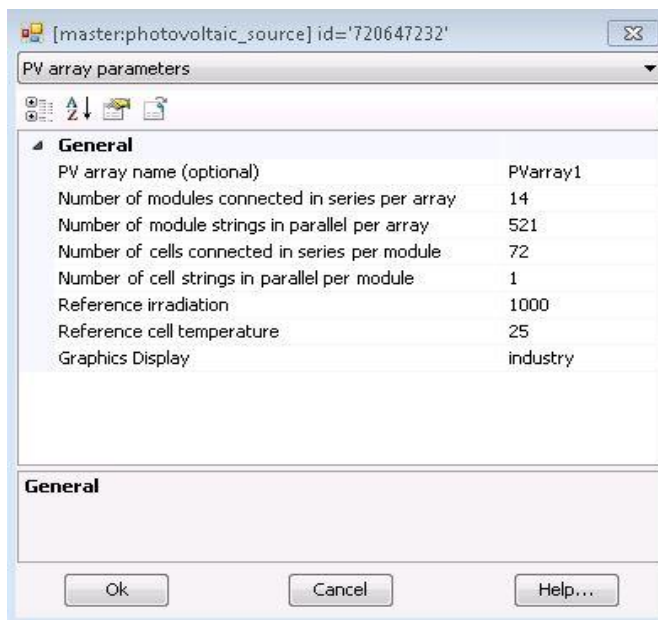


Figure 2.6 PV array parameters in PSCAD

The PV array circuit has been validated in PSCAD for 2MW DC load using the following circuit shown in Figure 2.7

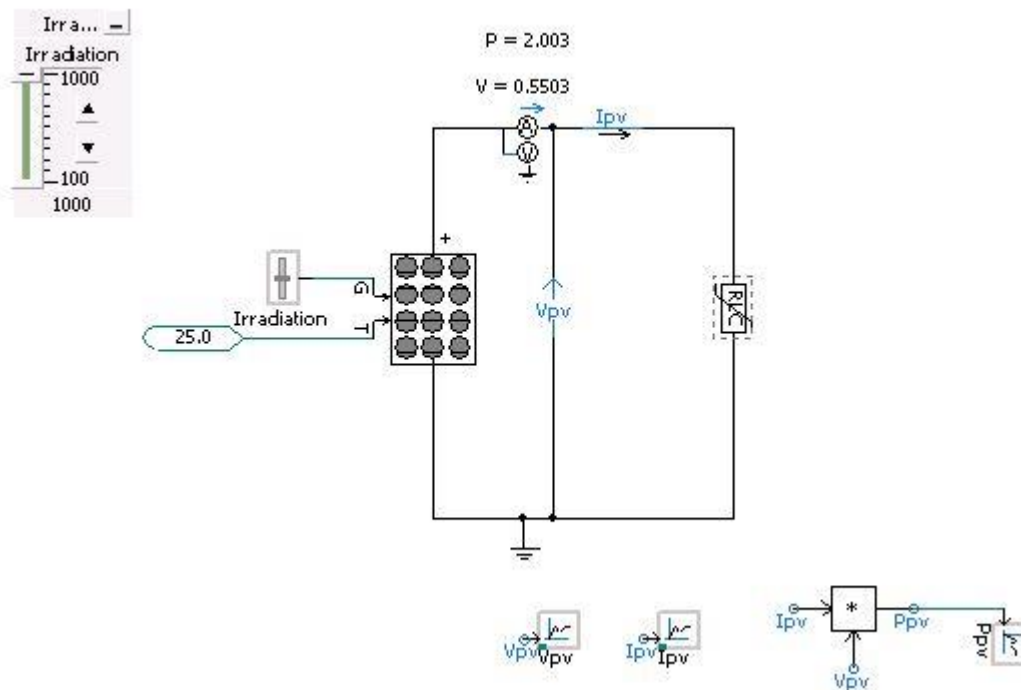


Figure 2.7 PV array validation circuit in PSCAD for 2 MW of rated load

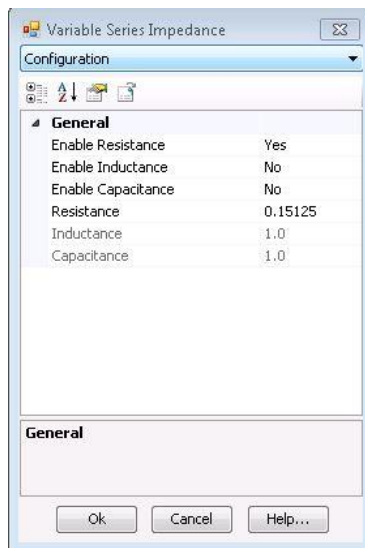


Figure 2.8 Load resistance corresponding to 2 MW of load

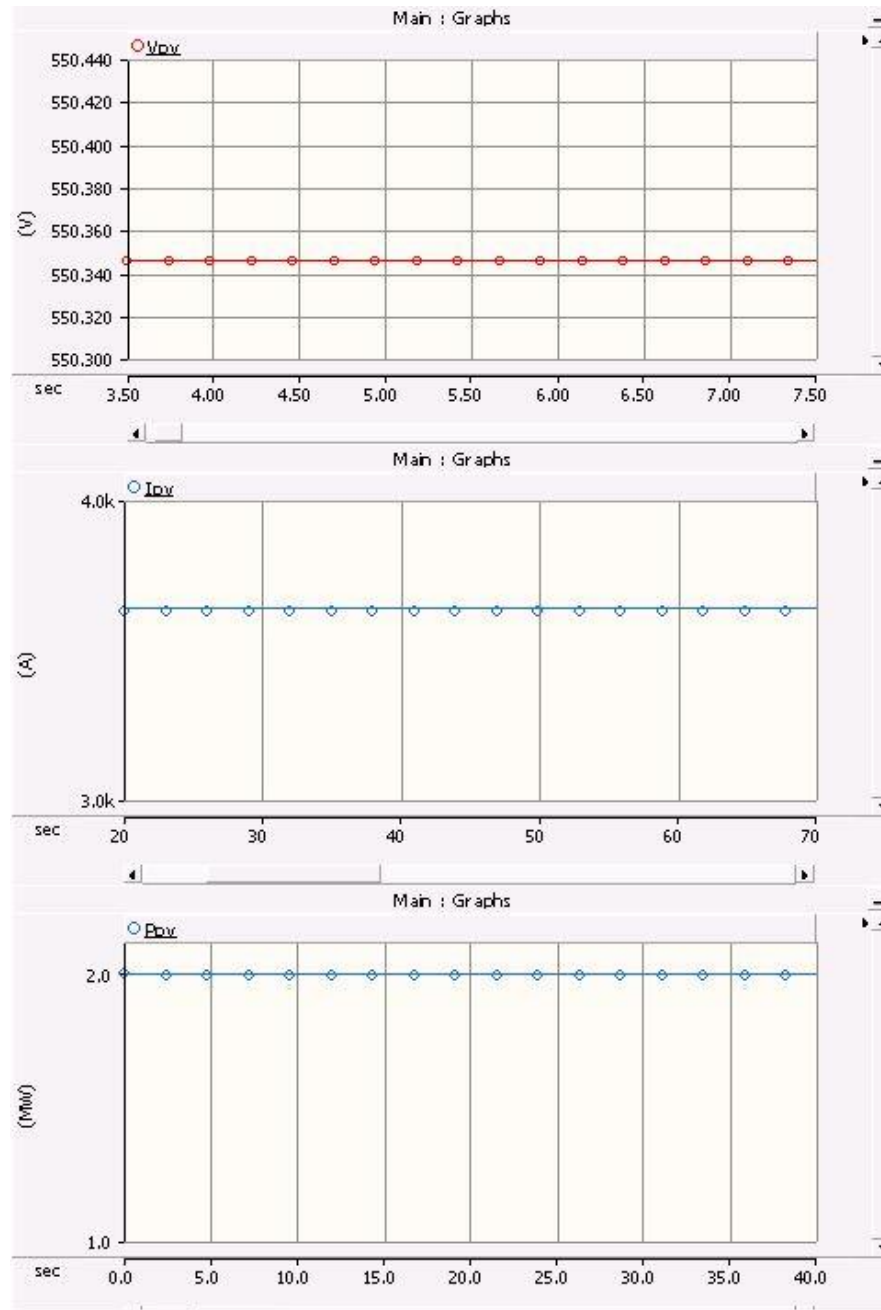


Figure 2.9 Voltage ( $V_{pv}$ ), Power ( $P_{pv}$ ) and Current ( $I_{pv}$ ) for rated load demand of 2 MW

From the above figures it can be understood that the PV array is capable of supplying 2MW of load at rated voltage of 550 V DC. This validates the PV array design for our system.

## 2.4 PV Array with Variable Irradiance

The PV array design in the topic above needs to be validated with changing irradiance since we will be considering irradiance as one of the testing parameters when the complete system is built. To test the PV response to changing irradiance we use the irradiance data of a sunny day and a cloudy day.

The Figures 2.10 through 2.13 validate the PV response to changing irradiance.

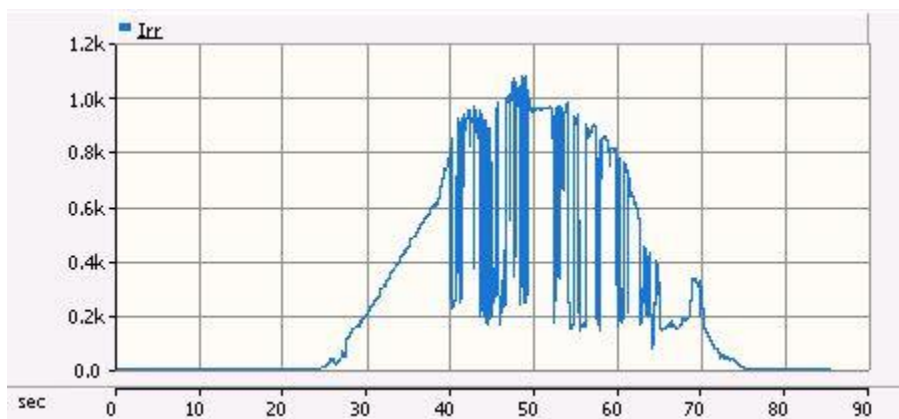


Figure 2.10 Irradiance data for a cloudy day simulated between 20 seconds and 80 seconds in PSCAD

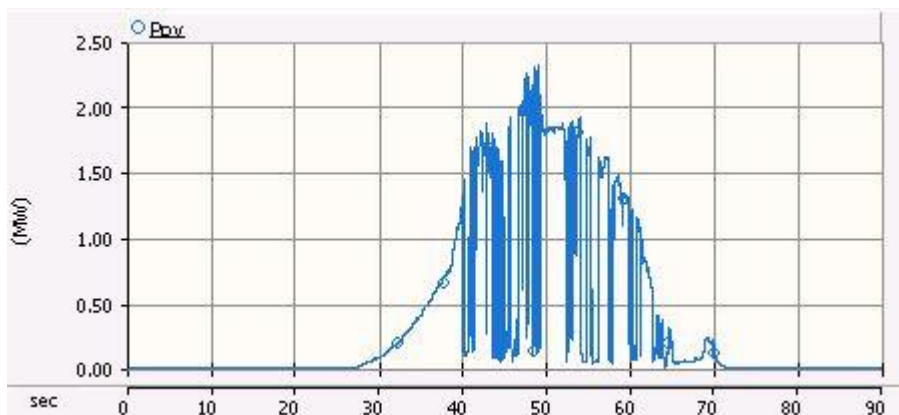


Figure 2.11 PV response to changing Irradiance for cloudy day



Figure 2.12 Irradiance data for a sunny day simulated between 20 seconds and 80 seconds in PSCAD

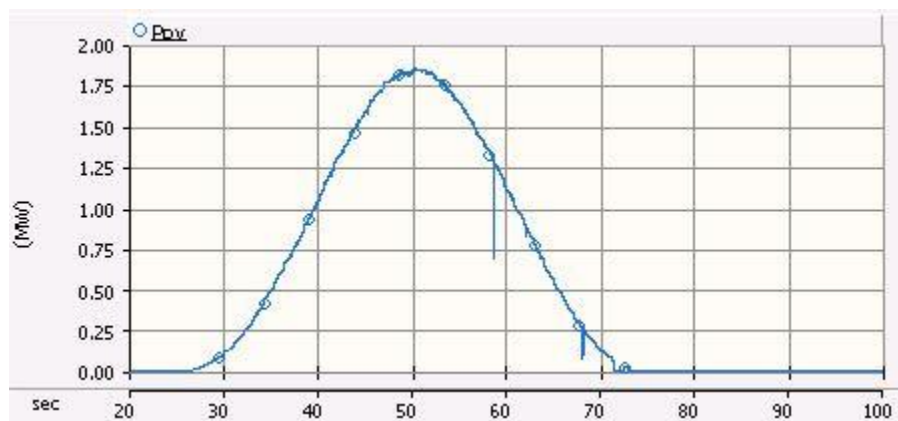


Figure 2.13 PV response to changing Irradiance for cloudy day

## 2.5 Design and Modeling of DC-DC Boost Converter

### 2.5.1 Mathematical Model of DC-DC Boost Converter

To exercise control over voltage/current output from the PV source we employ DC-DC boost converter. The output of the boost converter is the desired voltage/current which can be cascaded to another power electronic module in our system. Both the DC-DC boost converter and the Inverter comprise of our power conditioning system. In this section we summarize the mathematical equation for modeling an average linearized circuit of a DC-

DC boost converter. The state-space equation for average linearized model of a DC-DC boost converter can be written as follows:

$$\frac{d\bar{i}_L}{dt} = \frac{\bar{v}_{in}}{L} - d' \frac{\bar{v}_0}{L} \quad (2.1)$$

$$\frac{d\bar{v}_0}{dt} = \frac{\bar{v}_0}{RC} + d' \frac{\bar{i}_L}{C} \quad (2.2)$$

Where,  $d' = (1 - d)$

Considering small perturbations in  $V_{in}$ ,  $D$ ,  $V_{out}$  and  $I_L$ :

$$\begin{aligned} \bar{V}_{in} &= V_{in} + \widetilde{v}_{in} \\ \bar{i}_L &= i_L + \widetilde{i}_L \\ \bar{v}_0 &= V_0 + \widetilde{v}_0 \\ d &= D + \widetilde{d} \end{aligned} \quad (2.3)$$

Substituting above values we get:

$$\begin{aligned} \frac{d\widetilde{i}_L}{dt} &= \frac{\widetilde{v}_{in}}{L} - \frac{D'}{L} \widetilde{v}_0 + \frac{V_0}{L} \widetilde{d} \\ \frac{d\widetilde{v}_0}{dt} &= -\frac{\widetilde{v}_0}{RC} - \frac{D'}{C} \widetilde{i}_L - \frac{I_L}{C} \widetilde{d} \end{aligned} \quad (2.4)$$

Applying Laplace transform to the above set of equations to derive transfer function in term of change in output voltage with respect to change in duty cycle and considering no perturbation in input voltage, we get:

$$s\widetilde{i}_L = -\frac{D'}{L} \widetilde{v}_0 + \frac{V_0}{L} \widetilde{d}$$

$$s\tilde{v}_0 = -\frac{\tilde{v}_0}{RC} - \frac{D'}{C}\tilde{i}_L - \frac{I_L}{C}\tilde{d} \quad (2.5)$$

Rearranging terms:

$$\frac{\tilde{v}_0}{\tilde{d}} = \frac{-s\frac{I_L}{C} + \frac{V_0 D'}{LC}}{s^2 + \frac{1}{RC}s + \frac{D'^2}{LC}} \quad (2.6)$$

The above transfer function has one right half plane zero (RHPZ) which means the system inherently unstable. Our goal is to maintain a constant output voltage by exercising a control on the duty ratio of the boost converter. For this we need to build a PI controller which will nullify the effect of the right half plane zero in the system and bring the PV and DC-DC boost converter system to stability.

### 2.5.2 PI Controller for DC-DC Boost Converter

As discussed in the section before the DC-DC boost converter has a right half plane zero in its control (duty ratio) to output (voltage) transfer function. This RHPZ has a destabilizing effect on the system. To remove this in-stability we use a Proportional-Integral (PI) controller. These compensators improve the steady-state error due to its Integral gain without affecting the transient response.

The transfer function is given by:

$$G_C(s) = K_p \left( \frac{1+T_z s}{s} \right) \quad (2.7)$$

The PI controller is designed using the bode plot method by calculating the GM and PM of the open loop transfer function of the converter and then designing a control loop based on PI around it for the desired PM and crossover frequency.

Figures 2.14 through 2.18 presents the bode analysis of the PI controller and its design.

The MATLAB code for the PI controller can be viewed from the APPENDIX.

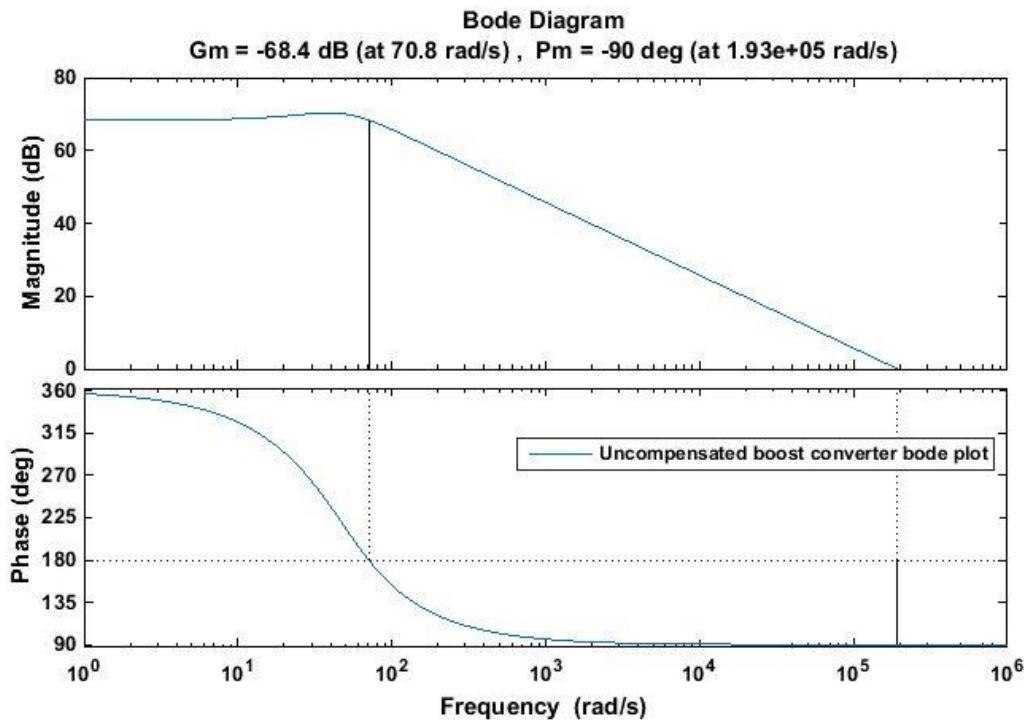


Figure 2.14 Bode plot of uncompensated system

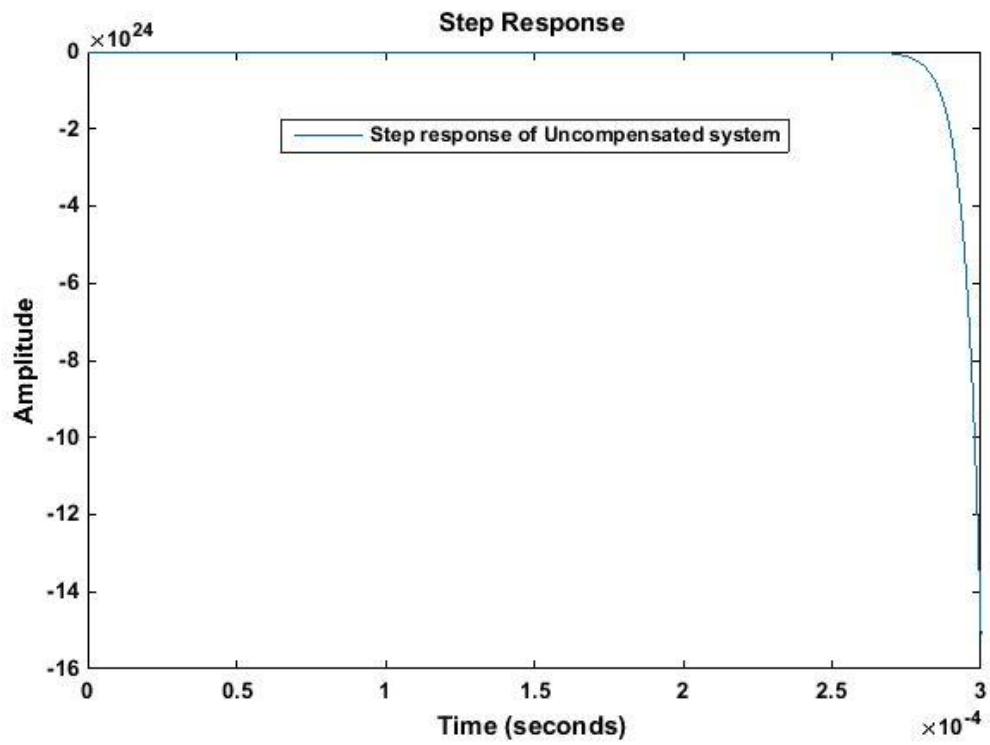


Figure 2.15 Step response of uncompensated system

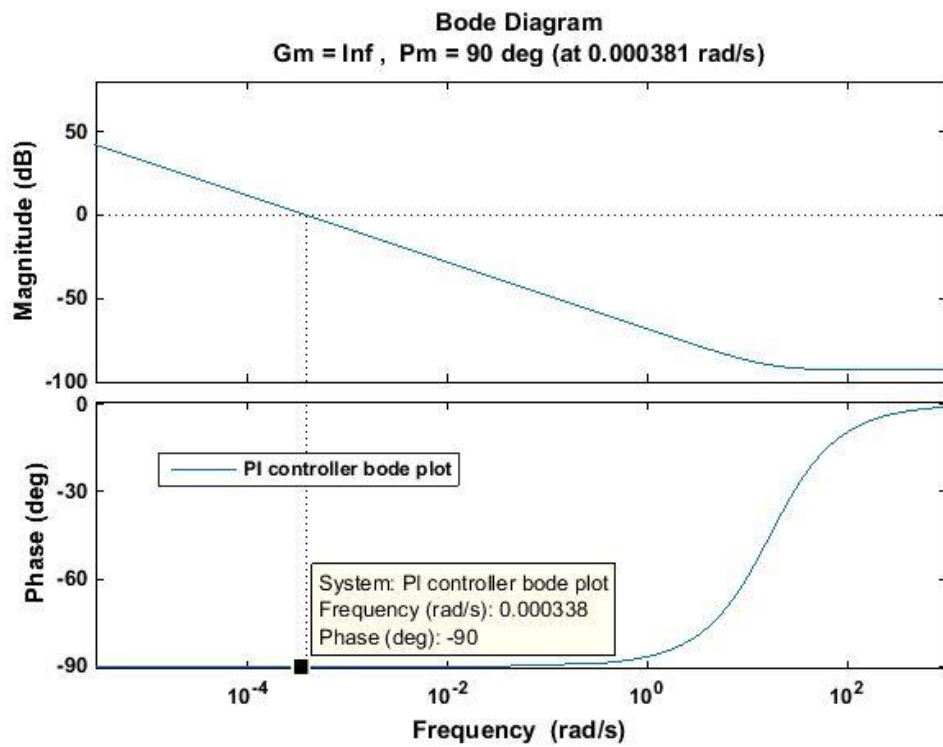


Figure 2.16 Bode plot of PI controller for the system

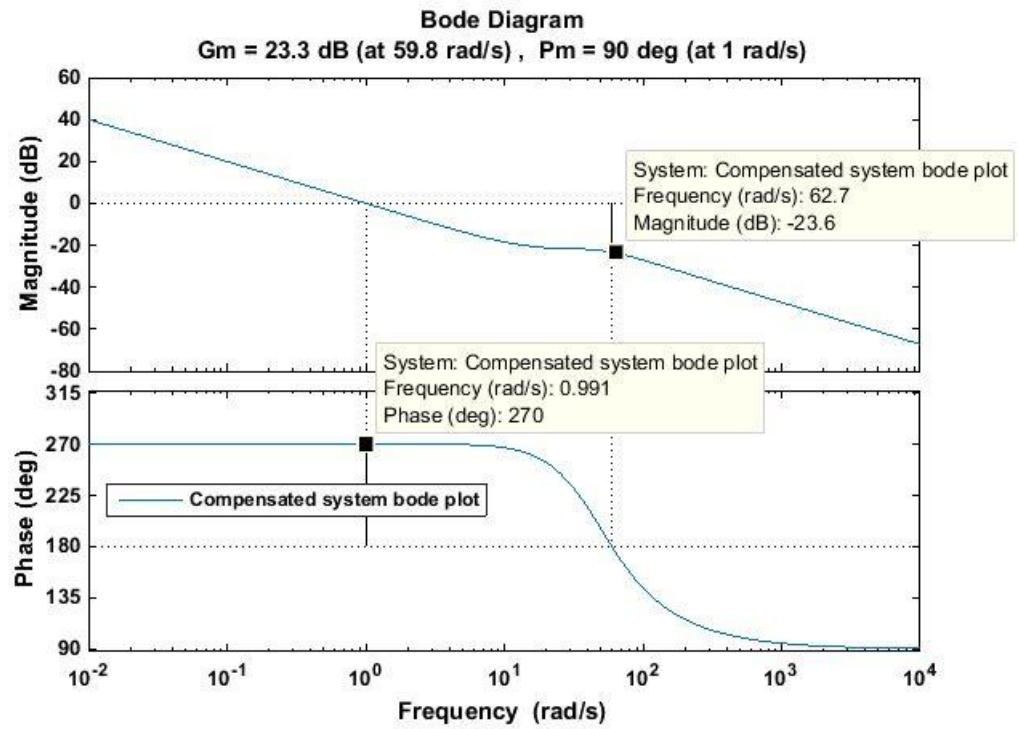


Figure 2.17 Bode plot of compensated system

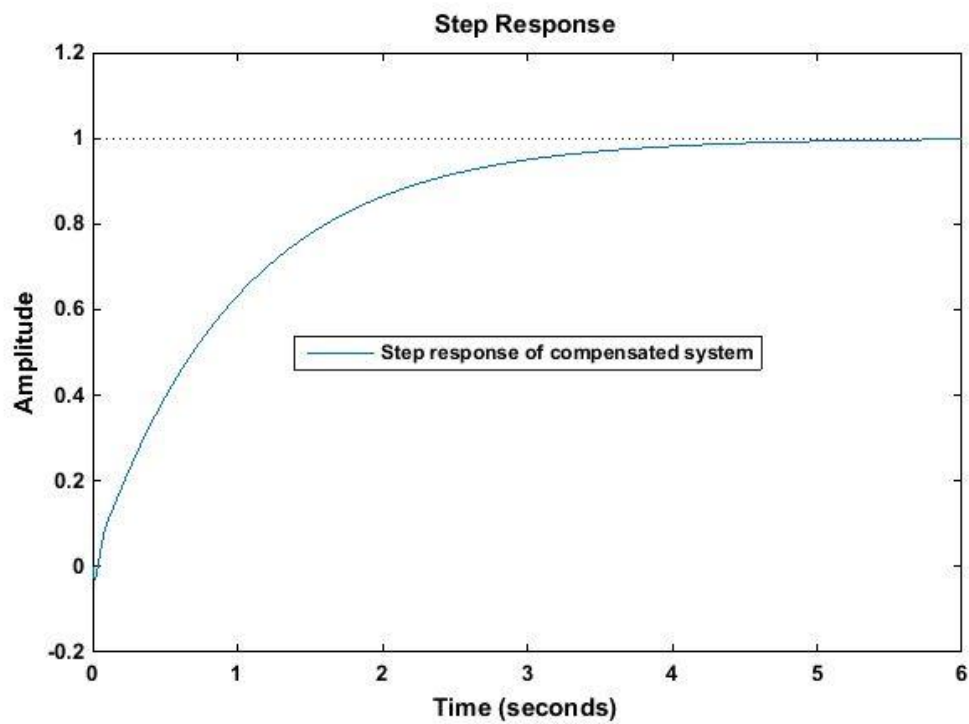


Figure 2.18 Step response of compensated system

### 2.5.3 Design, Modeling and Validation of DC-DC Boost Converter

The boost converter design is initiated by considering the input voltage available to the boost converter and the desired output voltage from the boost converter which will be the DC-link voltage of our system. Based on these values the duty ratio is calculated for the rated operating point. Then follow the inductor and the capacitor calculations along with the input and output capacitors for the DC-DC boost converter.

Table 2.1 details the DC-DC Boost Converter modeling for 1000 Hz of switching frequency.

Table 2.1 DC-DC Boost converter modelling parameters

Sr. No.	Parameters	Value
1.	Vin	550 V
2.	Vout	1200 V
3.	Pout = Pin	2 MW
4.	Inductor (L)	0.0056 H
5.	Capacitor (C)	0.0188 F
6.	Input capacitor	0.027 F
7.	Maximum allowable ripple	2%

The boost converter circuit used for the purpose of validation of the above proposed design is shown in Figure 2.19 through 2.23 presents the bode analysis for the design of PI control for duty cycle control of the boost converter.

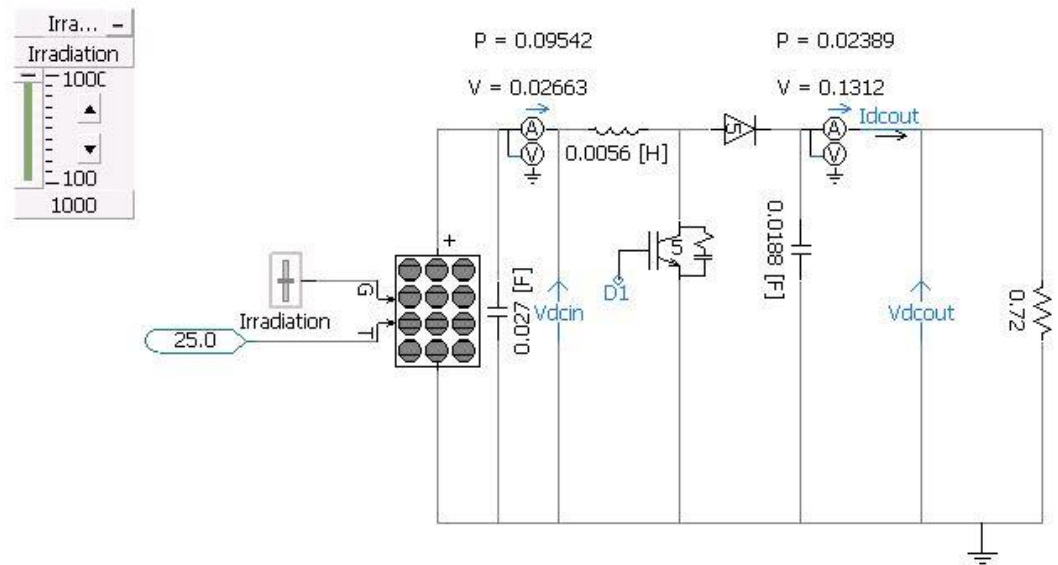


Figure 2.19 PV with DC-DC Boost converter model in PSCAD

The PI controller design using bode analysis is detailed for the above boost converter in APPENDIX.

The control loop is shown in Figure 2.20.

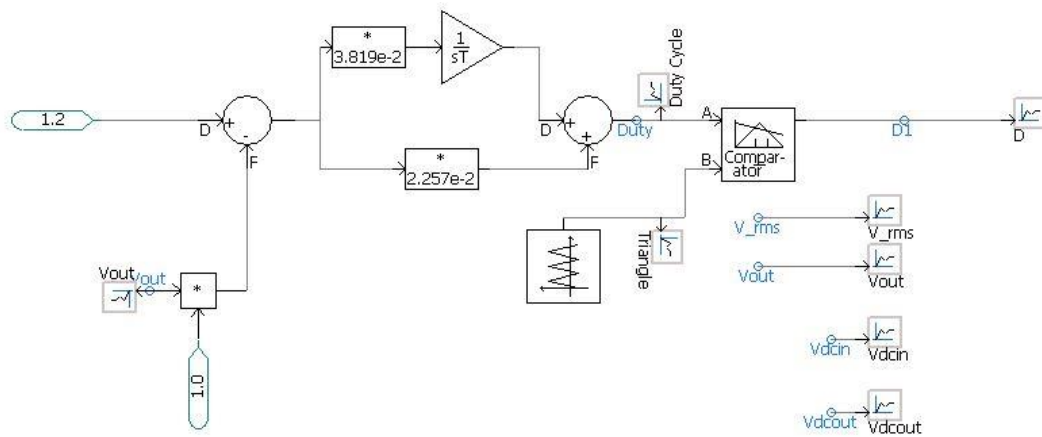


Figure 2.20 PI based controller for Duty cycle control of DC-DC Boost converter

Figures 2.21 through 2.25 detail the results of DC-DC boost converter simulation for validating the design and model of the converter when subject to changing load demands at the boost output.

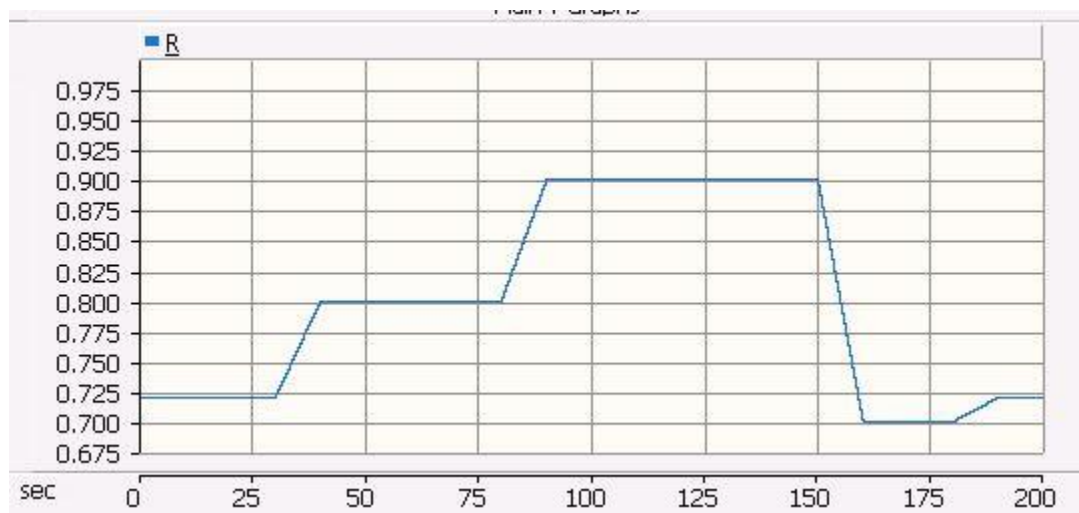


Figure 2.21 changing load resistance at the output of the boost converter

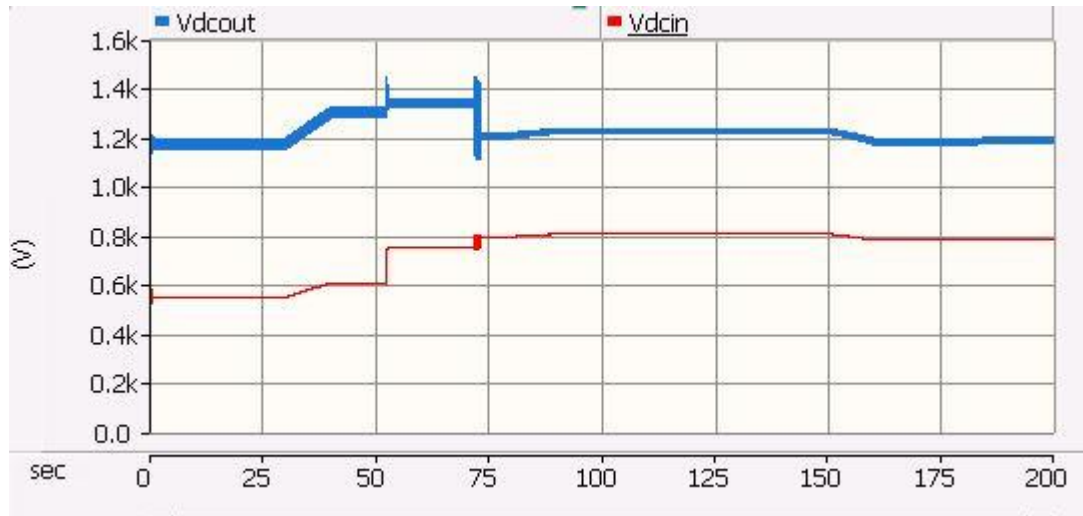


Figure 2.22 Input and Output voltage of the DC-DC boost converter

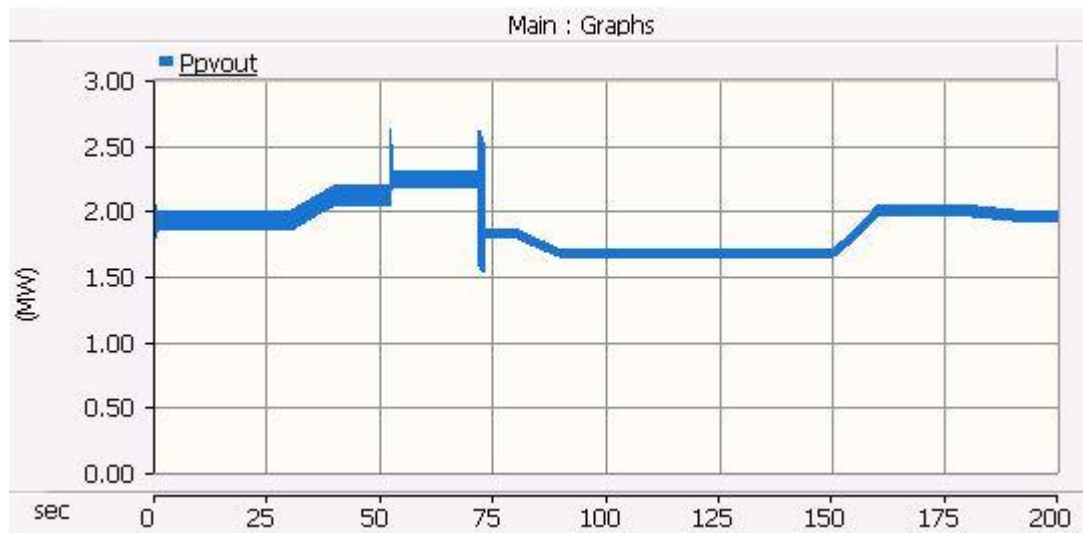


Figure 2.23 Power curve of the system to changing as per load demand



Figure 2.24 Duty ratio of the DC-DC boost converter adjusting to load demand

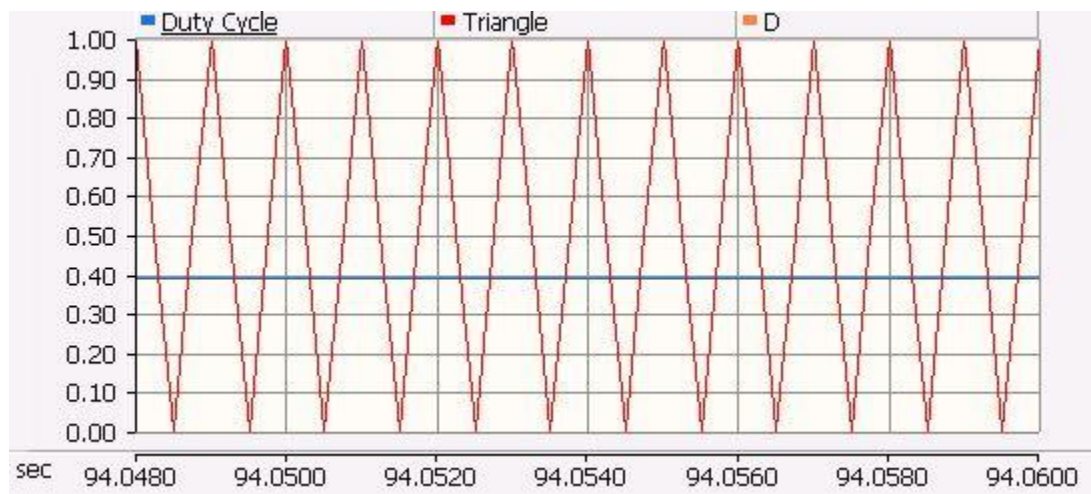


Figure 2.25 Triangular wave and duty ratio to generate the duty pulses for converter

The plot of output voltage being regulated at 1200 V for the changing load demands validate our controller design for duty cycle control loop.

### CHAPTER 3: DESIGN AND MODELLING OF HYBRID ENERGY STORAGE SYSTEM

Renewable energy sources are becoming increasingly popular in the world and are the favorites to take over the baton of power generation in the future. The clean energy perk comes with one disadvantage, i.e. intermittence. Be it solar or wind, the renewable energy sources suffer from irregular generation outputs due to the way they are extracted from nature. In case of Photovoltaics, temperature, irradiation and inclination of the PV arrays towards sun change the output and make the generation variable in nature. For PV to be considered as a standalone generating source, it needs to solve the problem of intermittence. This generates the need of energy storage devices which can store the surplus power and dispatch it when PV needs support during intermittence.

If we consider the load demands, there are fast and slow changing loads. In case of fast changing loads transient power changes are observed which the source has to supply. For this requirement high density power devices can work well, which can supply high amounts of power in a short period of time. For such applications energy storage devices like ultra-capacitors are suitable as they have one of the highest power density levels. These storage devices are known as ‘short term storages’.

In case of slow changing loads, “long term storages” like batteries can be employed which are capable of operating over a long period of time from a few minutes to hours. Thus, a combination of battery and ultra-capacitor storage system can be used to balance the power demand during intermittence and also during sudden and slow load changes in the system. Such a combination of battery and ultra-capacitor is known as a hybrid energy storage system (HESS) [34].

In this chapter the design, modelling, validation and application of hybrid energy storage system is discussed in detail.

### 3.1 Long Term Storage Device – Battery

Battery is a device which converts chemical energy into electrical energy. Like in a PV array, the battery comprises of cells connected in series and parallel combination to get the desired voltage and current at its output. Each cell consists of a positive and negative electrode and an electrolytic solution which serves as a medium to transfer charge between to electrodes. On completing the external circuit, the electron flow through the path generates electric current. Li-Ion, Nickel-Cadmium, Nickel-Metal-Hydride and Lead-Acid battery are the most commonly used batteries in the industry. Among these varieties, Li-Ion batteries are the most suitable for applications related to grid storage and distributed generating auxiliary sources. Lower weight, higher energy density, longer life cycle and no memory effects make Li-Ion based battery technology stand out among others. Especially in the case of distributed and portable generations like that of standalone PV

sets, the Li-Ion battery is more suitable due to the fact that it weighs one third the weight of lead-acid batteries and two third the weight of NIMH batteries.

### 3.1.1 Mathematical model of Li-Ion Battery

There are basically 3 types of battery models reported in literature: experimental, electrochemical and electric-circuit based models. The electric-circuit based model takes the State of charge (SOC) of the battery into consideration and is our model of interest because it is a useful representation of the battery characteristics.

The Li-Ion battery model is based on modified Shepard model equations which uses a simple controlled voltage source in series with a constant resistance, as shown in the Figure 3.1.

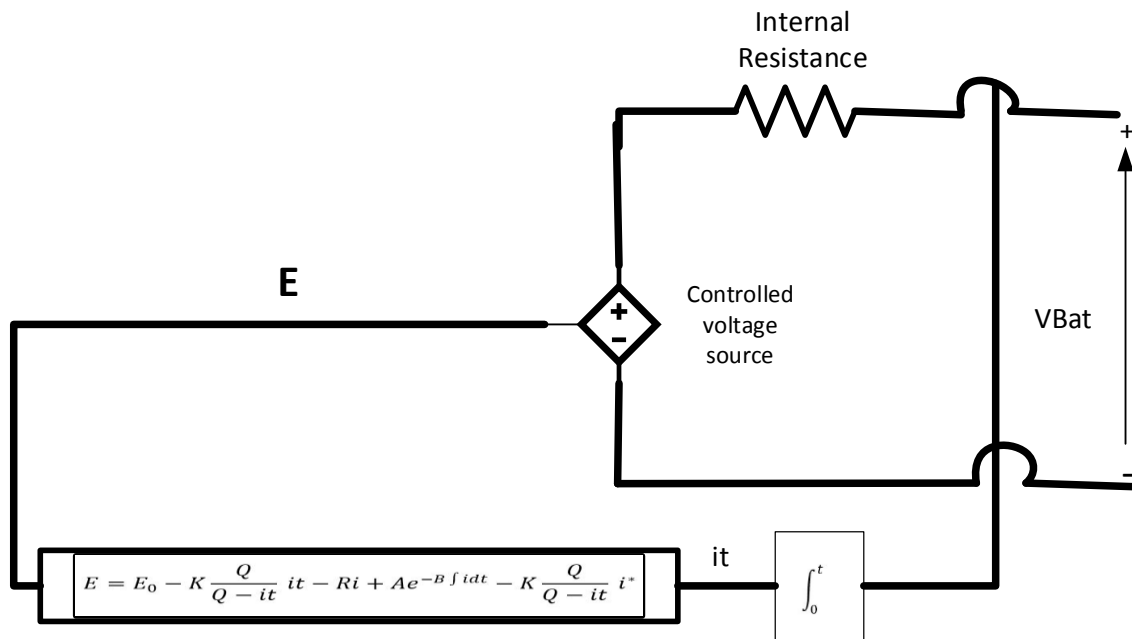


Figure 3.1 Equivalent circuit of battery [37]

The main feature of the model is that the parameters can be easily deduced from a manufacturer's discharge curve.

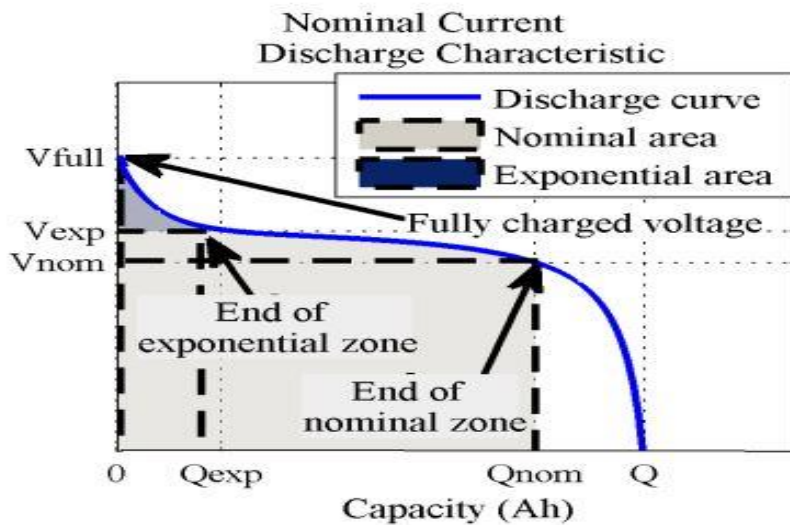


Figure 3.2 Typical Discharge curve [40]

Only 3 points on the manufacturer's discharge curve, in steady state are required to obtain the parameters. The fully charge voltage ( $V_{full}$ ), the end of the exponential zone ( $Q_{exp}$ ,  $V_{exp}$ ), the end of the nominal zone ( $Q_{nom}$ ,  $V_{nom}$ ) are enough to determine the all the necessary battery parameters to design the model.

### 3.1.2 The Charge and Discharge Model of Battery

#### 3.1.2.1 The Discharge Model

The model shown in Figure 3.1 considers the open circuit voltage as the function of SOC. The battery voltage is described by equation (3.1):

$$V_{Bat} = E_0 - K \frac{Q}{Q-it} it - Ri + Ae^{-B \int idt} - K \frac{Q}{Q-it} i^* \quad (3.1)$$

Where,

$V_{Bat}$  : Internal battery voltage (V)

$E_0$  : Battery voltage constant (V)

$K$  : Polarization constant (V/Ah)

$Q$ : Battery capacity (Ah)

$\int idt$  : Actual battery charge (Ah)

$A$ : Exponential zone amplitude (V)

$B$  : Exponential zone time constant inverse (Ah)<sup>-1</sup>

$R$ : Internal resistance of the battery ( $\Omega$ )

$i$ : Battery current (A)

$i^*$ : filtered current (A)

The equation means that when the battery is completely discharged and no current is flowing through the circuit, the voltage will be nearly zero.

### 3.1.2.2 The Charge Model

For Li-Ion batteries the voltage increases as the battery reaches its full charge. This is modelled by the polarization resistance term (K). In charge model, the polarization resistance increases until the battery is almost fully charged, meaning  $it=0$ .

Hence for the charge model the polarization resistance terms becomes  $K \frac{Q}{it}$ .

Theoretically, when  $it=0$ , the polarization resistance is infinite. This is not exactly the case in practice. Experimental results prove that K is shifted by 10%. Hence the Polarization resistance can be written as;

$$\text{Polarization Resistance} = K \frac{Q}{|it|-0.1Q} \quad (3.2)$$

Thus the battery voltage becomes:

$$E_{Bat} = E_0 - K \frac{Q}{Q-it} it - Ri + Ae^{-B \int idt} - K \frac{Q}{|it|-0.1Q} i^* \quad (3.3)$$

The model is based on the following assumptions and limitations:

Assumptions:

Internal resistance is assumed to be constant during charge and discharge cycles and does not vary with amplitude of the current.

The model parameters deduced from the discharge characteristics apply to charging as well.

The battery does not follow Peukert effect.

The battery model is unaffected by temperature change.

The battery has no memory effect.

Charge and discharge history does not affect battery characteristics.

Limitation:

Minimum capacity of the battery is 0 Ah and the maximum capacity is Q. Thus the maximum SOC is 100% for an overcharged battery.

### 3.1.3 Battery Model in PSCAD

Based on the modified Shepard's equation for Li-Ion battery discussed in the earlier topic the battery is modelled in PSCAD. The battery component and its SOC based charge-discharge logic has been provided by PSCAD technical support team for this thesis.

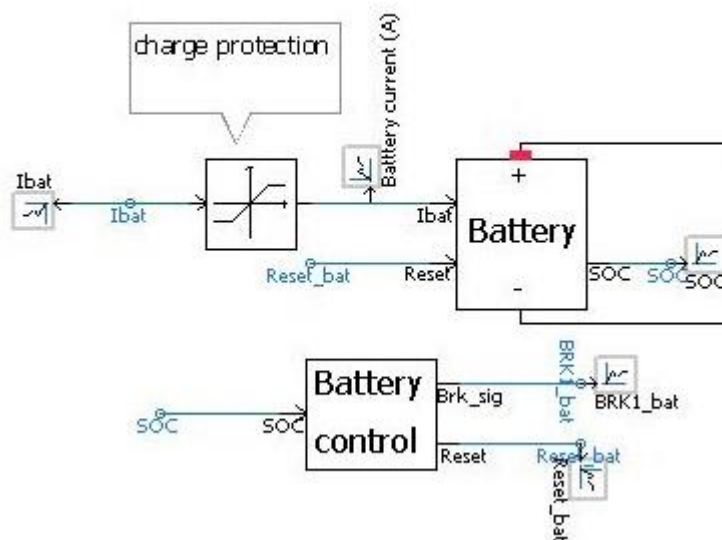


Figure 3.3 Battery component and the SOC based charge-discharge logic in PSCAD

In the figure above the battery component and the control logic has been shown.

Where,

I<sub>bat</sub>: output current from the battery, input signal.

Reset: control signal used to control the charge and discharge cycles based on SOC.

SOC: State of charge of the battery which generates the Reset signal.

The battery control logic will not be discussed in this thesis as it can be readily studied from the model example in PSCAD library, just as the battery model can be verified from the same library.

To scale and configure the Li-Ion battery to a user suitable size the following parameters are required by the battery model in PSCAD/EMTDC.

Nominal Voltage (V): Voltage at the end of nominal zone of the discharge curve.

Rated capacity (Ah): Rated capacity of the battery.

Initial Capacity (Ah): Initial battery condition for simulation.

Nominal Capacity (Ah): Extracted from battery until the voltage drops below nominal voltage.

Voltage at the exponential (V): Voltage corresponding to the end of the discharge characteristics.

Maximum voltage (V): Fully charged voltage.

Internal Resistance ( $\Omega$ ): Internal resistance which is a constant value.

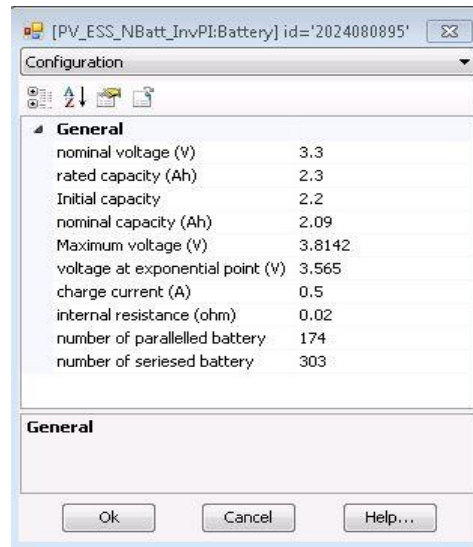


Figure 3.4 Battery model dialogue box in PSCAD

In this thesis the battery is sized to supply 20% of peak load demand. This brings the battery size to 400kWh considering 2MW of peak load demand. The battery pack is size for 400kWh with 1000V of nominal voltage and 400Ah of rated capacity. The Li-Ion battery parameters seen in Figure 3.4 have been extracted from Simulink battery model.

The number of series and parallel battery cells are calculated as follows:

$$N_s = \frac{\text{Desired battery pack voltage}}{\text{Cell nominal voltage}} = \frac{1000}{3.3} = 303$$

$$N_p = \frac{\text{Rated Ah capacity}}{\text{Cell rated Ah capacity}} = \frac{400}{2.3} = 174$$

Thus the calculated battery ratings can be tabulated as follows:

Table 3.1 Calculated battery pack rating

Sr.No.	Parameters	Value
1.	Nominal Voltage	1000V (design)
2.	Nominal capacity	363 Ah
3.	Rated capacity	400 Ah
4.	Fully charged voltage	1155.8 V
5.	Internal resistance	0.02 $\Omega$
6.	Nominal discharge current	174 A
7.	Voltage at exponential	1080 V

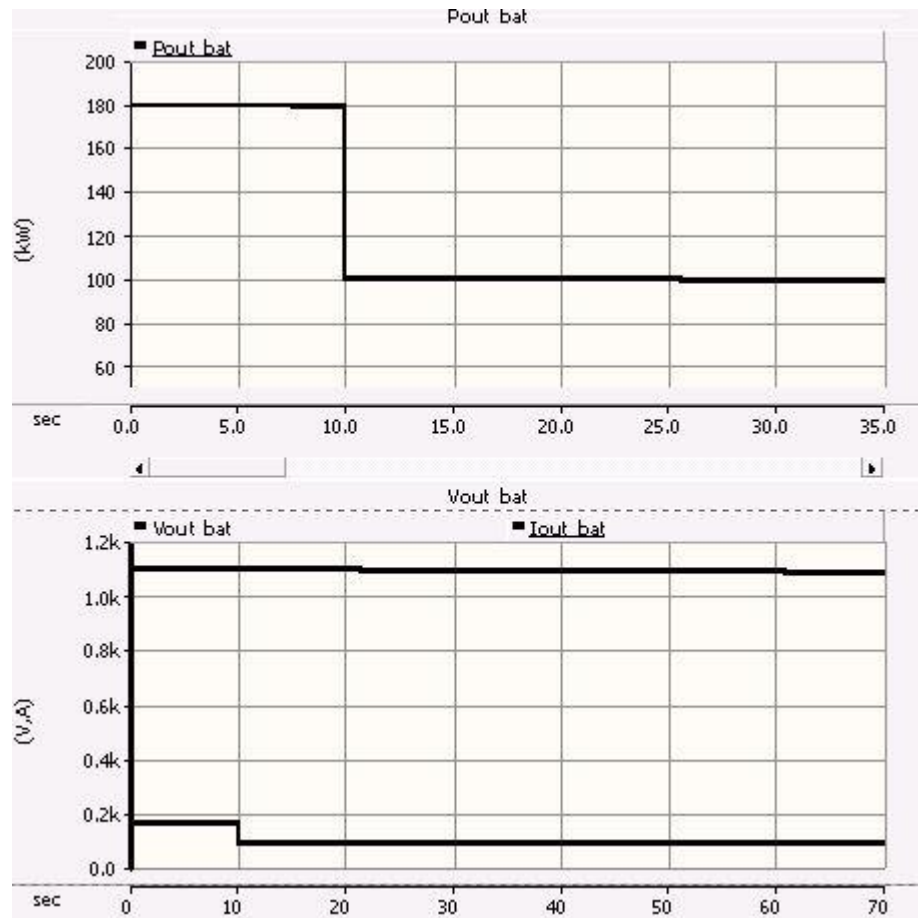


Figure 3.5 Battery pack voltage, current and power for model validation.

Response of the modelled battery pack to step change in the load from Figure 3.5 validates our battery pack model in PSCAD.

### 3.1.4 Power Conditioning for Battery System in PSCAD

The Power conditioning requirements of the battery primarily depends on how the battery is going to be utilized in the system. In case of our thesis, both the battery and the Ultra-capacitor are considered to be storage devices which are not supposed to supply power in normal operating conditions when the PV system is capable of supplying the load. Only when there is intermittence in the PV or additional loading on the PV than what the PV can supply should the battery and ultra-capacitor supply power. The prime objective of

the power storage devices is to maintain 1200V DC V at the DC link where the system connects to the inverter. This can be done by modelling a DC-DC boost converter in current control mode. By doing this the battery and ultra-capacitor will supply the commanded power in terms of current discharge. This discharge reference will correspond to the slow and fast changing power demand on the system. Figure 3.6 depicts the topology to be implemented among the PV and the HESS systems.

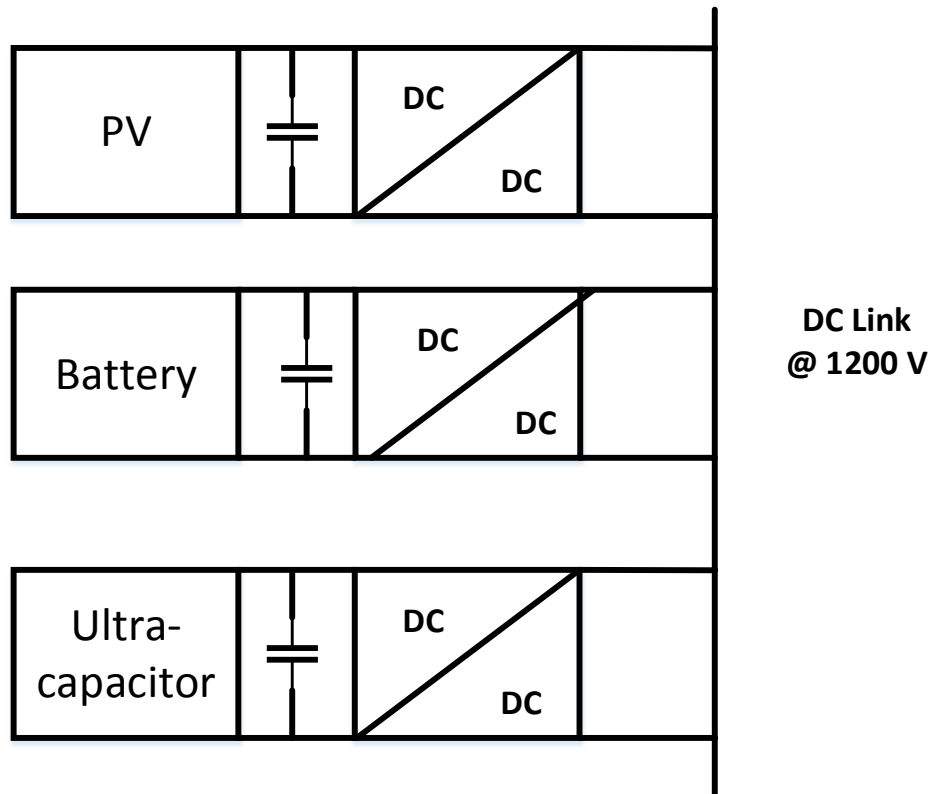


Figure 3.6 DC link topology showing PV and HESS in parallel.

### 3.1.5 DC-DC Boost Converter for Battery

The Mathematical model of the boost converter for the battery is similar to that discussed in 2.6.1 for the PV system. The difference here is that we will employ the current control mode of the boost converter instead of duty cycle control.

Thus the transfer function for the DC-DC boost converter becomes:

$$\frac{\tilde{i}_l}{\tilde{d}} = \frac{s \frac{V_0}{L} + \frac{V_0}{RLC} + \frac{I_l D'}{LC}}{s^2 + \frac{1}{RC}s - \frac{D'^2}{LC}} \quad (3.4)$$

Figures 3.7 through 3.11 details bode analysis and the compensation for the DC-DC boost system based on the analysis.

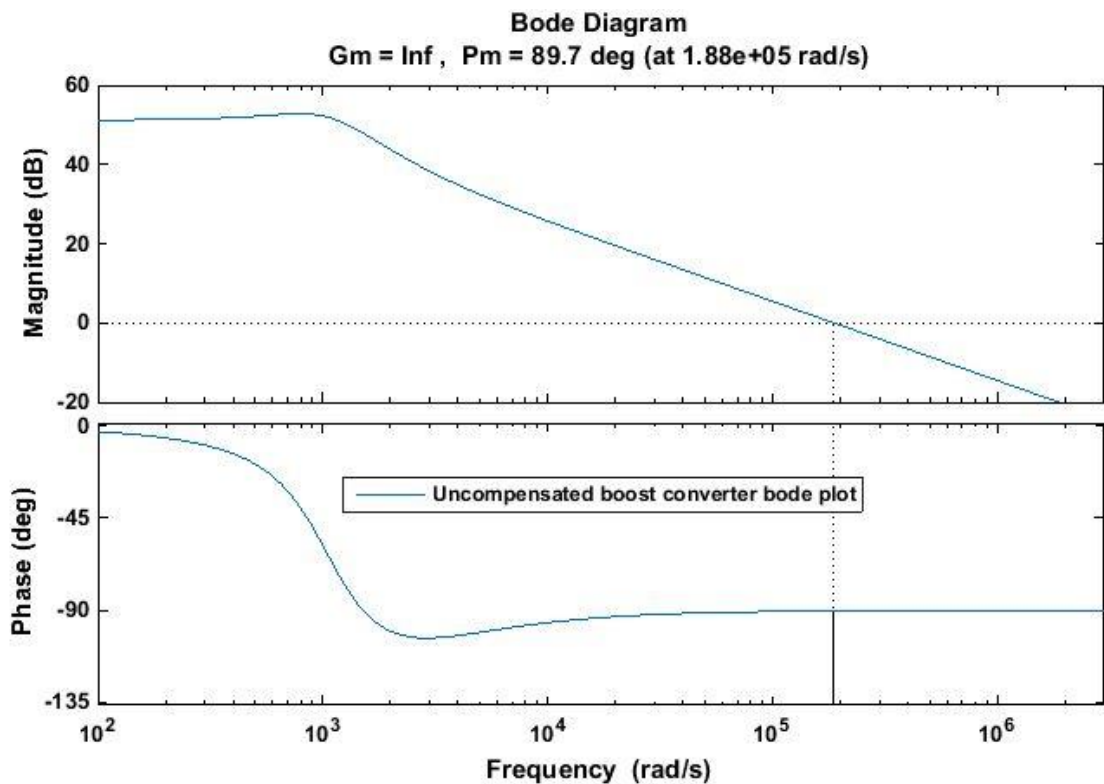


Figure 3.7 Bode plot of uncompensated system

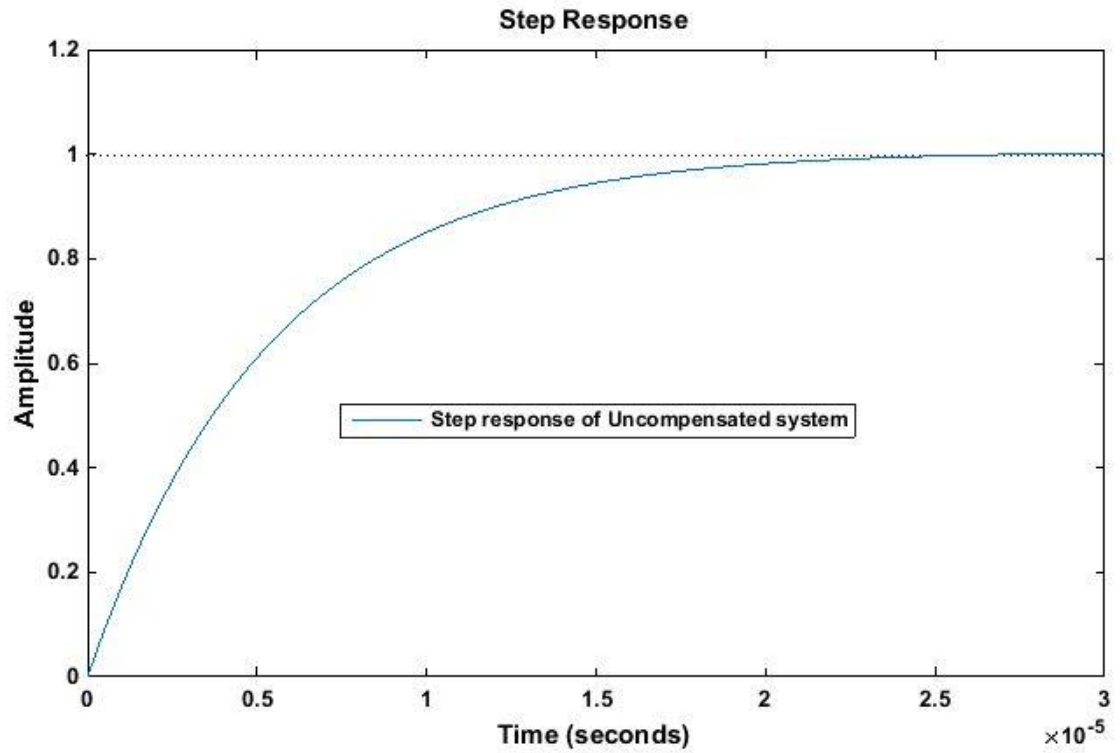


Figure 3.8 Step response of uncompensated system

After bode analysis we calculate the  $K_p$  and  $K_i$  values for the PI controller to compensate the system with desired Phase Margin and crossover frequency.

The transfer function of the PI control as shown in the earlier chapter will be:

$$G_C(s) = K_p \left( \frac{1+T_z s}{s} \right)$$

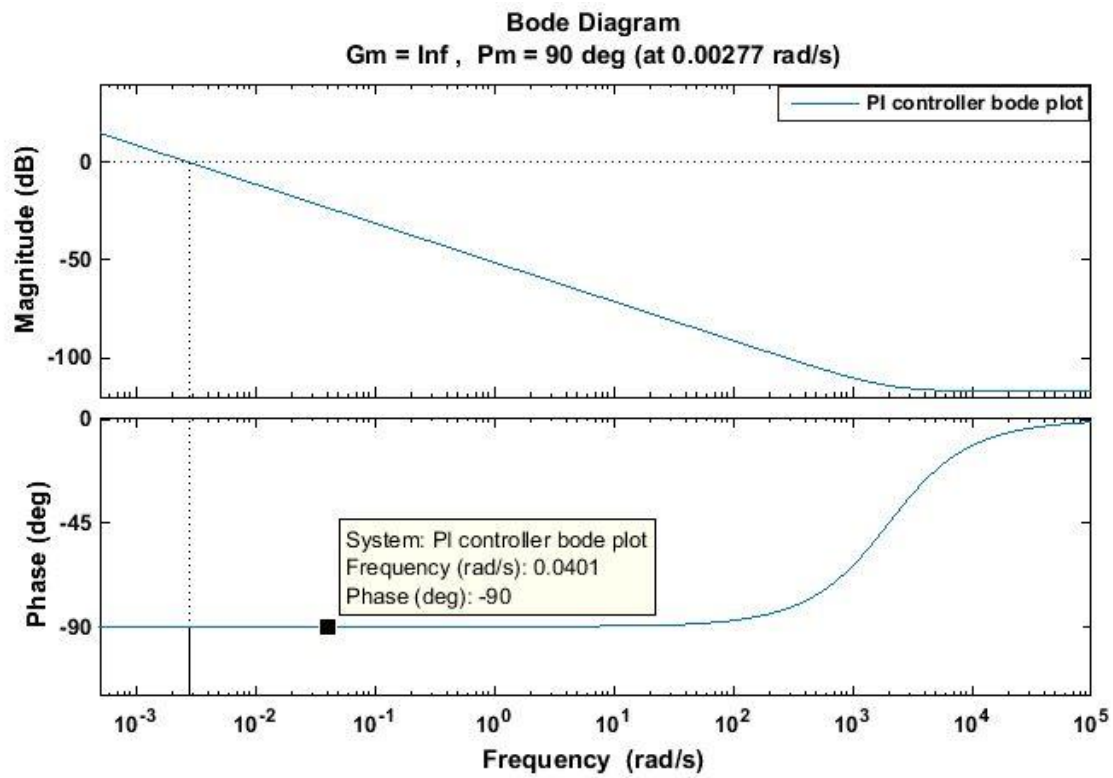


Figure 3.9 Bode plot of PI controller

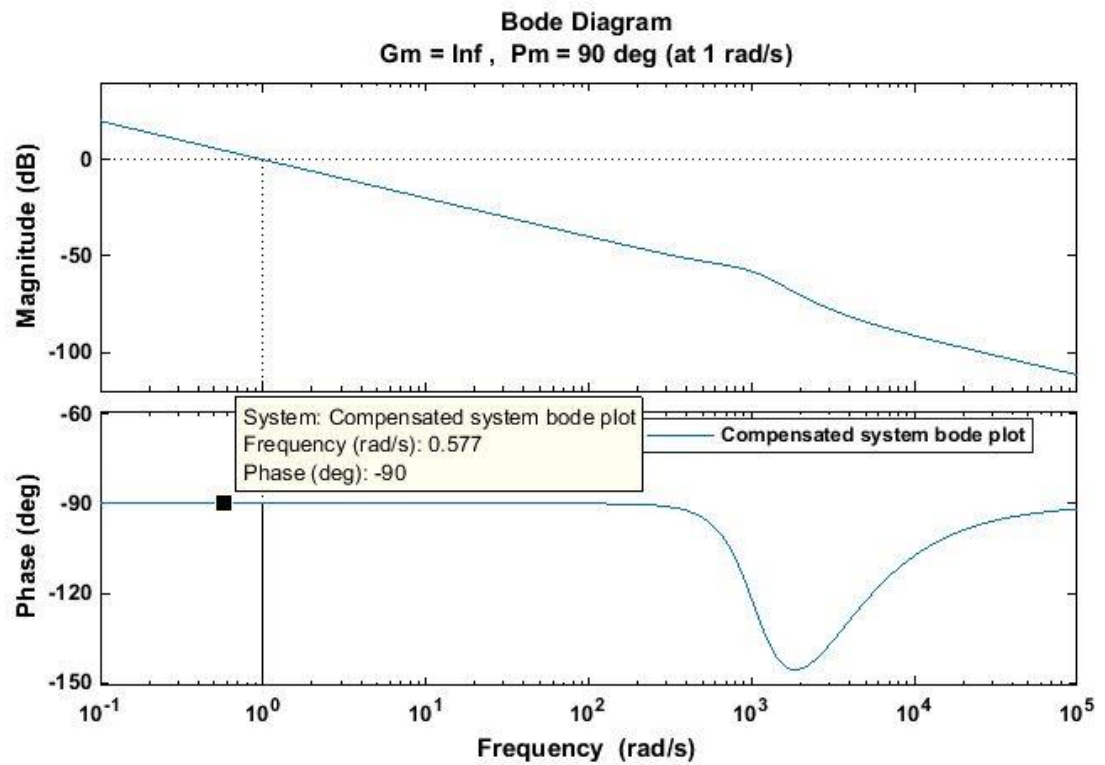


Figure 3.10 Bode plot of compensated system

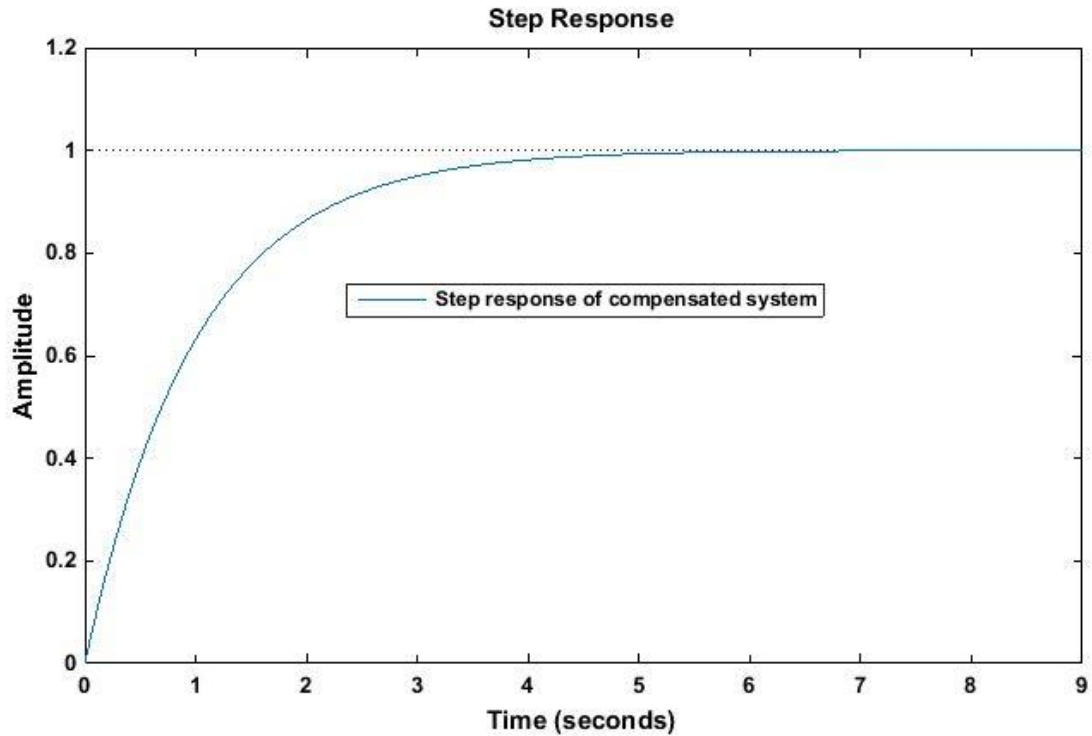


Figure 3.11 Step response of compensated system

From the bode plot of the compensated system in Figure 3.10 can see that we have a Phase margin of 90 Degrees at 1 rad/s of cross-over frequency. This was our design criteria while developing the controller from MATLAB based code.

The control loop developed based on the PI controller will control the Inductor current of the battery (which is also the input current to the boost converter) based on a current reference by exercising a control on the duty ratio of the boost converter. This makes sure that the battery supplies the demanded current corresponding to the power reference for the battery to be supplied.

Table 3.2 Summarizes the design of DC-DC boost converter for the battery for 1000 Hz of switching frequency and a rated duty cycle of 3.68%

Table 3.2 DC-DC boost converter for battery @ 1000 Hz

Sr. No.	Parameters	Value
1.	Vin	1155.8 V
2.	Vout	1200 V
3.	Pout = Pin	400 kWh
4.	Inductor (L)	0.008 H
5.	Capacitor (C)	0.00012789 F
6.	Maximum allowable ripple	2%

Figure 3.12 shows the battery and current controlled DC-DC boost converter model with a changing load for the purpose of validating the control loop.

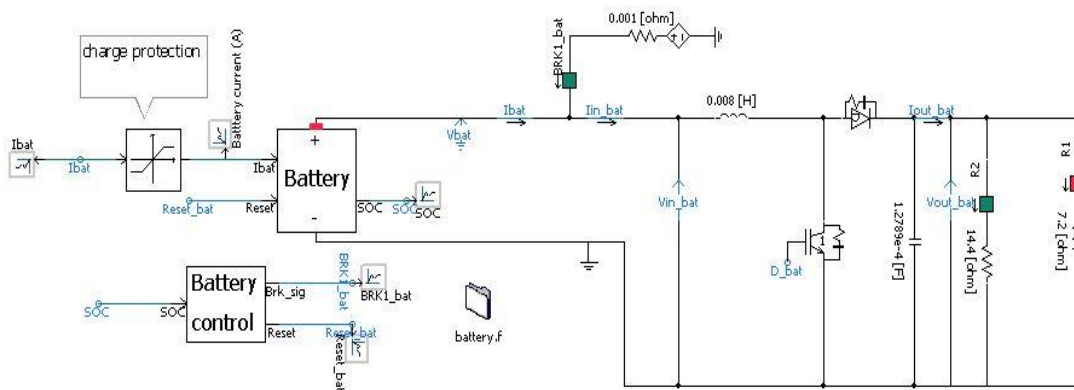


Figure 3.12 Battery and DC-DC boost converter simulation

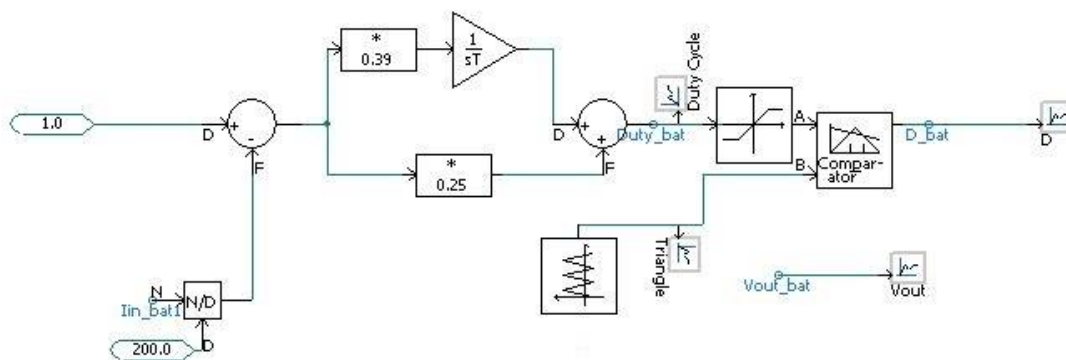


Figure 3.13 Current control loop for the DC-DC boost converter

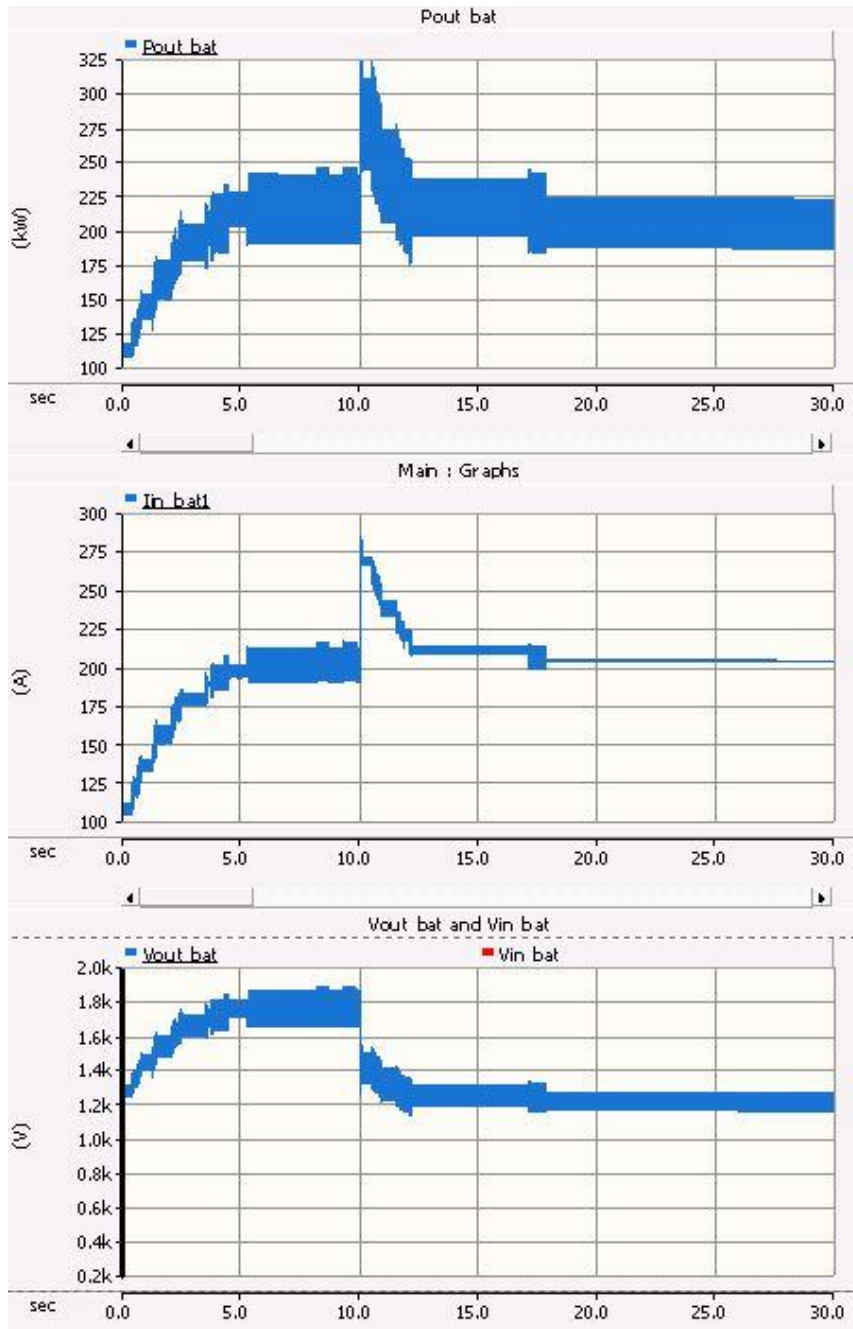


Figure 3.8 Voltage, current and power graphs for step changing load.

From Figures 3.12 and 3.13 it can be observed that the battery reference current is 1 (p.u.) on the base of 200 A. Even though the load demand was changed from 100kW to

200kW the battery continues to supply 1 (p.u.) of current. This validates our current control mode design for the DC-DC boost converter on the battery.

### 3.2 Short Term Storage Device – Ultra-capacitor

#### 3.2.1 Ultra-Capacitor Modelling

Some notable characteristics of Ultra-capacitors are faster charging time, thousand times more storage capacity than conventional capacitors, tens of thousand times more power deliverability than batteries, higher capacities with lower cell voltage. Just like batteries, the ultra-capacitor can also be modeled into a series-parallel combination of cell forming an array to achieve desired voltage and current [42].

The simplest form of Ultra-capacitor would be a capacitor with an Equivalent Series Resistor (ESR), which together can simulate the ohmic loss and the ultra-capacitor's capacitance during charge and discharge cycles. This model is easier to implement but cannot capture the voltage dynamics after charging and discharging stops [43].

For this thesis we are going to employ Zubeita's multi-time constant model which uses the third order system of resistances and capacitors, all having different time constants [42].

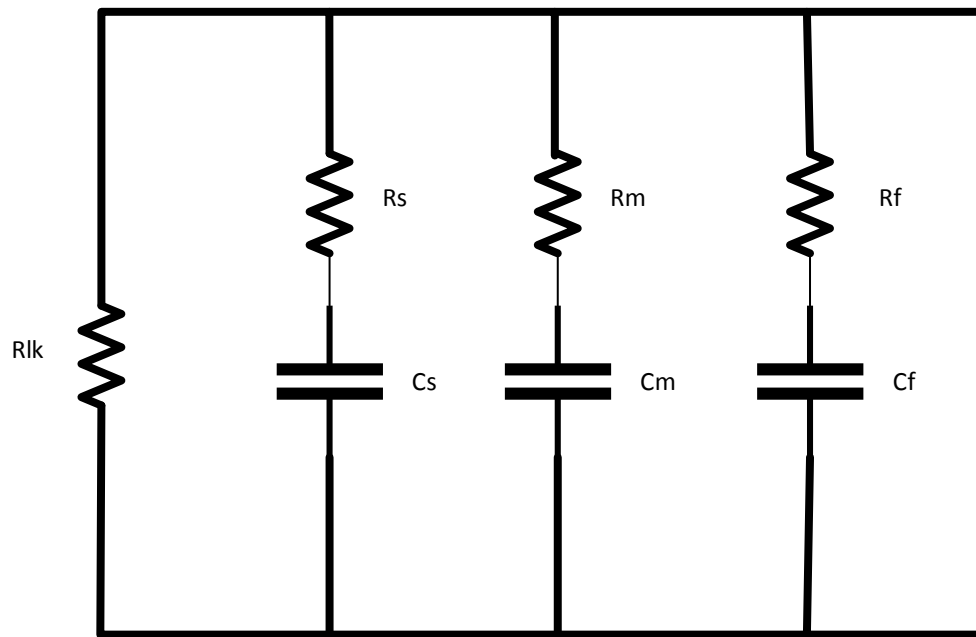


Figure 3.14 Equivalent circuit of Zubeita's multi-time constant model [42]

To meet the capacity and voltage rating for applications the short-term model shown in the Figure 3.14 can be scaled to an equivalent n-cell model. The Ultra-capacitor cell parameters, single cell model and n-cell model calculations are detailed in the Tables 3.3, 3.4 and 3.5 respectively.

Table 3.3 Ultra-capacitor cell model parameters

Sr. no.	Specifications	Units
1.	Rated Capacitance	Farads (F)
2.	Max. ESR initial	mili-ohms (mΩ)
3.	Rated Voltage	Volts (V)
4.	Maximum continuous current @ 40° C	Amperes (A)
5.	Maximum continuous current @ 15° C	Amperes (A)
6.	Maximum peak current 1 second (non-repetitive)	Amperes (A)
7.	Leakage current, maximum	mili-amperes (mA)

From the parameters obtained above we can develop the single cell Ultra-capacitor model. The calculations are given in the Table below.

Table 3.4 Ultra-capacitor Model calculation [44]

	Slow	Medium	Fast	Leakage
Resistance	$\frac{2}{3}\alpha^{-(2k+1)}ESR$	$\frac{2}{3}\alpha^{-(2k-1)}ESR$	$\frac{2}{3}ESR$	$R_{lk} = \frac{V_r}{I_{leak}}$
Capacitance	$1.05\alpha^{(2j-1)}C_0$	$1.05\alpha^{(2j+1)}C_0$	$1.05C_0$	
Where $\alpha = 0.5(\sqrt{5}-1)$ , $j = 2$ and $k = 8$				

To scale the above model to an equivalent n-cell model we use Table 3.5.

Table 3.5 N-Scaled Ultra-Capacitor Model [44]

	Slow	Medium	Fast	Leakage
Resistance	$\frac{2N}{3} \alpha^{-(2k+1)} ESR$	$\frac{2N}{3} \alpha^{-(2k-1)} ESR$	$\frac{2N}{3} ESR$	$R_{lk} = \frac{NV_r}{I_{leak}}$
Capacitance	$\frac{1.05}{N} \alpha^{(2j-1)} C_0$	$\frac{1.05}{N} \alpha^{(2j+1)} C_0$	$\frac{1.05}{N} C_0$	
Where $\alpha = 0.5(\sqrt{5}-1)$ , $j = 2$ and $k = 8$				

The Ultra-capacitor system in our thesis has been modelled for a 2 MW peak power, 150 A of maximum current and 750 V of output voltage. The following Table details the data extracted from a Maxwell BCAP 1500 capacitor which is used to design our Ultra-capacitor model in PSCAD.

Table 3.6 Maxwell BCAP 1500 datasheet for UC design

Sr. no.	Specifications	Units
1.	Rated Capacitance	1500 (F)
2.	Max. ESR initial	0.47 (mΩ)
3.	Rated Voltage	2.7 (V)
4.	Maximum continuous current @ 40° C	150 (A)
5.	Maximum continuous current @ 15° C	84 (A)
6.	Maximum peak current 1 second (non-repetitive)	1200 (A)
7.	Leakage current, maximum	3 (mA)

In order to achieve a total voltage of 750 V of the UC pack we do the following calculations:

$$N_p = N_s \frac{C_{eq}}{C_{cell}}$$

$$N_s = \frac{\text{Total voltage of UC pack}}{\text{Total voltage of a UC cell}} = \frac{750}{2.7} = 278$$

For,  $N_p = 1$ ;

$$C_{eq} = \frac{C_{eq}}{N_s} = \frac{1500}{278} = 5.3856 \text{ F}$$



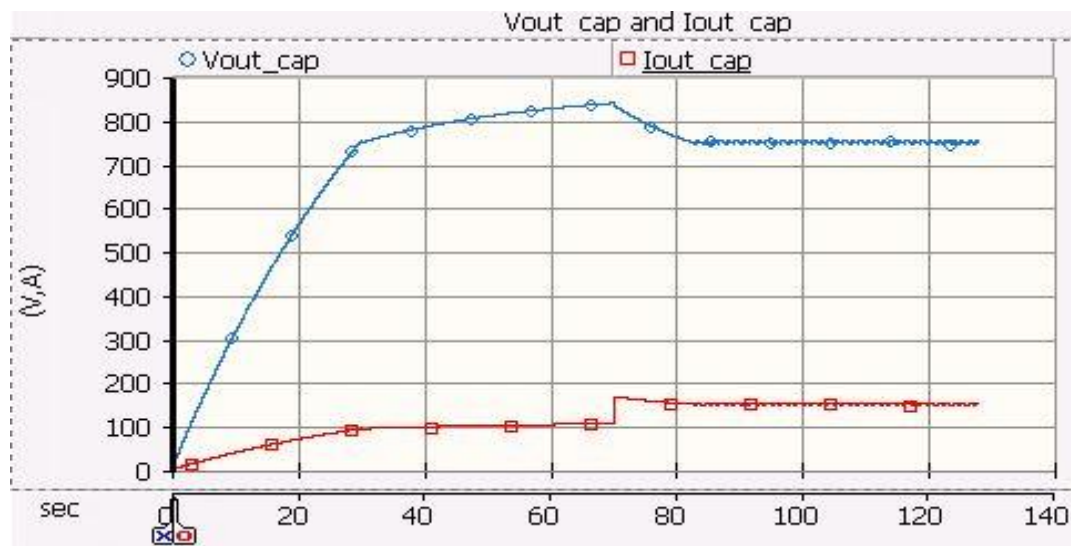


Figure 3.16 Step changing load validation for N-scaled UC model in PSCAD, graph of output voltage and current

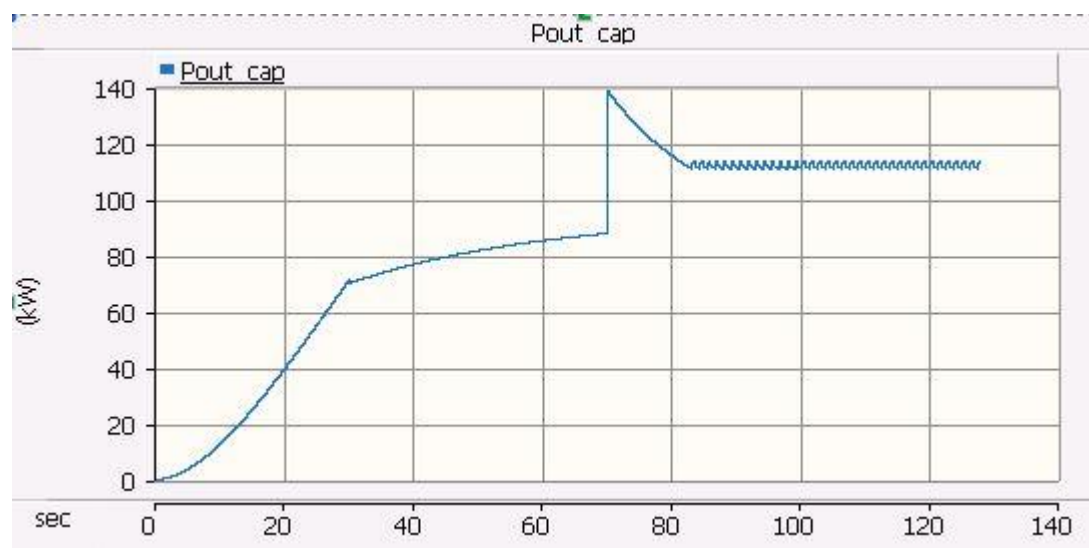


Figure 3.17 Step changing load validation for N-scaled UC model in PSCAD, graph of output power on ultra-capacitor system

The Figures 3.16 and 3.17 validates the design of UC system to a step changing load. As soon as the voltage reaches 750 V corresponding to power demand of 70 kW from

UC, a step change in load to 110 kW is initiated. The voltage re-tracks the 750 V rated value once the step transition is completed. This validates the UC system design in PSCAD.

### 3.2.3. Design and Modelling of a DC-DC Boost Converter for Ultra-capacitor

As discussed earlier about the power conditioning requirements for the battery system in our thesis in section 3.1.4, the same logic applies to the Ultra-capacitor since they both are connected in parallel along with the PV system to a common DC link. On the same lines as the DC-DC boost converter for the Battery was developed, we will design a boost converter operating in the current control mode.

Table 3.7 details the DC-DC boost converter modelled for our UC system.

Table 3.7 DC-DC boost converter model for UC system @ 1000 Hz

Sr. No.	Parameters	Value
1.	Vin	750 V
2.	Vout	1200 V
3.	Pout = Pin	2 MW
4.	Inductor (L)	0.0053 H
5.	Capacitor (C)	0.013 F
6.	Maximum allowable ripple	2%

Figure 3.18 shows the UC system and current controlled DC-DC boost converter model with a changing load for the purpose of validating the control loop.

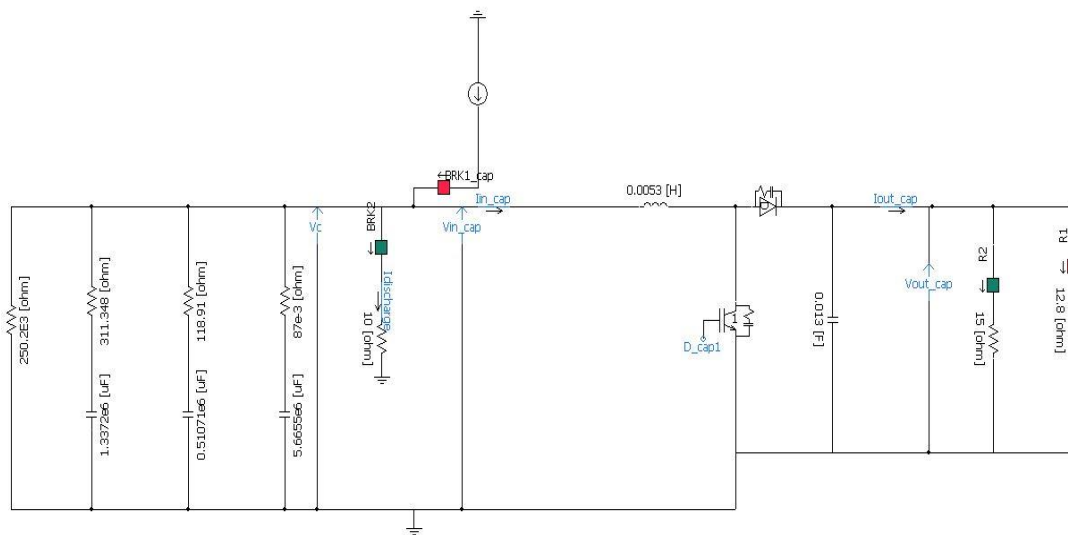


Figure 3.18 Current controlled DC-DC boost converter model with UC system in PSCAD

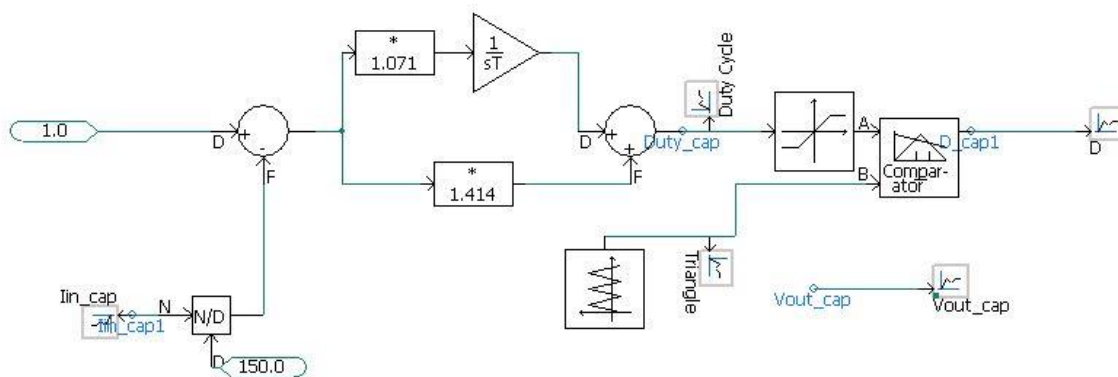


Figure 3.19 Current control loop of the DC-DC boost converter in PSCAD

Figure 3.19 shows the control loop from current control of DC-DC boost converter.

Figures 3.20 through 3.23 shows the controller response to step change in the load and the corresponding Power, Voltage, current and duty ratio graphs.

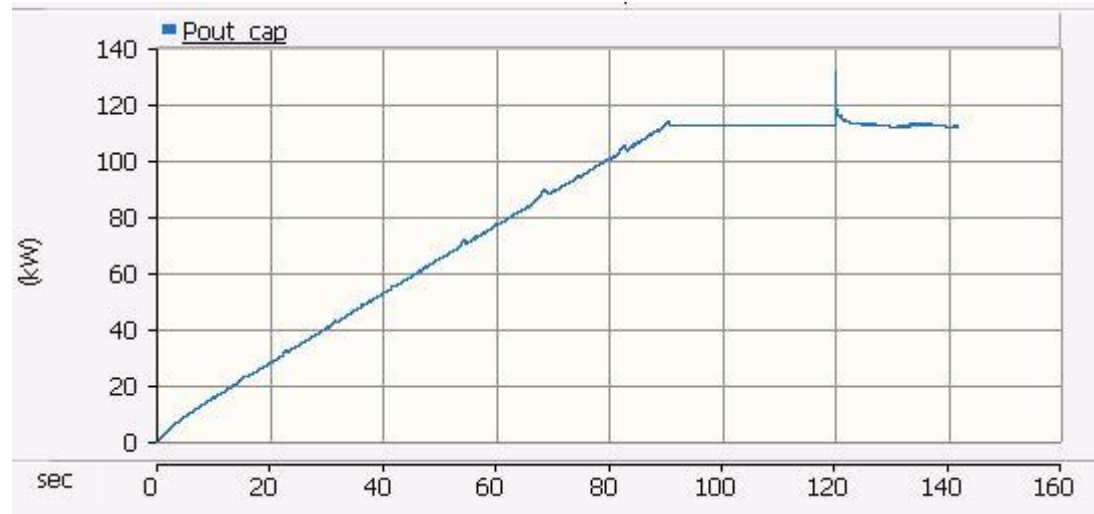


Figure 3.20 Power graph for step change in load

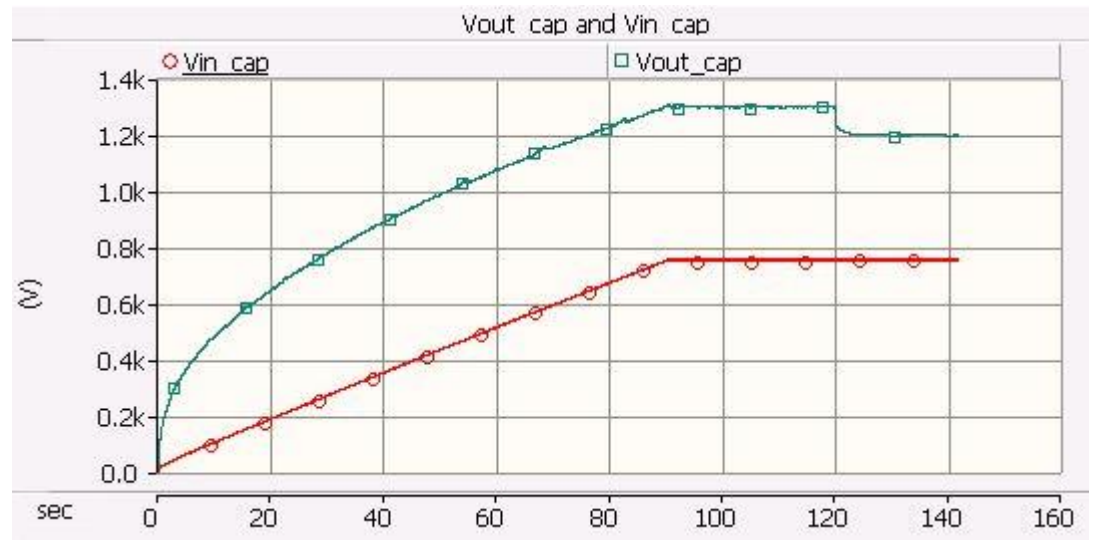


Figure 3.21 Input and output voltage graphs for step change in load

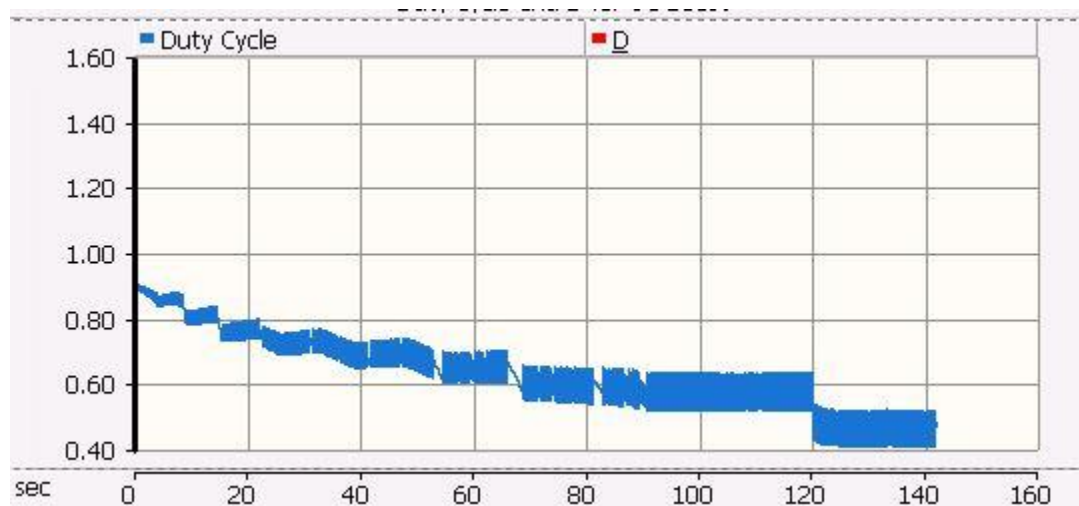


Figure 3.22 Change in duty cycle as a response to step change in load

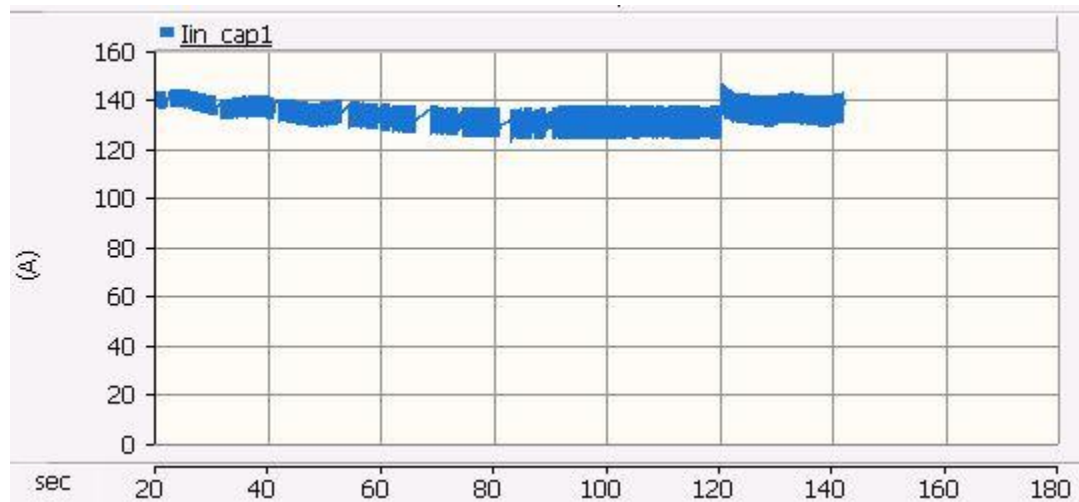


Figure 3.20 Input current response for step change in load

From the above graphs we can see that even though there is a step change in the load demand for the UC system the current still remains the same. This is because we have employed the DC-DC boost converter in the current control mode which demands 1 p.u

(around 150 A) current from the system irrespective of the load demand set for the UC system. This validates our DC-DC boost converter design in PSCAD for the UC system.

### 3.3 Cascade Control on HESS

As we have seen from the above topics the DC-DC boost converter gives us a current reference for the inner loop current control to work on. The outer loop for this scheme will be a power to current conversion loop. The power reference will be scheduled by the load and will be coming through a low pass filter. Figure 3.21 will explain the power scheduling for the HESS structure. In the Figure 3.21, the DC demanded power is the mismatch which the battery and the ultra-capacitor has to supply. This is the case as we do not have the PV farm connected in the system and are simulating the HESS system in standalone mode for the DC load demand.

The Power equation for the given topology is:

$$P_{dc\text{demand}} = P_{pv} + P_{HESS}$$

Since  $P_{pv} = 0$ , we have:

$$P_{dc\text{demand}} = P_{HESS}$$

Where,

$P_{dc\text{demand}}$ : Power demand at the DC link

$P_{pv}$ : Power output from the PV farm

$$P_{HESS} = P_{bat} + P_{uc}$$

$P_{HESS}$ : Power output from the Hybrid Energy Storage System

$P_{bat}$ : Power output from the battery

Puc: Power output from the ultra-capacitor

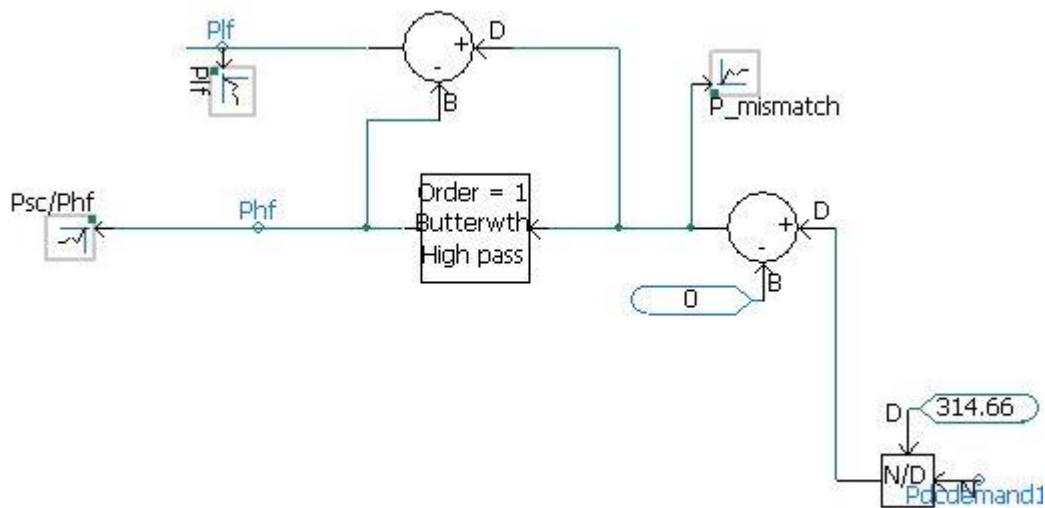


Figure 3.21 Power scheduling for battery and ultra-capacitor in terms of high frequency and low frequency reference.

These power reference  $P_{lf}$  and  $P_{hf}$  are our reference signals for the outer power loop. We now need to design the outer loop such that current references may be generated from these references. To do this we are going to employ Zeigler-Nichols based PI controller for the outer loop.

Figure 3.22 describes the cascade control structure, with the ZN PI for the outer loop and current controlled inner loop.

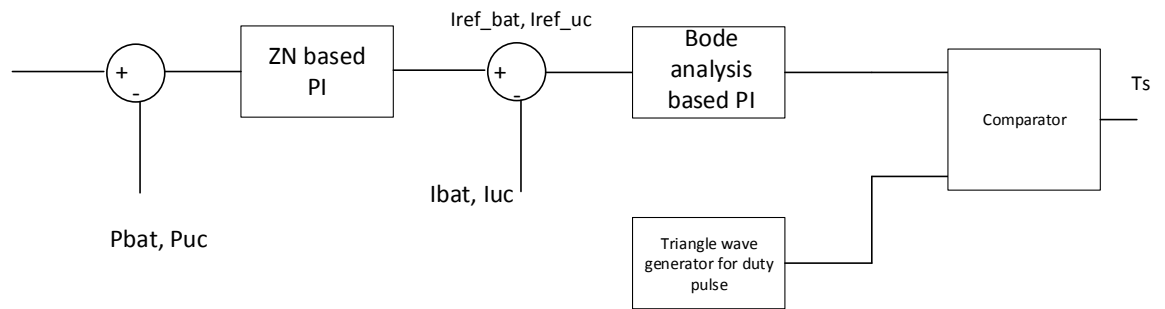


Figure 3.22 Cascade control structure for HESS

### 3.3.1 Zeigler-Nichols Tuning

For Zeigler Nichols method of tuning we need to obtain the plant step response. The advantage of this method is that it avoids the need of the plant model to design controller and only relies on the step response of the plant.

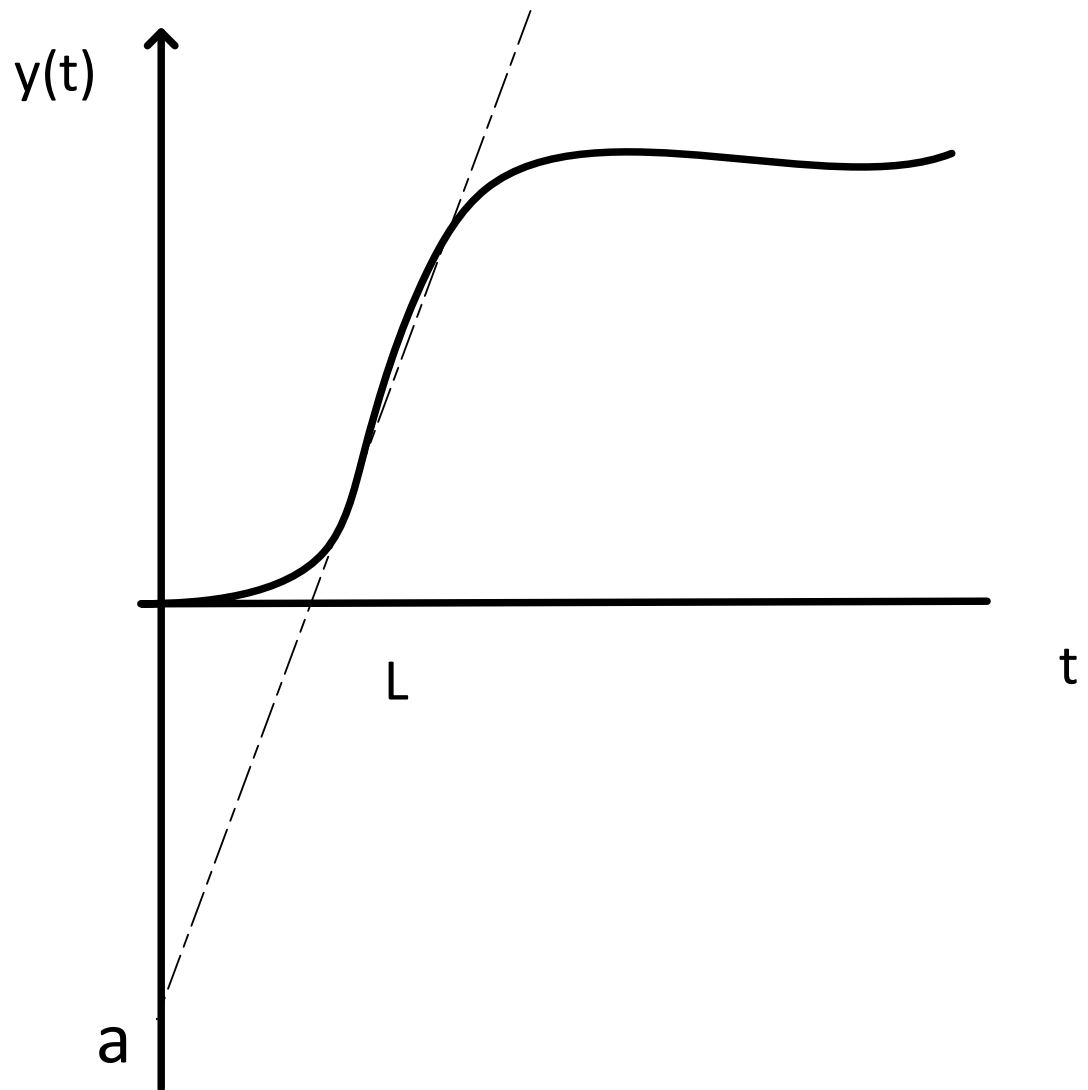


Figure 3.23 Step response of plant model [46]

Table 3.8 shows the controller parameters derived from the Zeigler Nichols step response [46].

Controller Type	$K_p$	$T_i$	$T_d$
P	$1/a$	-	-
PI	$0.9/a$	$3L$	-
PID	$1.2/a$	$2L$	$L/2$

Table 3.8 Controller calculation from the ZN plot [46]

The method of obtaining the controller parameters is as follows:

- 1) Get the step response of the plant
- 2) Draw the steepest tangent line to the curve
- 3) Get  $a$  and  $L$  (which are the Y and X intercepts respectively)
- 4) Design the desired controller using Table 3.8

The ZN approach for battery will be shown here. Figure 3.24 presents the step response of a single cell unit of battery in terms of Voltage.

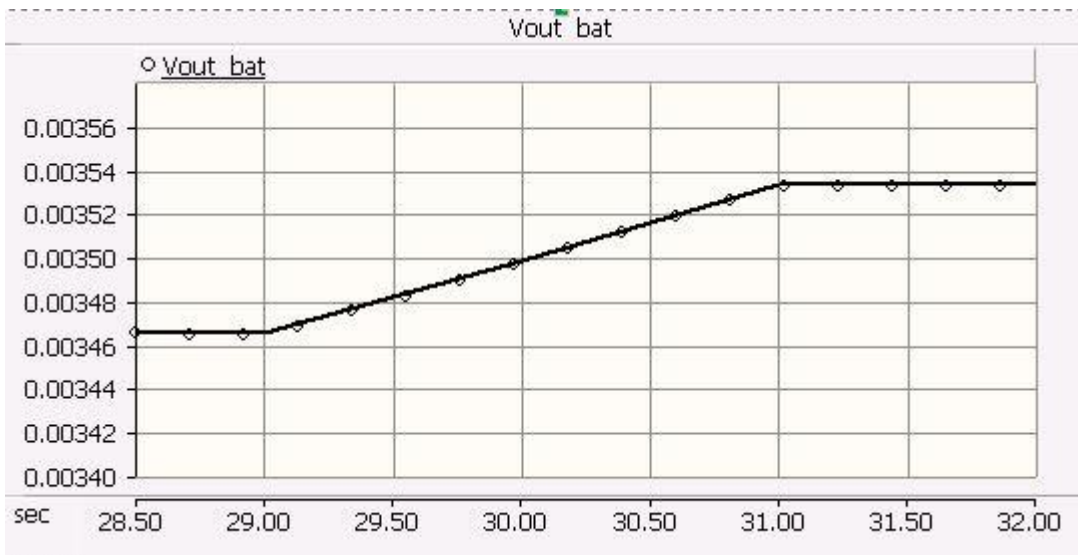


Figure 3.24 Step response in terms of voltage for a single cell battery unit [46]

From the above plot we can get 3 points on the tangent to the curve as: (29, 2.4647), (30, 3.49807) and (31, 3.53359). Based on these 3 points we calculate the X and Y intercept for the tangent line.

Hence,  $a = 2.465795$  and  $L = -71.5864$ .

From the Table 3.8 the  $K_p$  and  $K_i$  were calculated to be:

$K_p = 0.364944$  and  $K_i = 0.00169925$

The Bode plot of the PI controller can be seen in Figure 3.25.

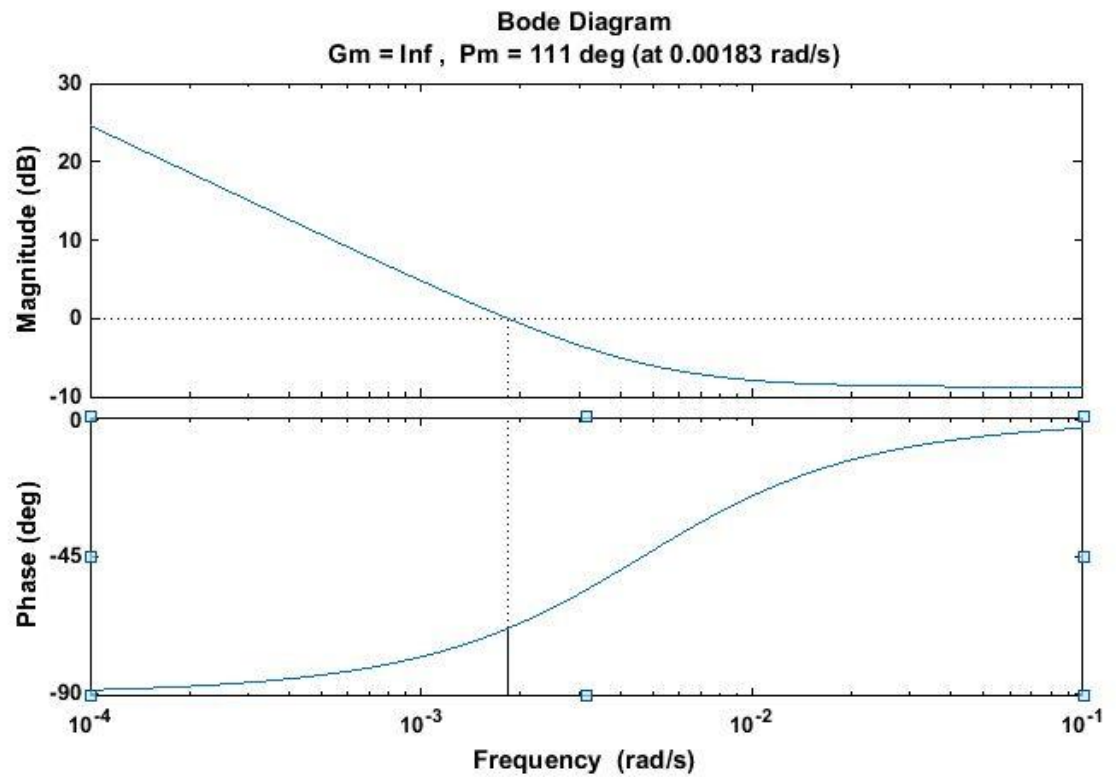


Figure 3.25 Bode plot of ZN Based PI controller for battery system

From the bode plot we can say that the developed PI controller will contribute toward positive Phase Margin to the system.

On similar lines the Zeigler Nichol results for the UC system can be in Figure 3.26 and Figure 3.27.



Figure 3.26 Step response in terms of voltage for UC pack [46]

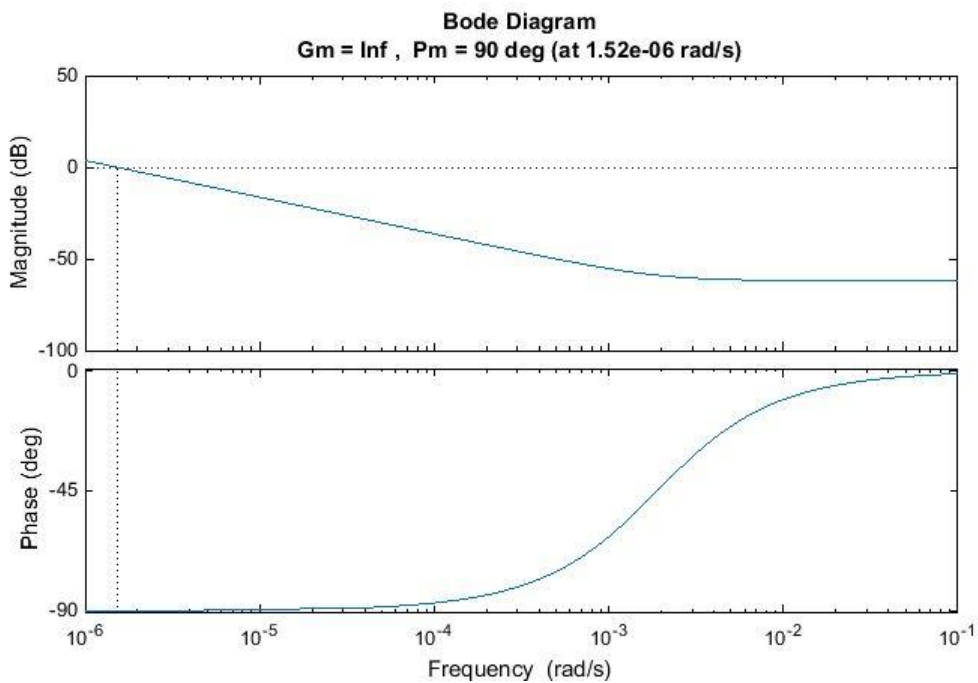


Figure 3.27 Bode plot of ZN Based PI controller for UC system

### 3.3.2 HESS in Standalone Mode of Operation

After deriving the Outer loop control based on ZN tuning we will now simulate the HESS in standalone mode for a step change in load and validate the results with the help of graphical analysis.

Figures 3.28 through Figure 3.35 represent the standalone mode analysis of the HESS connected to a varying DC load for the case of slow varying load

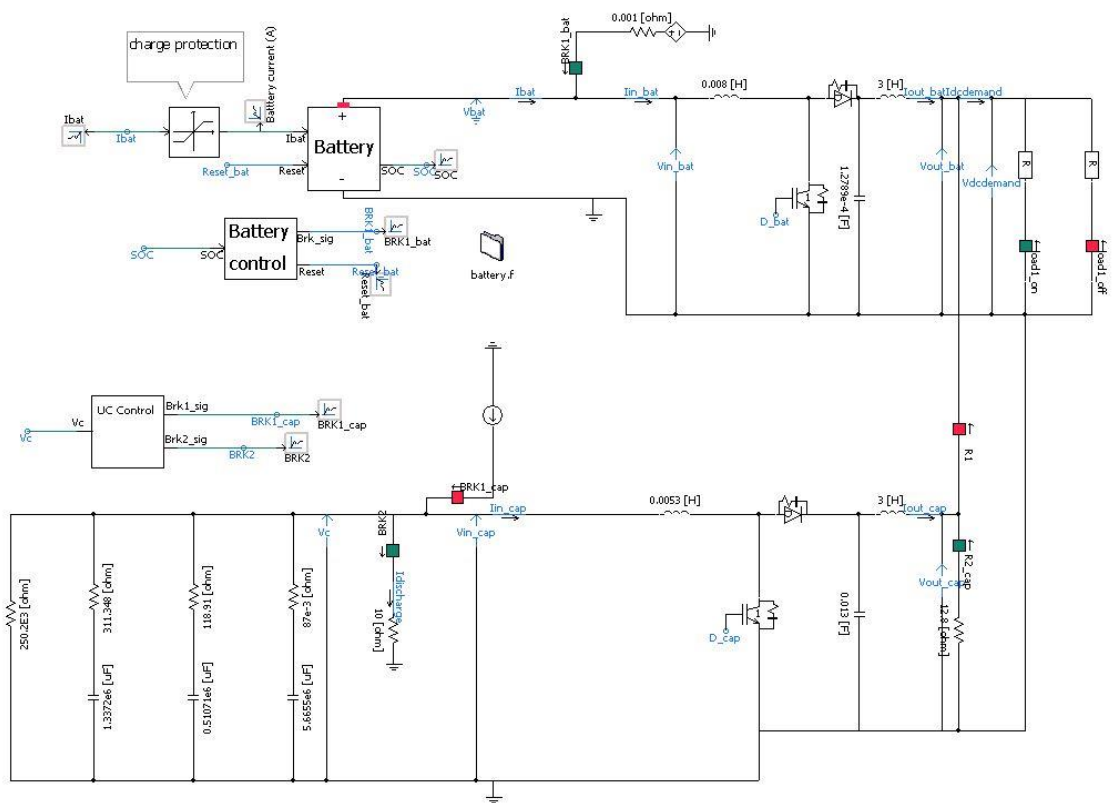


Figure 3.28 HESS model in standalone configuration

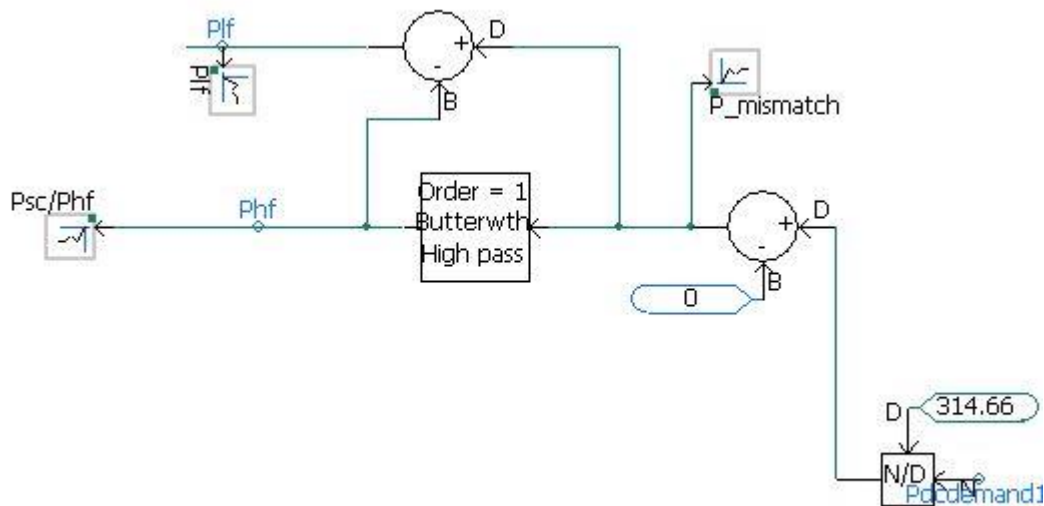


Figure 3.29 Power reference generation for cascade control using Low pass filter

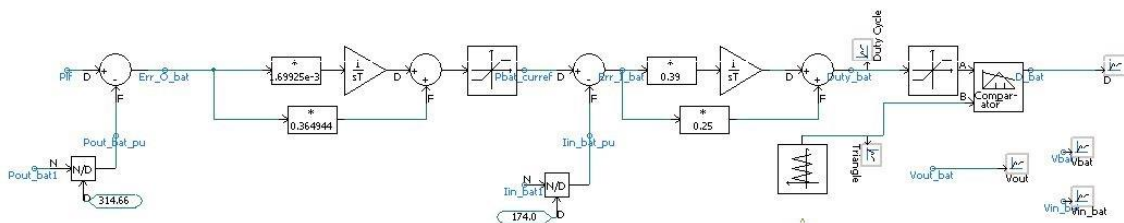


Figure 3.30 Cascade control on battery

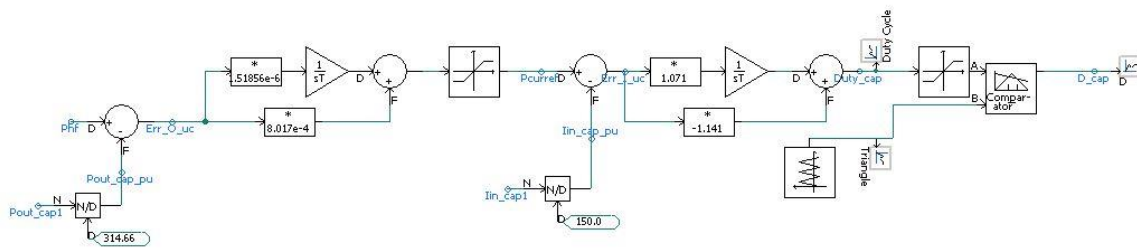


Figure 3.31 Cascade control on UC system

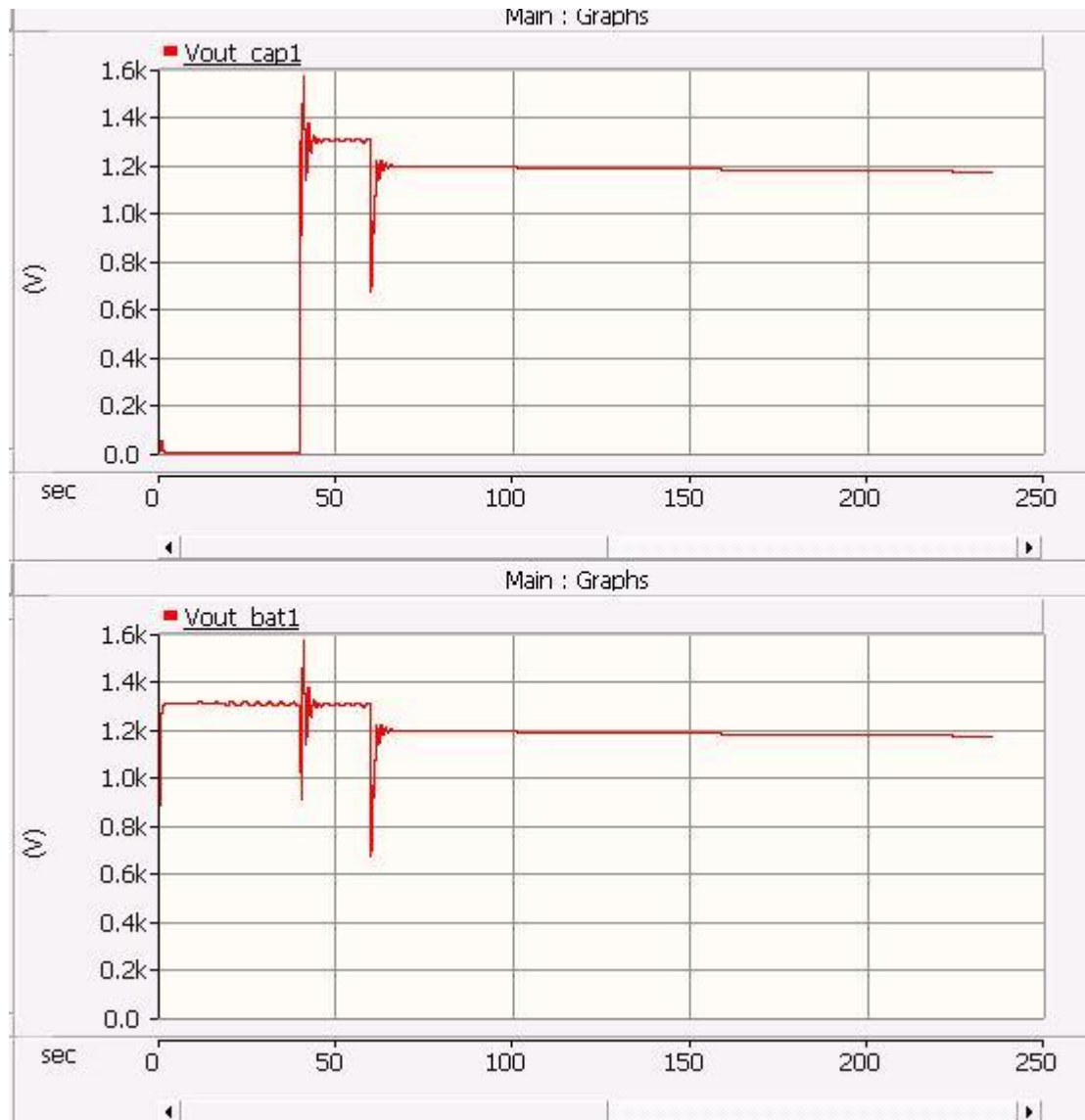


Figure 3.32 Voltage graphs for battery and UC system to step changing load for slow varying load conditions

Since the HESS is controlled using the current control mode of DC-DC boost converter we can see in Figure 3.32 that we do not have a control on the DC link voltage and hence

here we see that for non-rated power demand the DC link does not regulate to 1200V. That part will be taken care by the duty cycle control employed on the PV farm when the system integration takes place.

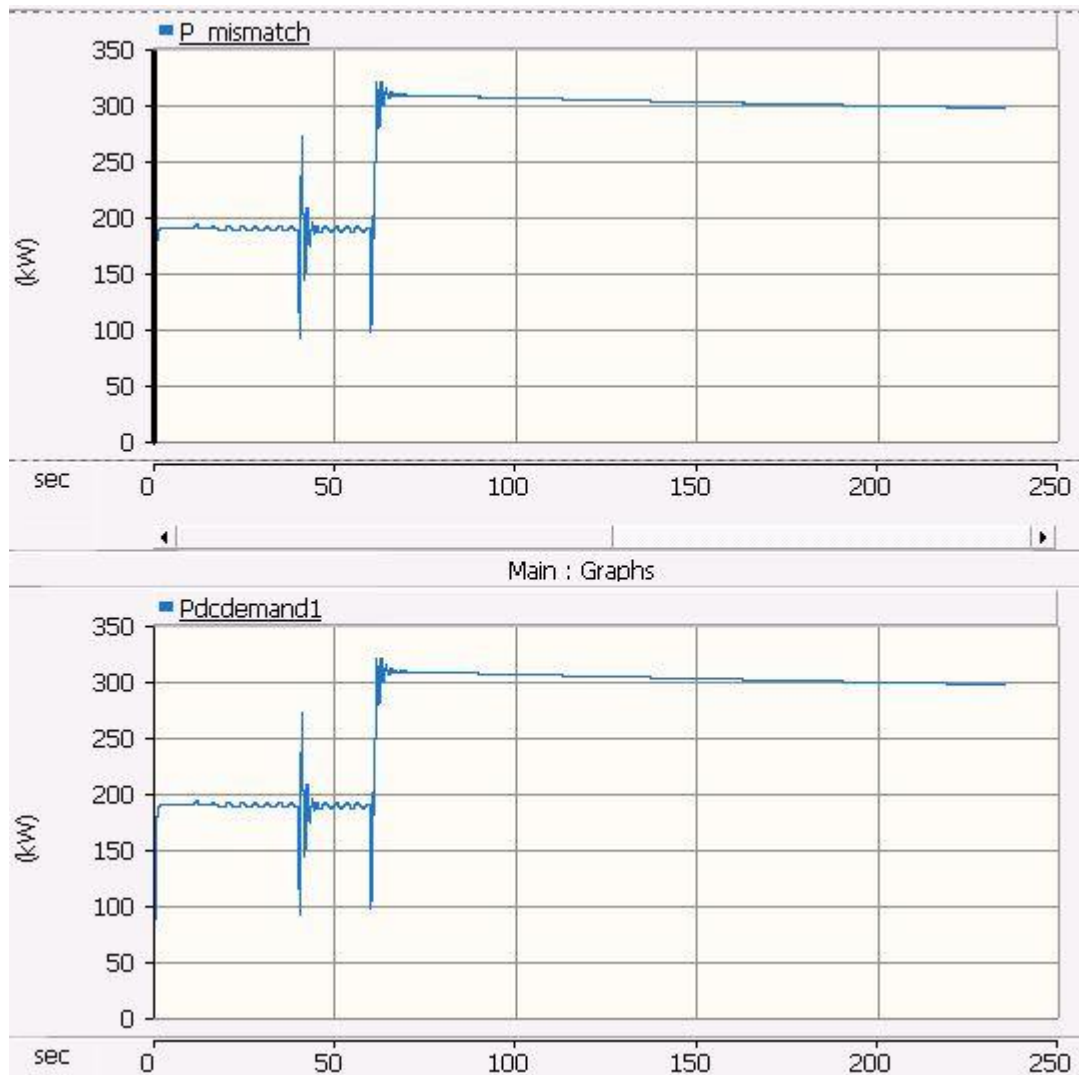


Figure 3.33 DC demand power for the standalone HESS and mismatch for slow varying load conditions

The DC demand power and mismatch in Figure 3.33 will be the same since the HESS is being operated in standalone mode ( $P_{pv} = 0$ ;  $P_{dcdemand} = P_{mismatch}$ ).

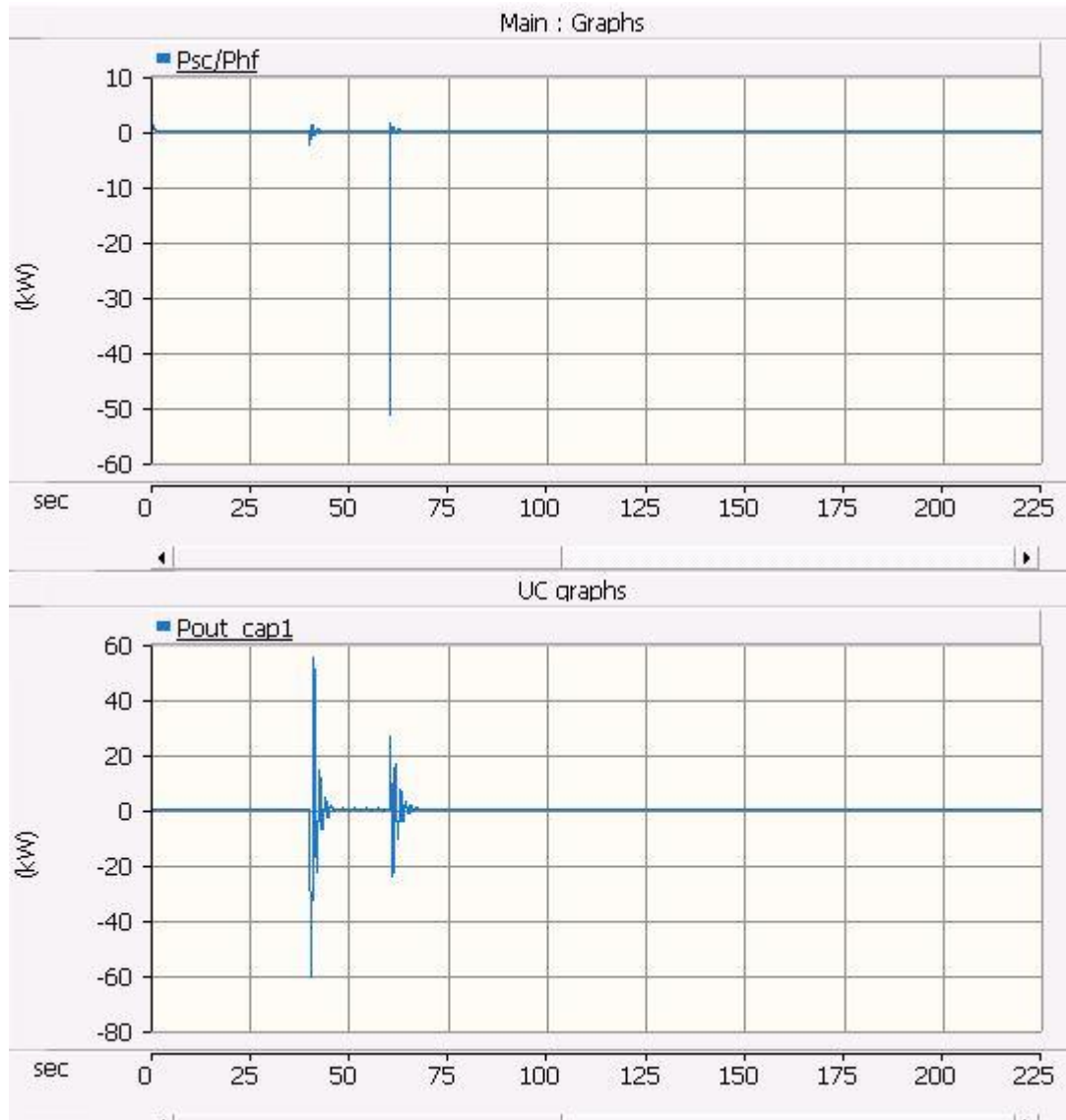


Figure 3.34 Power output of UC system compared to its reference Phf for slow varying load conditions

In Figure 3.34, since this simulation was done for a slow varying load the Ultra capacitor contribution is negligible towards the total  $P_{\text{HESS}}$ . It should be noted that the UC cannot charge when the power reference is negative because we haven't implemented bidirectional operation of the system yet.

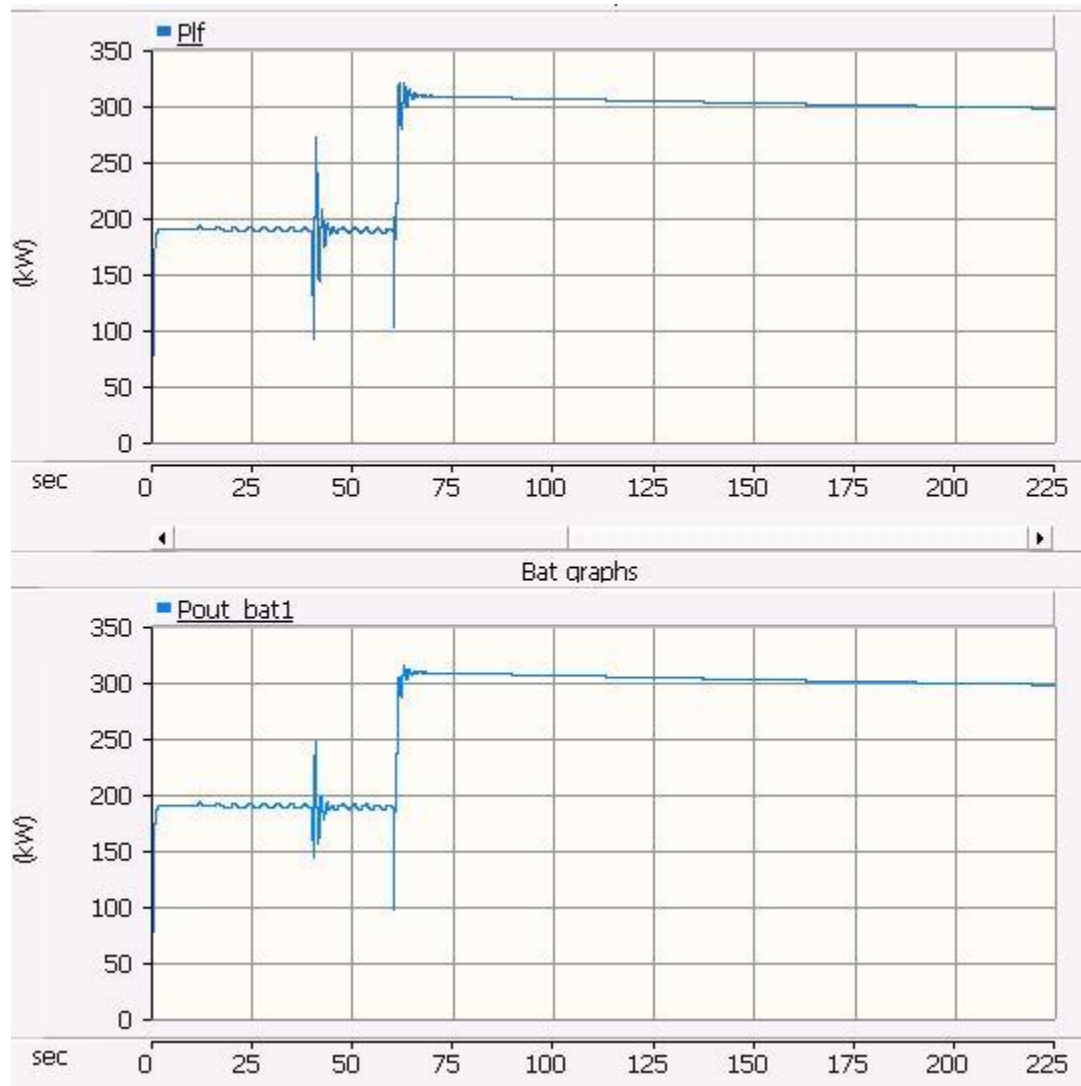


Figure 3.35 Output power of the battery system compared to the referenced PIf for slow varying load conditions

Comparing Figure 3.33 and Figure 3.35 we can understand that most of the demanded power is supplied by the battery system and the ultra-capacitor hardly contributes during the slow varying change.

Now we will perform the same standalone operation of HESS for a fast changing load demand. Figures 3.36 through 3.38 present and validate the fast varying load response of the HESS system.

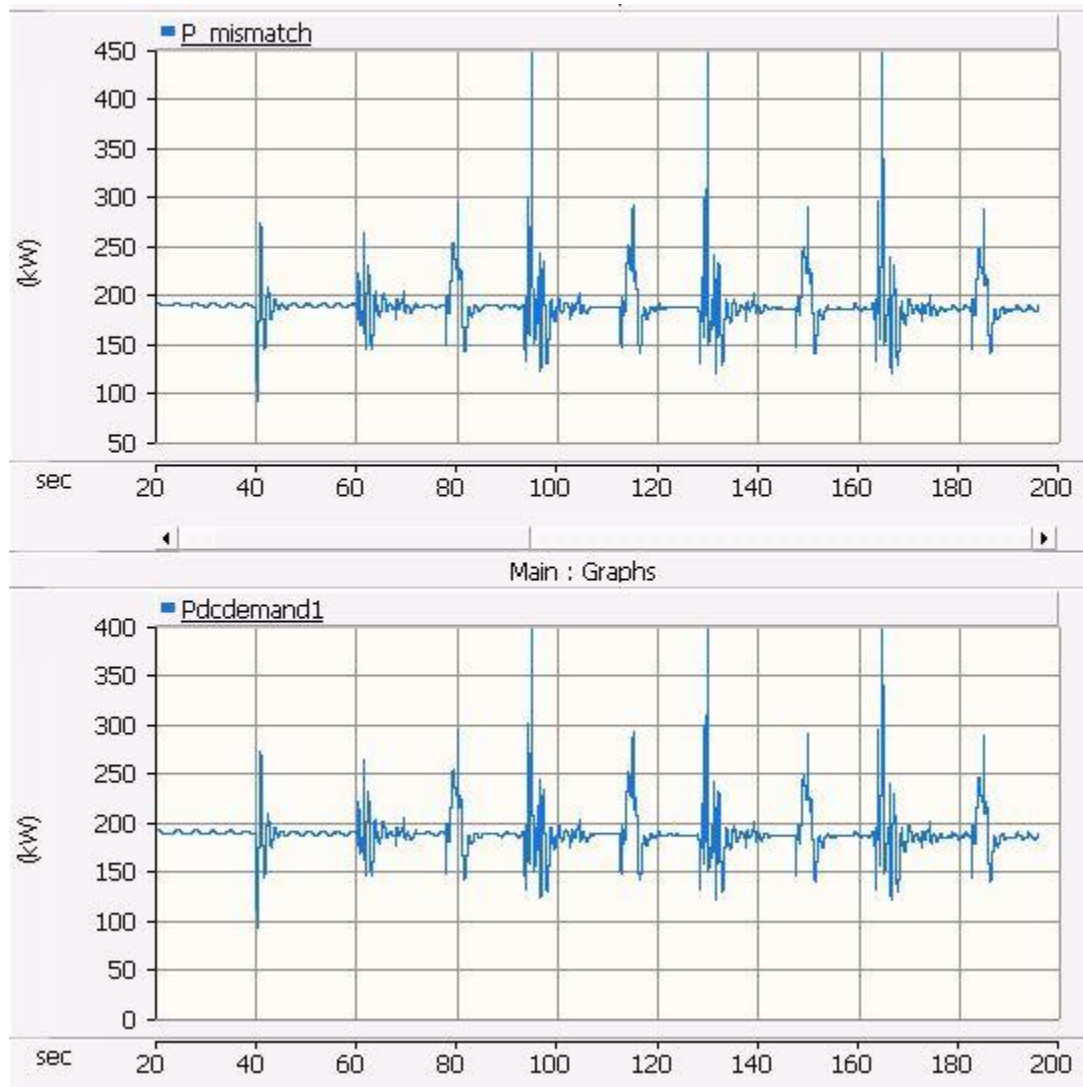


Figure 3.36 DC demand power for the standalone HESS and mismatch for fast varying load conditions

On account of the fast changing load we can see in Figure 3.36 that the  $P_{dc}$  demand and hence the  $P_{mismatch}$  has more spikes as compared that from the slow changing load simulation.

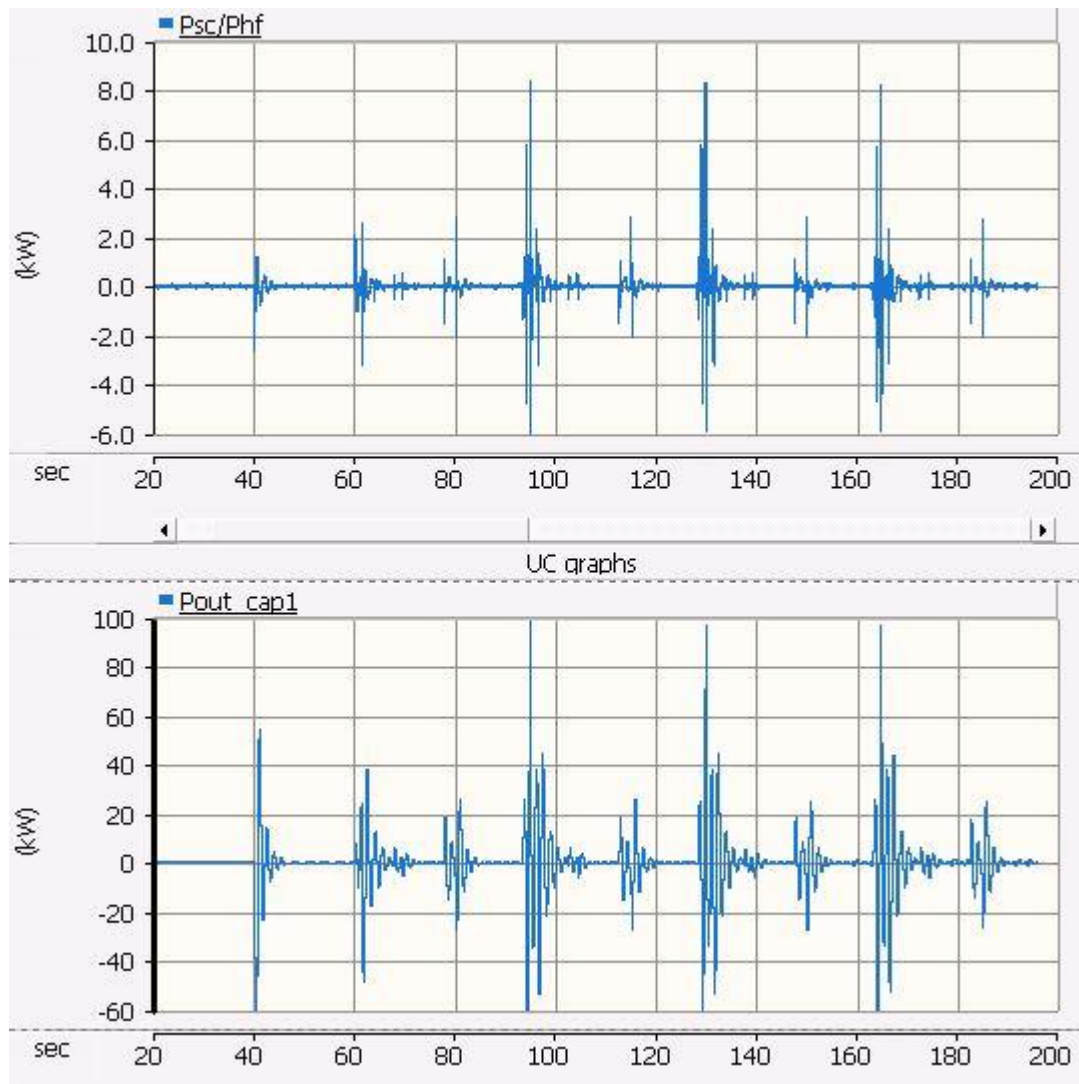


Figure 3.37 Power output of UC system compared to its reference Phf for fast varying load conditions

From Figure 3.37 we can see that the Ultra capacitor contributes more actively towards total power supplied by the HESS as compared to the slow changing simulation.

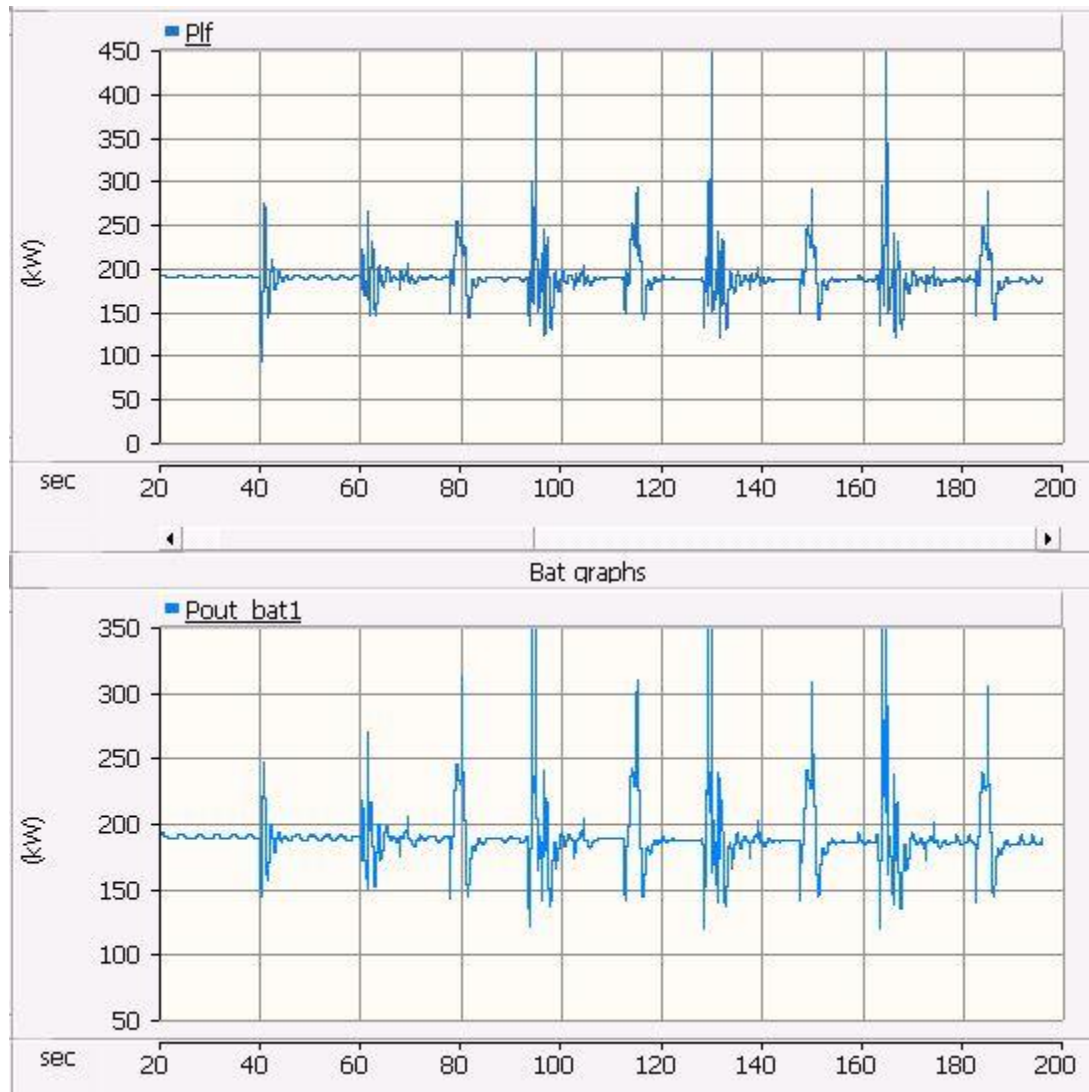


Figure 3.38 Output power of the battery system compared to the referenced P/f for fast varying load condition

In Figure 3.38 the reference tracking output of the battery and the UC system to slow varying and fast varying load validates the cascade controller design for the HESS

## CHAPTER 4: PV FARM AND HESS CONNECTED TO DC LOAD

In the previous chapter we designed and validated the HESS in standalone mode of operation. In this chapter we will integrate the PV farm with the HESS at the DC link. We saw previously that for standalone HESS the voltage at the DC link was not been regulated. This was because we modelled the control architecture that way for the HESS. But the PV farm has a duty cycle control implemented from the boost converter which will be responsible to maintain 1200 V at the DC link when the PV farm is integrated with HESS. This chapter will present the integrated PV-HESS micro system seeing a common DC load. We will also change the PV intermittence according to a standard irradiance chart for a sunny day and a cloudy day along with fast and slow varying changes in the loads to invoke a reaction from the battery and UC system as far as power sharing is concerned. It must be noted that from this chapter onwards we will be employing the bidirectional converters on HESS to simulate for both charging and discharging actions.

The power equations for PV-HESS integrated system can be given as:

$$P_{dc\text{demand}} = P_{pv} + P_{HESS}$$

Where,

$P_{dc\text{demand}}$ : Power demand at the DC link

$P_{pv}$ : Power output from the PV farm

$$P_{\text{HESS}} = P_{\text{bat}} + P_{\text{uc}}$$

$P_{\text{HESS}}$ : Power output from the Hybrid Energy Storage System

$P_{\text{bat}}$ : Power output from the battery

$P_{\text{uc}}$ : Power output from the ultra-capacitor

### 4.1 Slow Varying Load

Figure 4.1 describes the integrated model of PV farm and HESS.

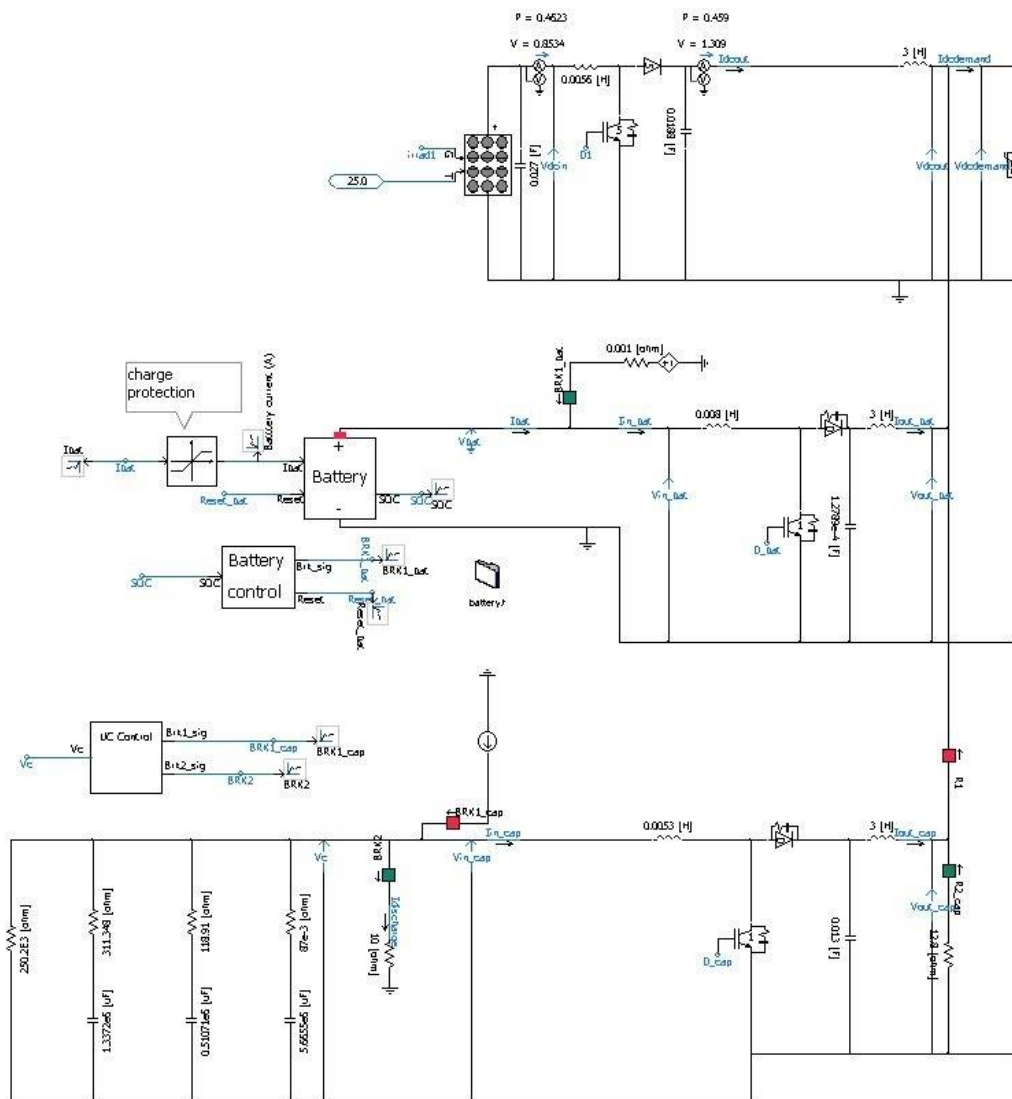


Figure 4.1 PV farm and HESS integrated model

In case of the integrated model the Power mismatch will now be the difference between the DC demand power and the output of the PV power. Thus there will be a slight change in the mismatch generation block where now we will have PV power to be subtracted from the DC demand. The Figure 4.2 explains show this change.

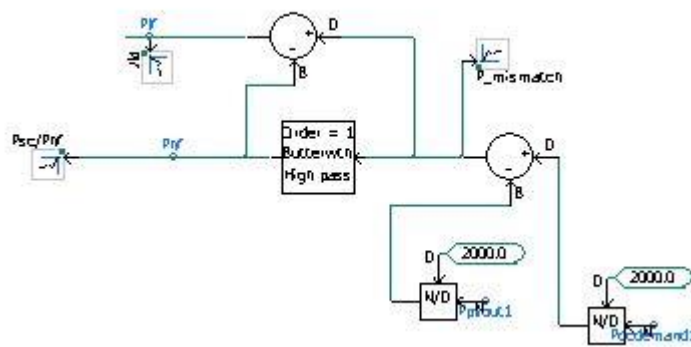


Figure 4.2 Power reference generation from mismatch power

In the first case we are going to use a slow varying load as the DC demand. The PV farm will be subject to standard irradiance curve for a sunny day as shown in the Figure 4.3.

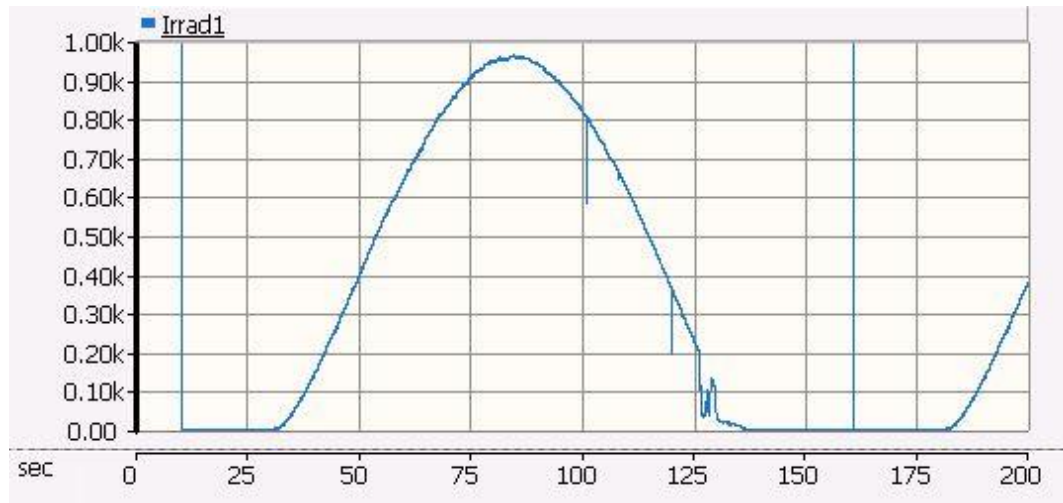


Figure 4.3 Irradiance for a sunny day

The PV output can be seen in Figure 4.4 as a response to changing irradiance. We see that the PV output varies proportionally to the irradiance.



Figure 4.4 PV farm output response to changing irradiance

The DC demand and the mismatch power can be observed as follows in Figure 4.5. We can see that as the irradiance drops the  $P_{mismatch}$  increases which demands more

power output from the HESS. It can also be observed that the  $P_{dc}$  demand remains roughly the same throughout this changing irradiance profile on the PV as the load demand does not look at intermittence in its source and commands all the power it requires.



Figure 4.5 DC demand and Power mismatch graphs

Figures 4.6 through 4.8 validates the load following characteristics of the HESS when subjected to a power reference. The voltage at the DC link is maintained at 1200V which validates the Boost converter operation on the PV farm, which can be observed in Figure 4.6.

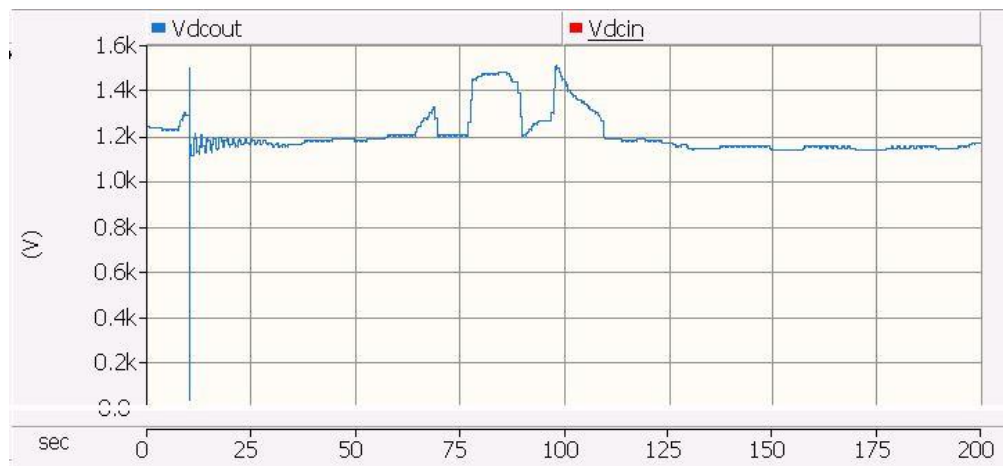


Figure 4.6 DC link voltage maintained at 1200V

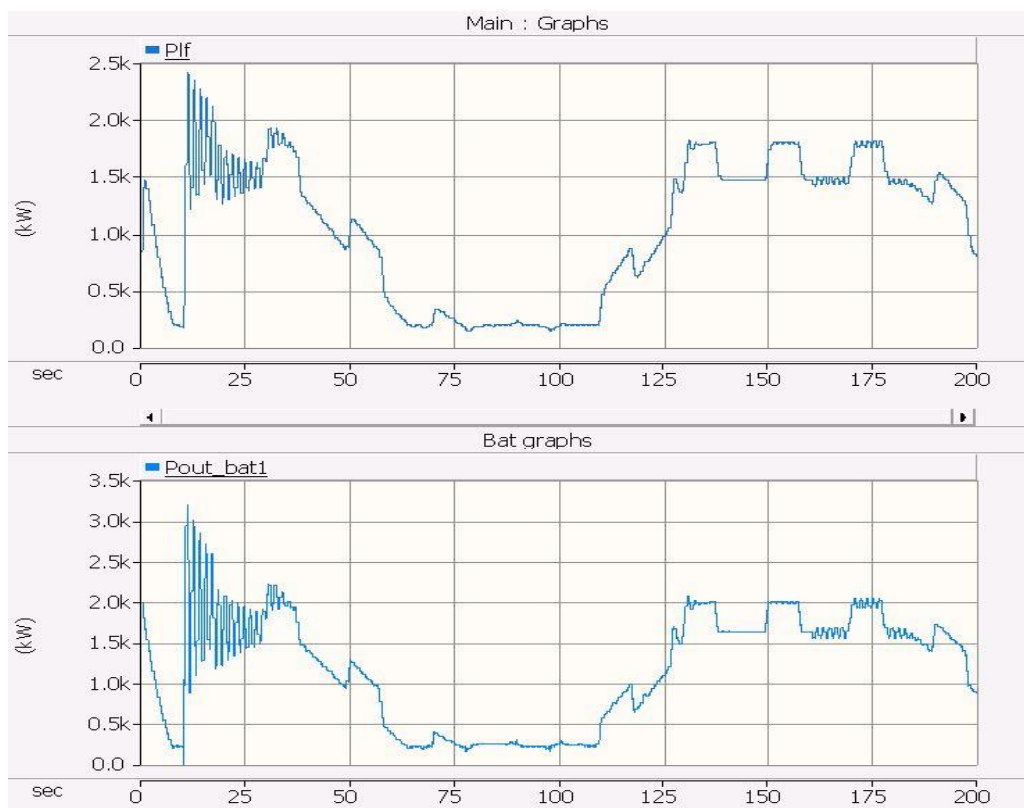


Figure 4.7 Battery power reference and battery output graphs

The low frequency and high frequency power reference is set looking at the Pmismatch which in turn is dependent on how much the PV farm can supply given the changing irradiance. Thus Figure 4.7 shows the battery reference power and the battery output response to the reference power. The reference following power graph of the battery validates the desired cascade control operation on the battery.

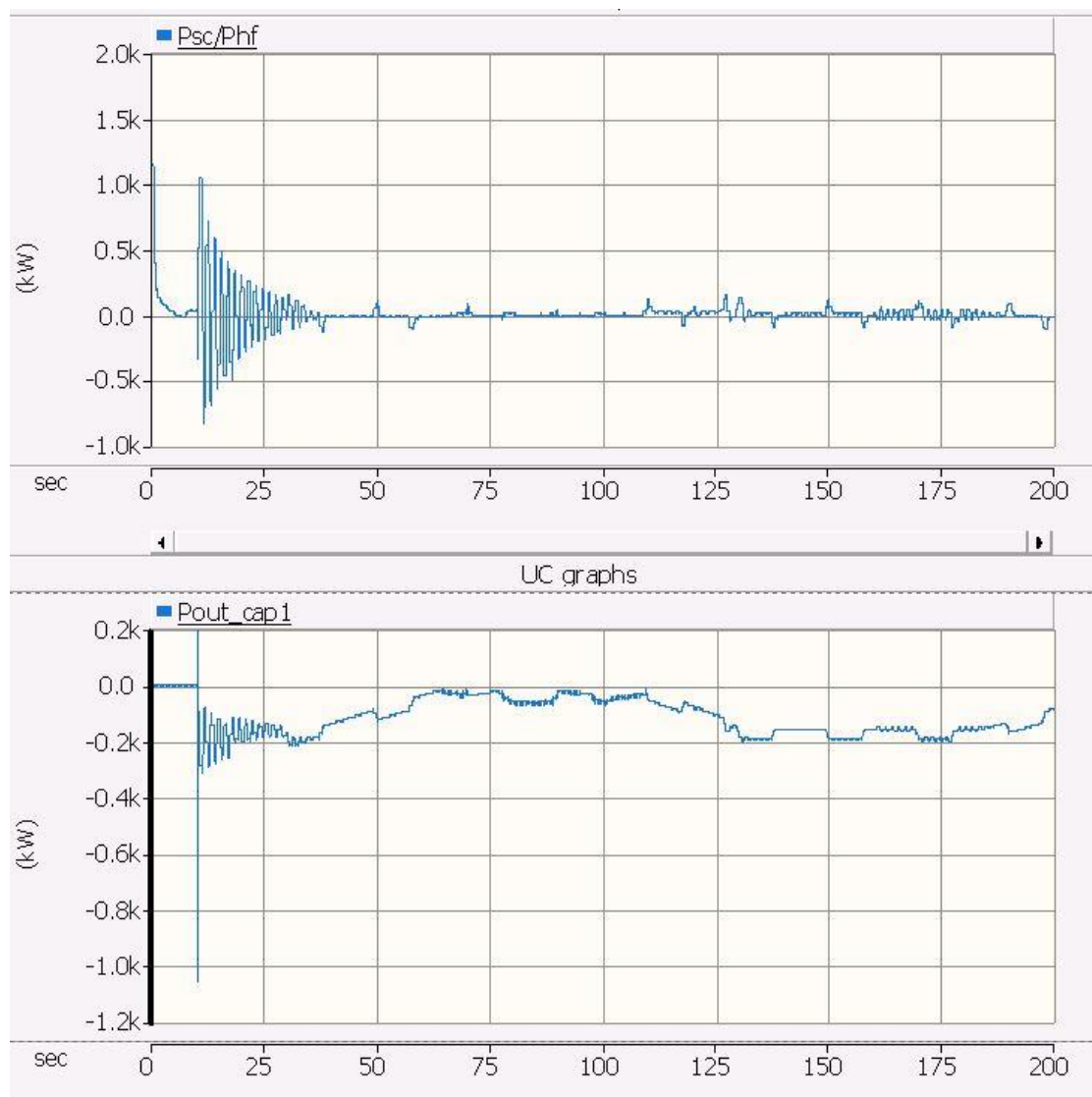


Figure 4.8 UC power reference and UC output graphs

Similar to Figure 4.7, the above Figure 4.8 validates the cascade control structure on the Ultra-capacitor system. In this case the Phf is negative for slow varying load which drives the DC-DC converter on the ultra-capacitor into bucking mode (charging). Thus we can see the charging of the ultra-capacitor in the above figure.

#### 4.2 Fast Varying Load

For the next case, we will give a fast changing load at the DC demand.

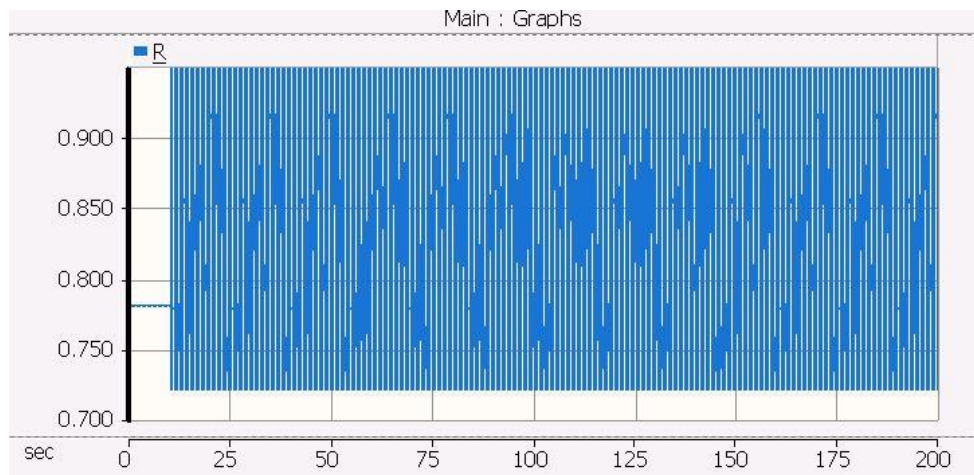


Figure 4.9 Fast changing load

Graphs 4.10 through 4.14 validates the PV integration with the HESS for a sunny day condition with a fast changing load demand. It can be seen that during the fast changing load simulation the ultra-capacitor plays an active part of power support during fast load switching transient durations.

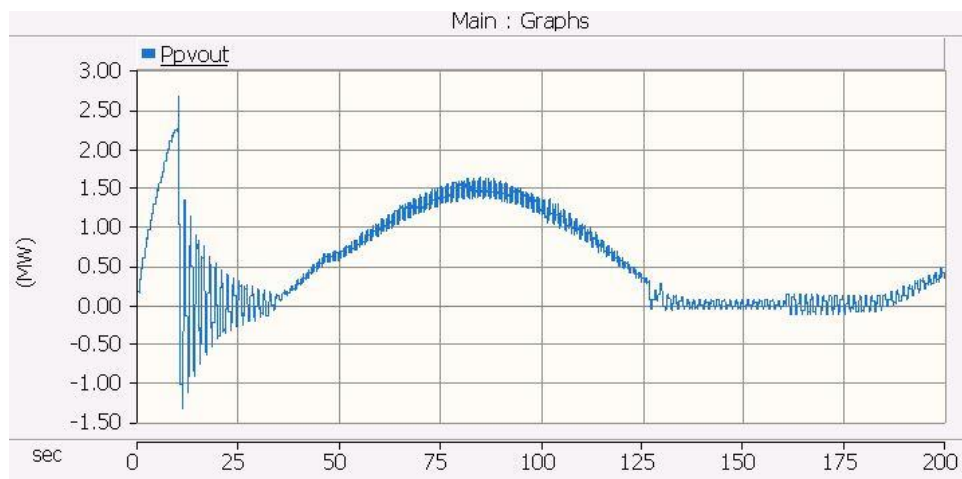


Figure 4.10 PV farm output for fast changing load

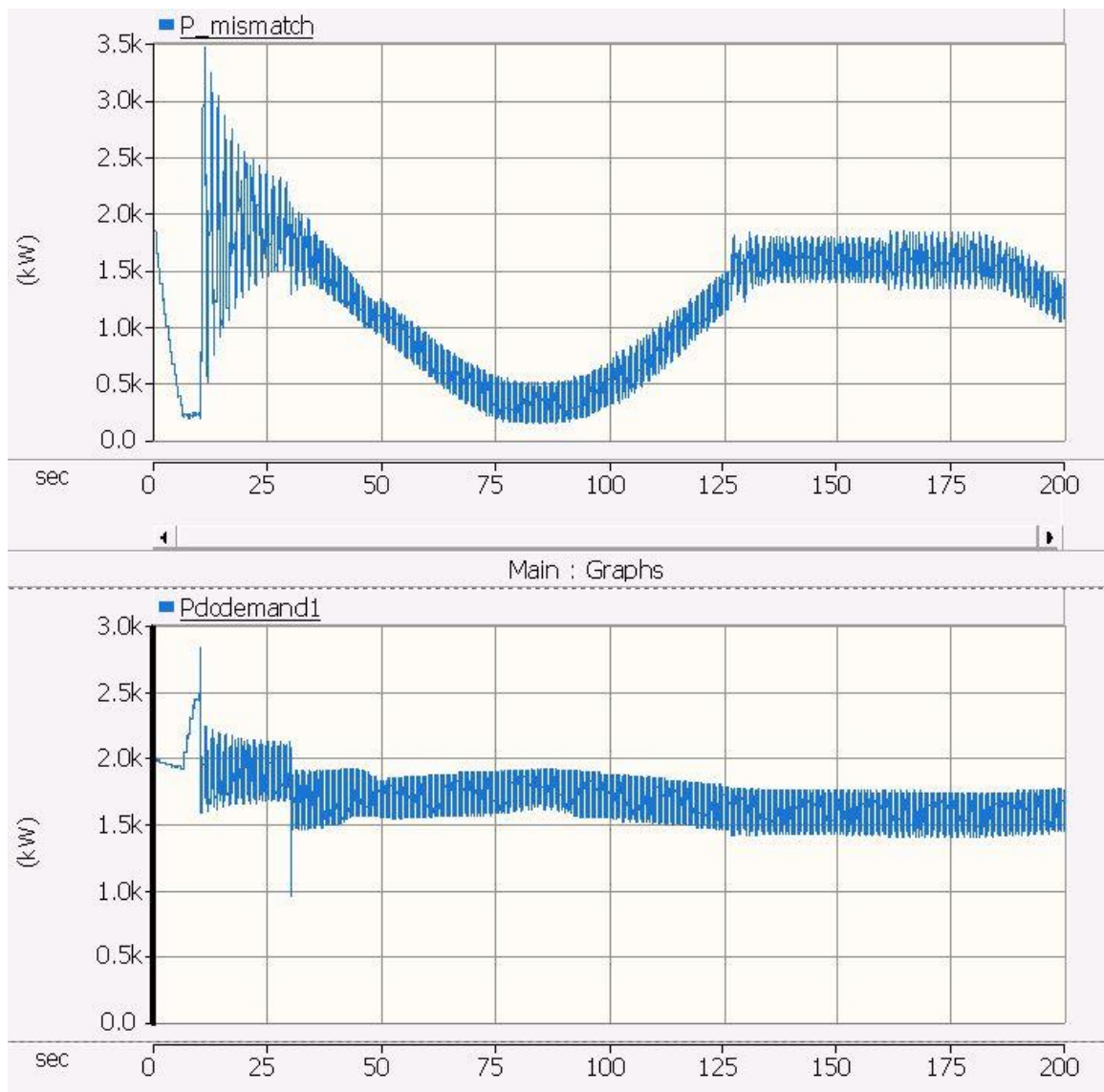


Figure 4.11 DC demand and PV mismatch for fast changing load

In Figure 4.11 we can see that for fast changing load simulation there are a lot of spikes (distortions) in the DC load demand and hence in  $P_{pv}$  and  $P_{mismatch}$ .

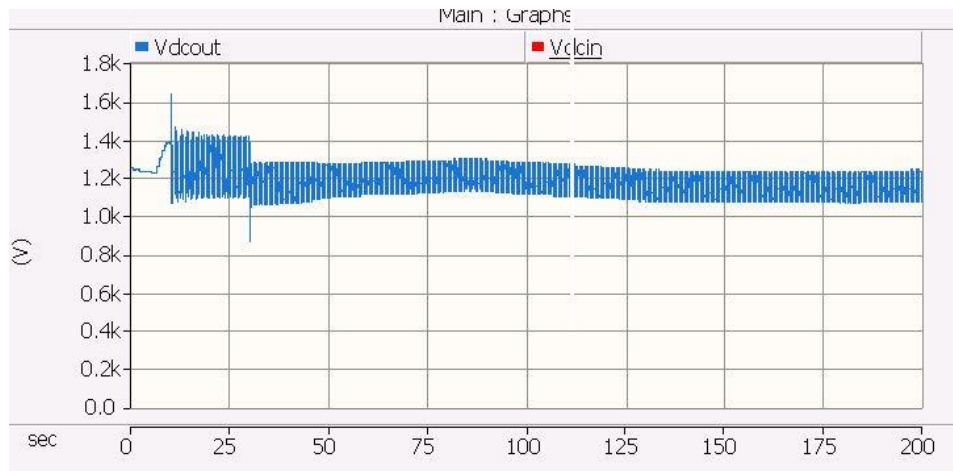


Figure 4.12 DC link voltage regulation for fast changing load

On comparing the above graph with the DC link voltage graphs from the previous chapter where we were running the HESS in standalone system we could see that we did not have regulation on the DC link voltage at around 1200 V. We now have that for the integrated system.

Despite the continuously changing load Figure 4.12 shows that the DC link voltage is still been maintained at 1200 V. This serves as a graph of validation for the DC-DC boost converter working on duty cycle control for the PV system.

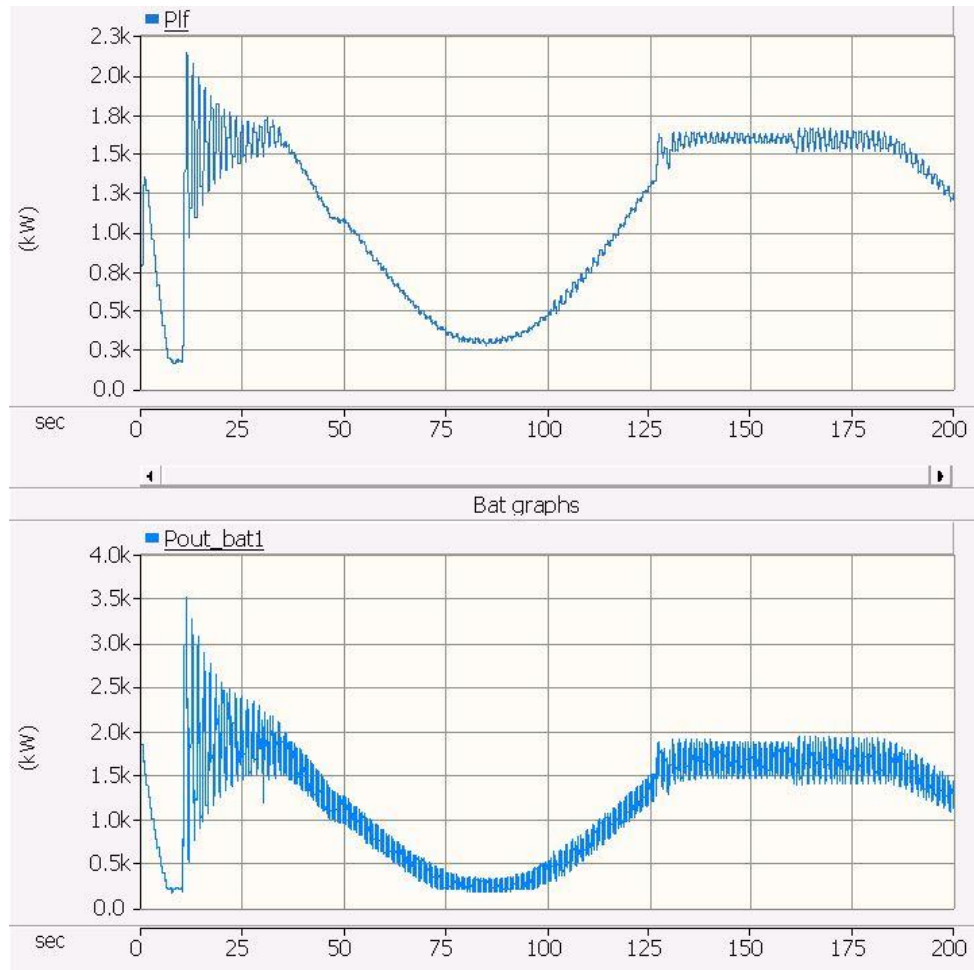


Figure 4.13 Battery reference and battery output for fast changing load

Figure 4.13 shows the battery reference and the corresponding response of the battery system to the fast changing load. We can see now that even the battery reference contains the spikes (distortions) which is the effect of the fast changing load simulation. The battery would still supply the majority of the power (1.6 MW of peak power) when we compare it with the ultra-capacitor response.

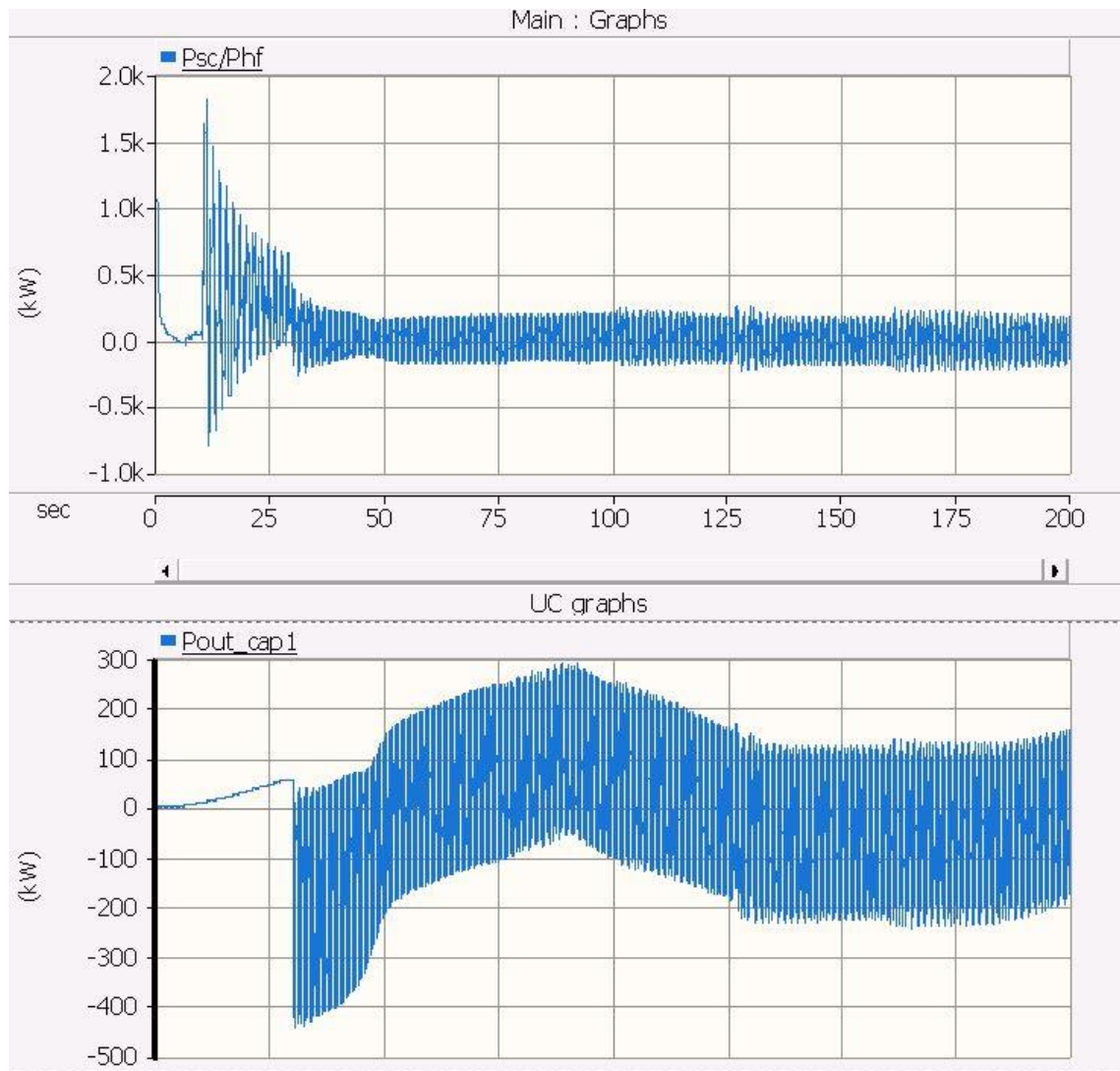


Figure 4.14 UC system reference and UC system output for fast changing load

In Figure 4.14 the ultra-capacitor is seen supplying 200 kW of peak power as compared to its charging operation during slow changing load (seen in Figure 4.8).

It should be noted that the UC system is connected to the DC link after 30 seconds of simulation time since that is the amount of time required for the UC voltage to build to 1200V.

## CHAPTER 5: PV SYSTEM AND 3 PHASE D-Q COUPLED INVERTER

In this chapter the inverter topology used in this thesis is discussed. A grid-side inverter effectively decouples the PV farm from the grid. This blocks the electrical faults occurring on the transmission line from the DC-side PV farm, preventing potential damage to the PV arrays. Similarly, the transients arising on the PV output due to intermittence are buffered from directly affecting the power grid on the AC side. This improves the power extraction of PV, allowing it to operate in a wider operating area with reduced risk of damage infliction on either side of the PCC due to interferences.

The ability of the inverter to control the current output at the grid-side both in magnitude and phase angle accomplishes the active and reactive power control of the inverter when operating in current control mode.

Figure 5.1 presents the inverter topology used in the thesis for DC to AC power conversion at the DC link voltage

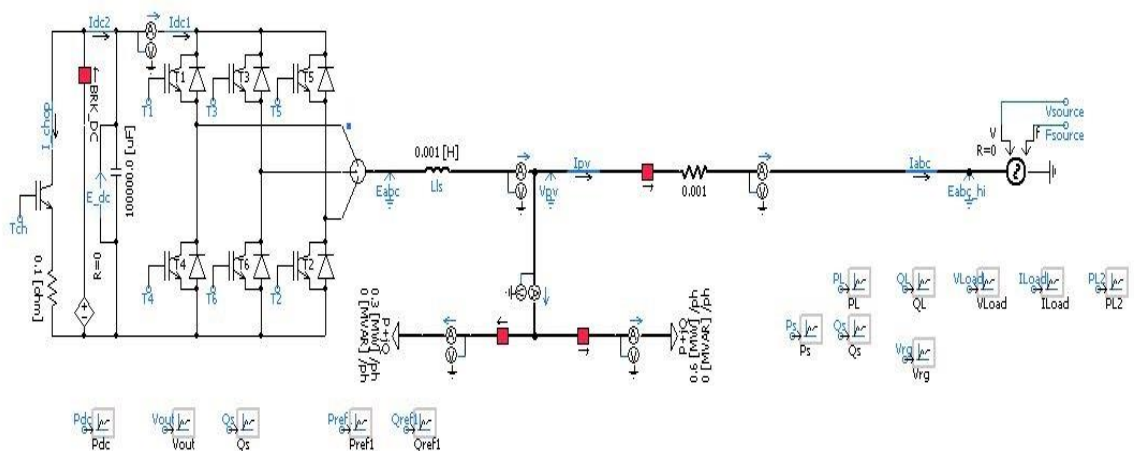


Figure 5.1 De-coupled Inverter topology connected to a constant voltage source

### 5.1 Real and Reactive Power Control on Inverter

The output current from the inverter ( $I_{pv}$ ) can be split into two components (Real and Imaginary). The real component ( $I_{real}$ ) is in phase with the voltage ( $V_s$ ) and imaginary component is in quadrature with  $V_s$ .

We know that,

$$P \text{ (active power)} = 3V_{pv}I_{real};$$

$$Q \text{ (reactive power)} = 3V_{pv}I_{imag};$$

The d-q coupled architecture uses the grid-side voltage  $V_{pv}$  to hold synchronism using the Phase locked loop (PLL) to track the phase angle of the grid voltage. Thus the inverter follows any changes on the grid angle or frequency automatically. In our

simulation the PLL is used to generate the phase angle theta which is used for doing any transformation of parameters from 3 phase to 2 phase, etcetera.

Figure 5.2 shows the implementation of the Phase locked loop in PSCAD.

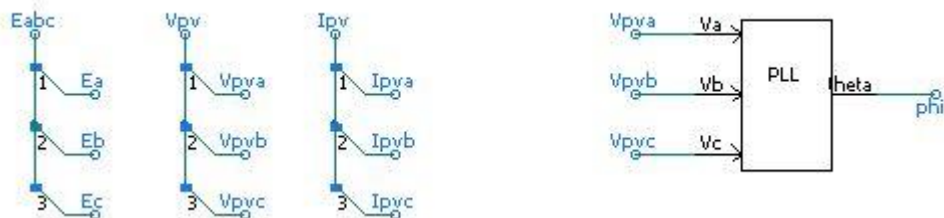


Figure 5.2 Phase Locked Loop in PSCAD.

3 Phase output line voltages and currents are converted into d-q reference frame using Clarke and Park Transformation. This can be seen in Figures 5.3 and 5.4. [49]

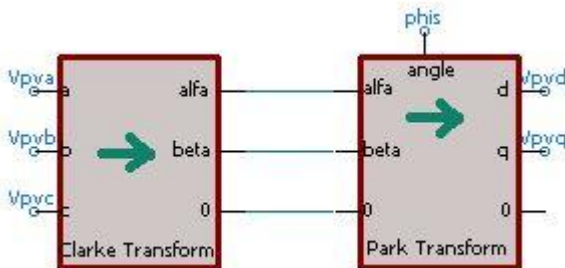


Figure 5.3 Clarke and Park Transform converting 3 Phase Output voltage to d-q reference frame.

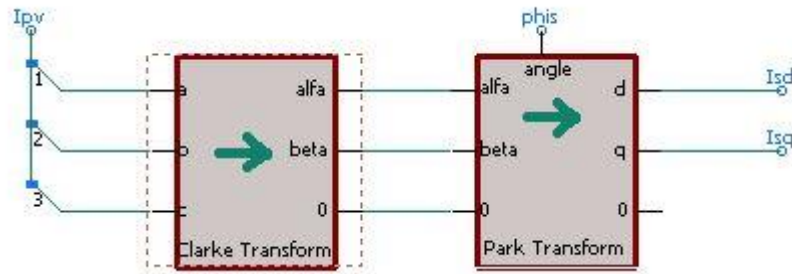


Figure 5.4 Clarke and Park Transform converting 3 Phase Output current to d-q reference frame.

The Mathematical equations converting voltage and currents from 3phase to d-q reference frame are as follows:

Clarke Transform changes 3phase abc to 3phase  $\alpha\beta 0$  frame.

$$\begin{bmatrix} V_\alpha \\ V_\beta \\ V_0 \end{bmatrix} = \frac{2}{3} \begin{bmatrix} 1 & -0.5 & -0.5 \\ 0 & 0.866 & -0.866 \\ 0.5 & 0.5 & 0.5 \end{bmatrix}$$

The Park Transform converts the  $\alpha\beta 0$  quantities to its corresponding dq0 values.

Thus the d-q reference frame transformation concludes.

$$\begin{bmatrix} V_d \\ V_q \\ V_0 \end{bmatrix} = \begin{bmatrix} \cos\theta & \sin\theta & 0 \\ -\sin\theta & \cos\theta & 0 \\ 0 & 0 & 1 \end{bmatrix} \begin{bmatrix} V_\alpha \\ V_\beta \\ V_0 \end{bmatrix}$$

The  $V_0$  component is called as the zero sequence component and it does not exist in normal operating condition. This component appears (gets a non-zero value) during fault conditions.

The Voltage components  $V_{pvd}$  and  $V_{pvq}$  are maximum and zero respectively since the synchronous frame is aligned to phase A of the 3 phase voltage  $V_{pv}$ . This may not be the other case if voltage is considered at another other node in the grid if there is a significant phase angle difference from the  $V_{pv}$ .

The real and reactive power can be written as:

$$P = \frac{3}{2} (V_q I_q + V_d I_d)$$

$$Q = \frac{3}{2} (V_q I_d - V_d I_q)$$

Thus  $I_{dref}$  and  $I_{qref}$  can be written as:

$$I_{dref} = \frac{\frac{2}{3} P_{ref} - V_q I_q}{V_d}$$

$$I_{qref} = \frac{V_q I_d - \frac{2}{3} Q_{ref}}{V_d}$$

Figure 5.5 and 5.6 present the generation of the  $I_{pcmd}$  and  $I_{qcmd}$  command signals using control loops each for P and Q reference at the Inverter output.

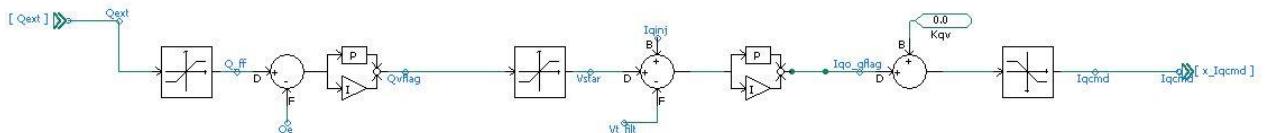


Figure 5.5  $I_{qcmd}$  Command generation from  $Q_{ref}$  (reference reactive power for Inverter)

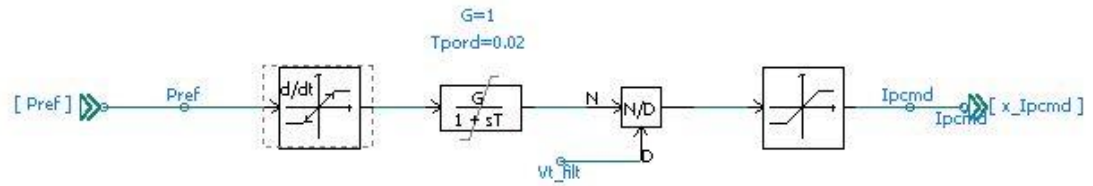


Figure 5.6 Ipcmd Command generation from Pref (reference active power for Inverter)

In our case the reference bus used is  $V_{pv}$  from Figure 5.1. Thus the impedance between the terminal voltage and  $V_{pv}$  must be included for calculating voltage drop. Including the voltage drop across  $X_{ls}$  from Figure 5.1 we get the following equation:

$$V_t = V_{pv} + jX_{ls}I_s$$

In control structure it can be written as:

$$U_{tq} - jU_{td} = (U_{sq} - jU_{sd}) + jX_s(I_{sq} - jI_{sd})$$

$$U_{tq} = U_{sq} + X_s I_{sd}$$

$$U_{td} = U_{sd} - X_s I_{sq}$$

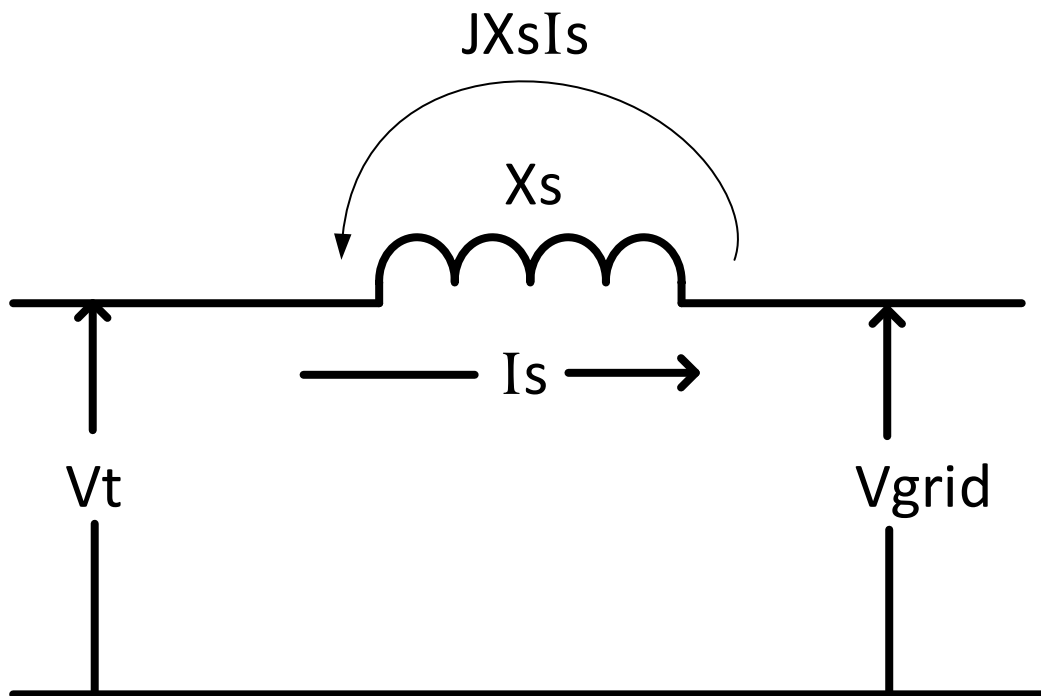


Figure 5.7 Voltage drop compensation for a remote bus as reference

The control structure realization in PSCAD simulation can be seen in Figure 5.8

below:

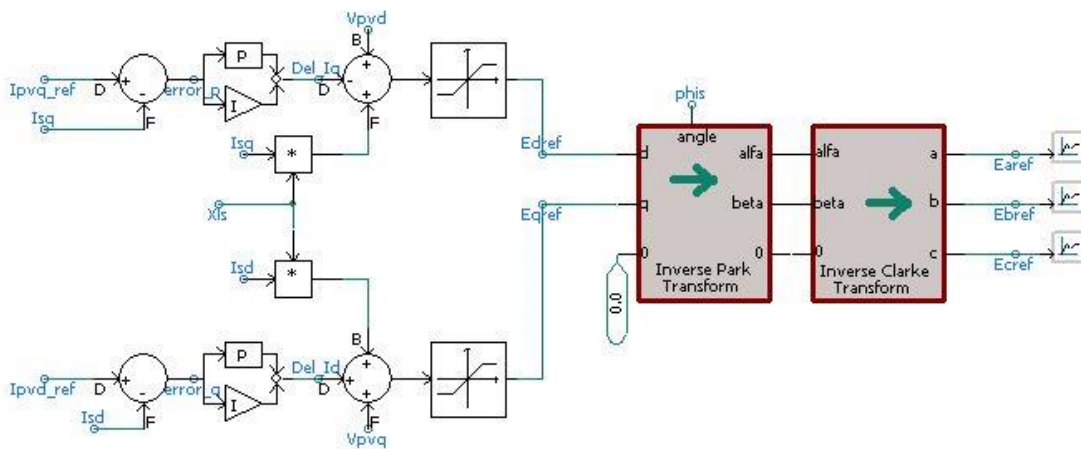


Figure 5.8 Control structure calculating the terminal voltage in dq0 reference

The control equations consists of  $I_{sd} \cdot X_L$  and  $I_{sq} \cdot X_L$  which are known as de-coupling terms in d-q based architecture. Voltages calculated from the control structures;  $E_{dref}$  and  $E_{qref}$  are converted back to 3 phase voltages using the Inverse Park and Inverse Clarke transforms. The 3 phase voltages  $E_{aref}$ ,  $E_{bref}$  and  $E_{cref}$  are given to the switching circuitry and are responsible for the inverter operation.

## 5.2 PV Farm and HESS Integration with Inverter in Off-Grid Mode

Figure 5.9 presents the circuit model for system integration with Inverter in PSCAD simulation. As we can see from the Figure inverter is connected to the Grid via a 3phase circuit breaker. We use the 3phase breaker to isolate the AC side Inverter from the grid to test simulation in off-grid mode. We need the grid in the simulation to be able to get the grid angle and keep the Inverter phase locked with the grid using the Phase Locked Loop discussed earlier.

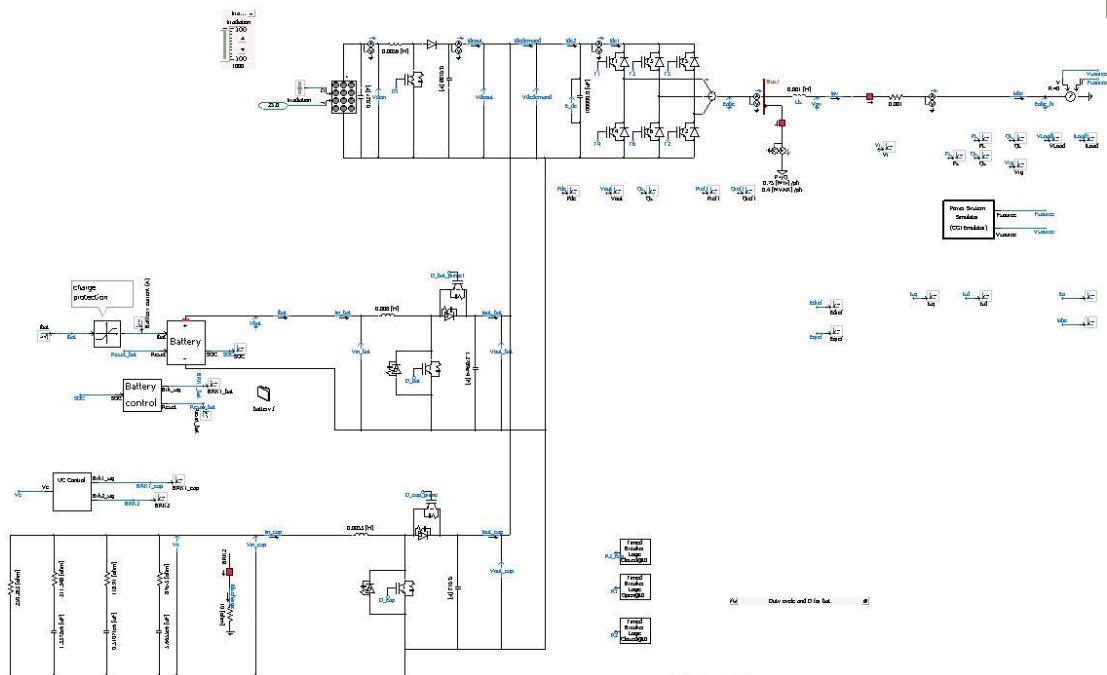


Figure 5.9 PV farm and HESS integration with Inverter in PSCAD for off-grid mode operation

The integrated system was tested with AC side load of 1.6 MW and 1.1 MVAR. Irradiance was reduced from standard condition of  $1000 \text{ W/m}^2$  to  $400 \text{ W/m}^2$  after 39 seconds of simulation time.

Figure 5.10 through 5.21 present the comparison of system parameters before and after change in irradiance.

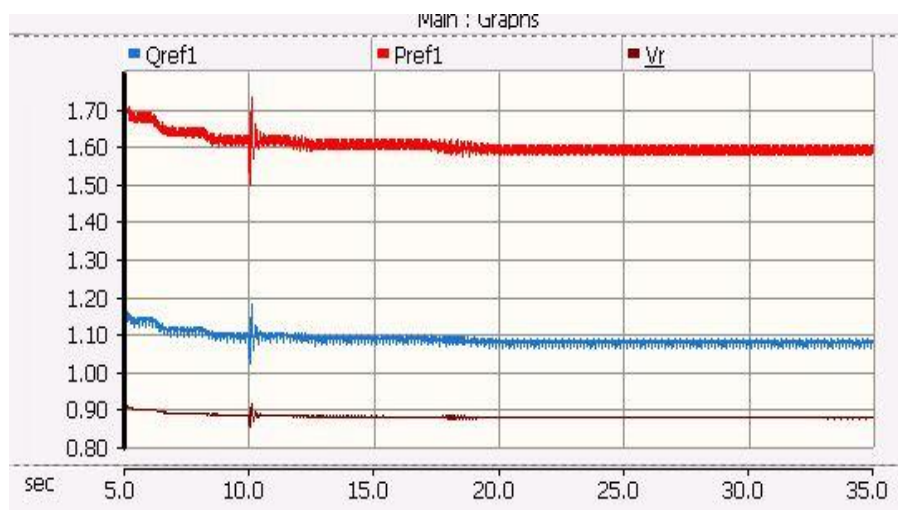


Figure 5.10 Inverter side load graph before irradiance change

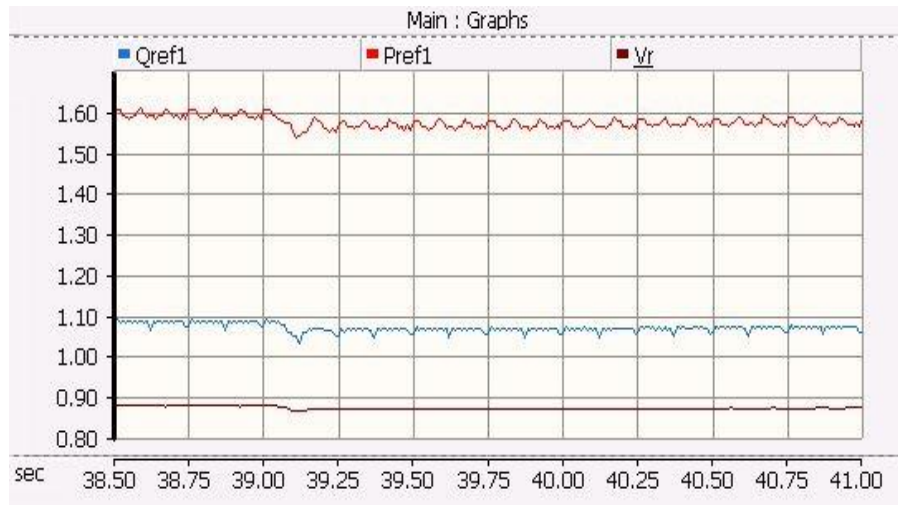


Figure 5.11 Inverter side load graph after irradiance change

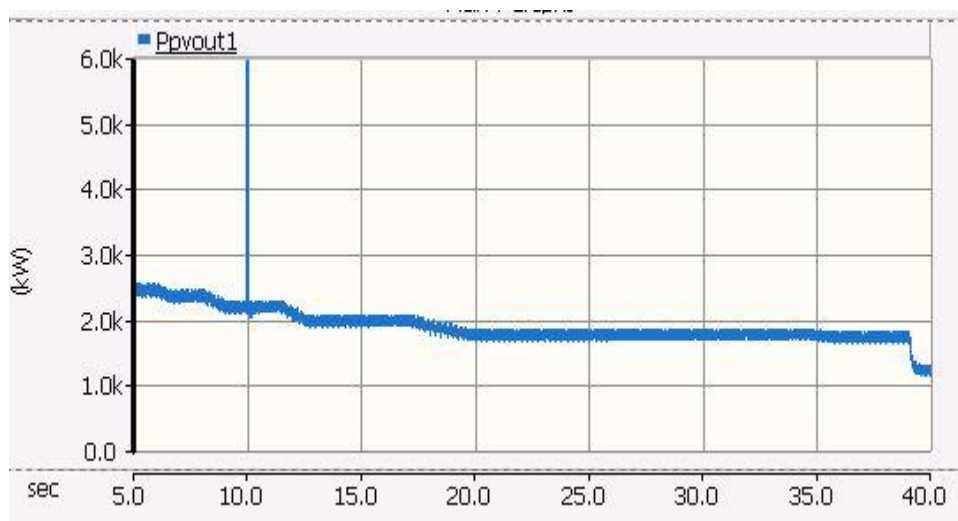


Figure 5.12 PV response before irradiance change

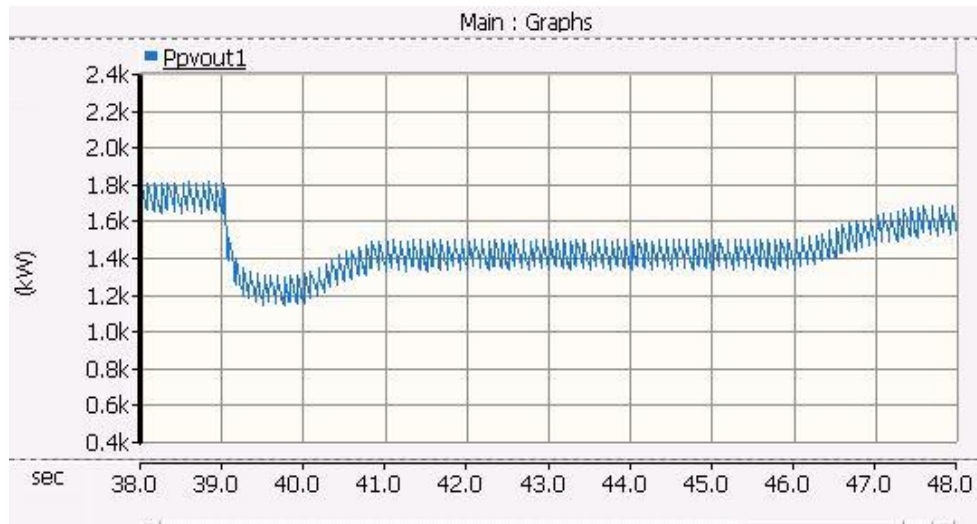


Figure 5.13 PV response after irradiance change

PV response before and after irradiance change can be seen in Figure 5.12 and 5.13. We can see that the PV output drops from 1.8 kW to 1.6 kW after the PV goes back to a steady state post-step change.

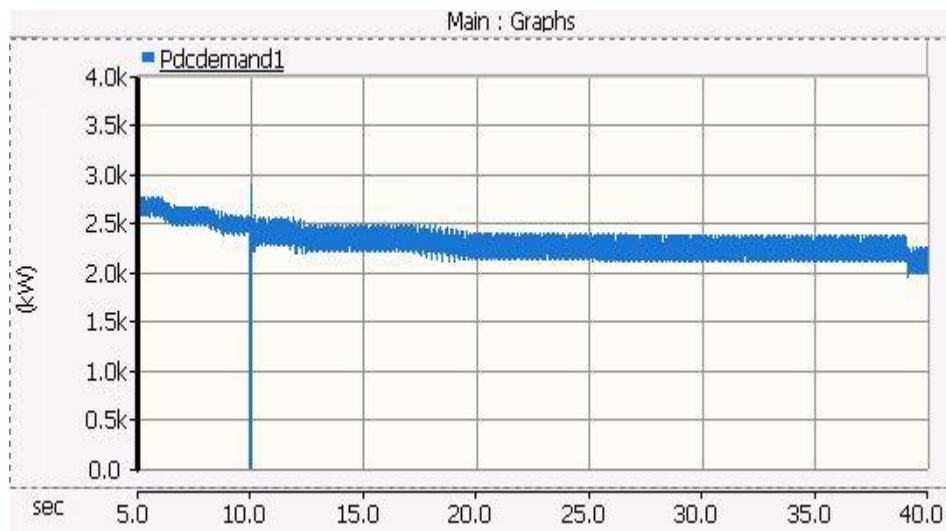


Figure 5.14 DC side demand before irradiance change

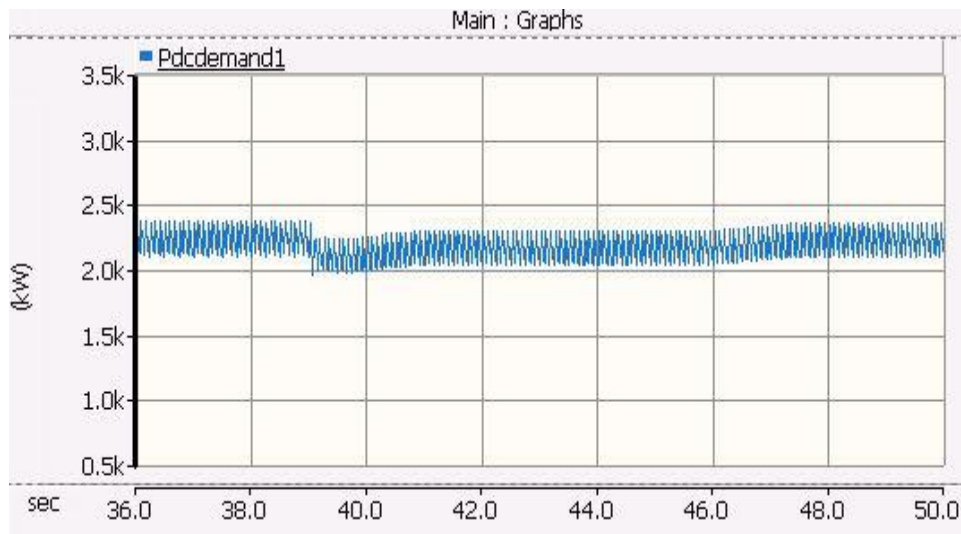


Figure 5.15 DC side demand after irradiance change

Pdcdemand and Pmismatch graphs in Figure 5.14 and 5.15 stay unchanged at 2.2 MW demand (except for the spike due to transient irradiance) because the load on the AC side is constant despite of the change in irradiance.



Figure 5.16 Low frequency power demand before irradiance change



Figure 5.17 Battery response to Low frequency power demand before irradiance change

The Plf and Pbat output is compared in Figures 5.16 and 5.17 for the system condition before the transient. We can see that the battery is supplying a peak power reference of around 550 kW as commanded by Plf.

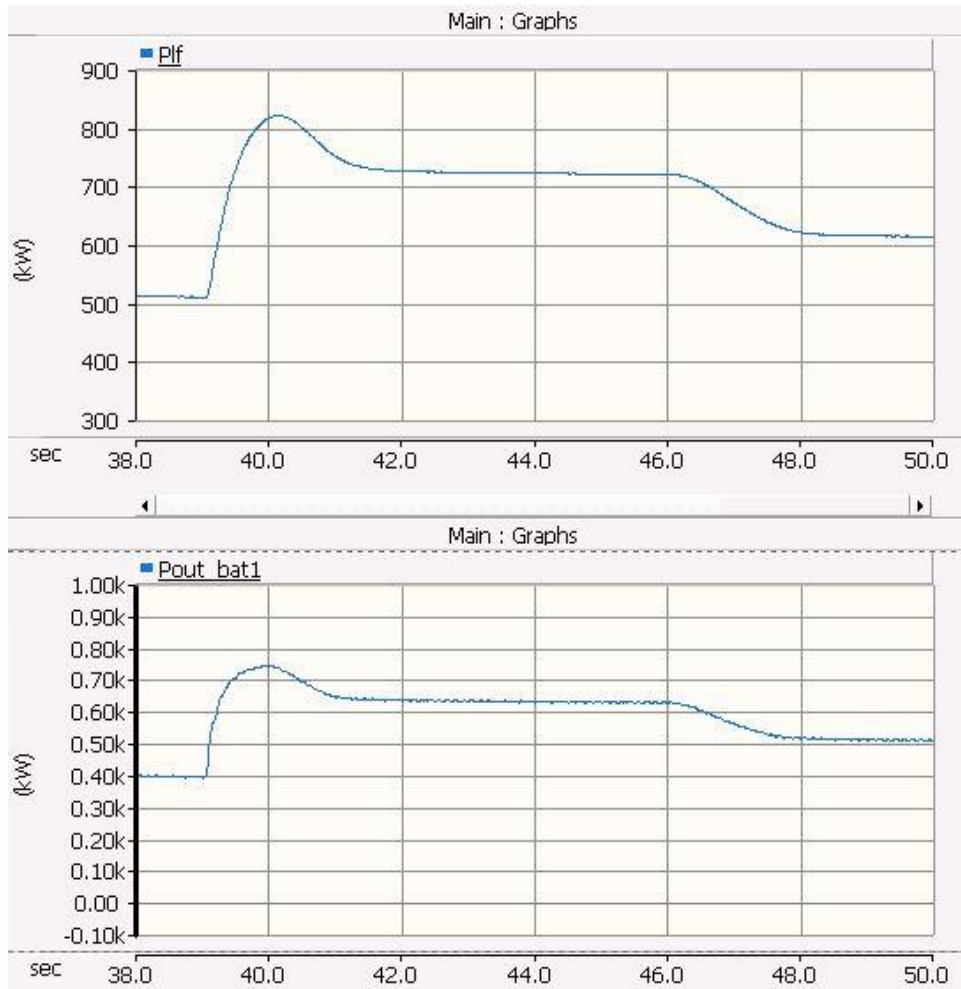


Figure 5.18 Low frequency power demand and the battery response after irradiance change

In Figure 5.18 we can observe that post-irradiance change the peak power demand rises to 750 kW from the 550 kW peak value when PV is supplying without intermittence. This is a result of the step change in irradiance from  $1000\text{ W/m}^2$  to  $400\text{ W/m}^2$ .

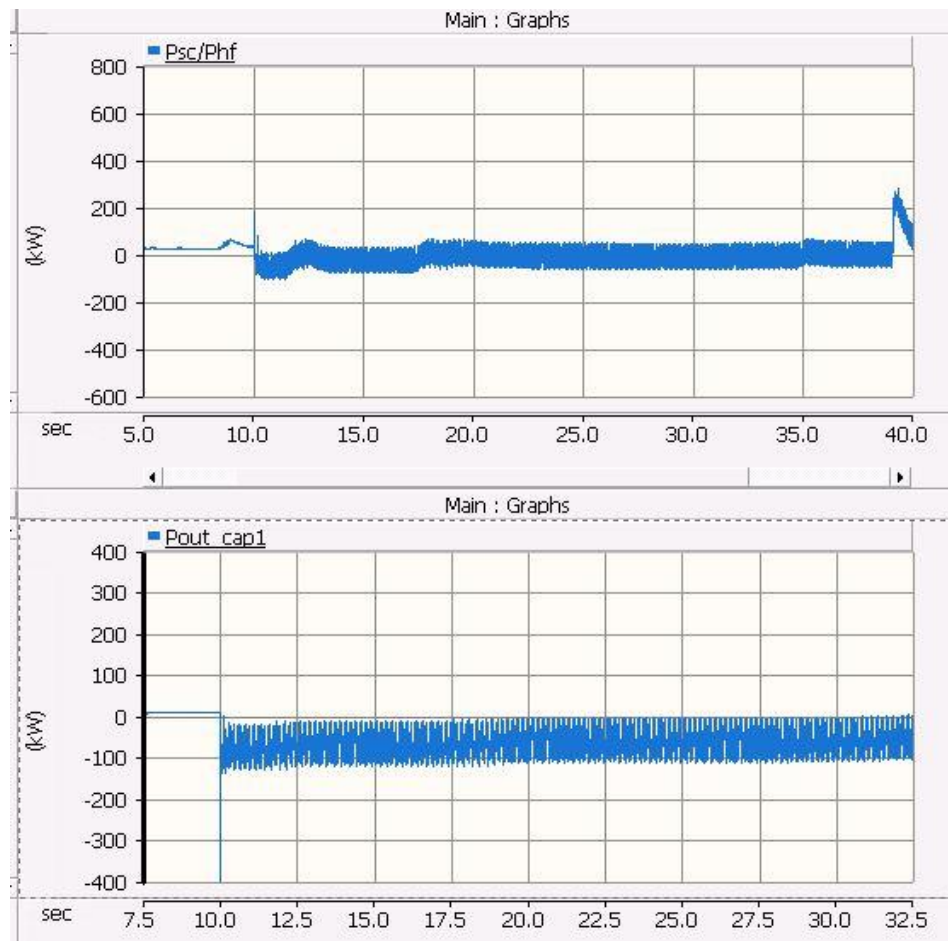


Figure 5.19 High frequency power demand and the UC response before irradiance change

Figure 5.19 presents the UC output before intermittence in PV. The negative power output means that the UC system is charging.

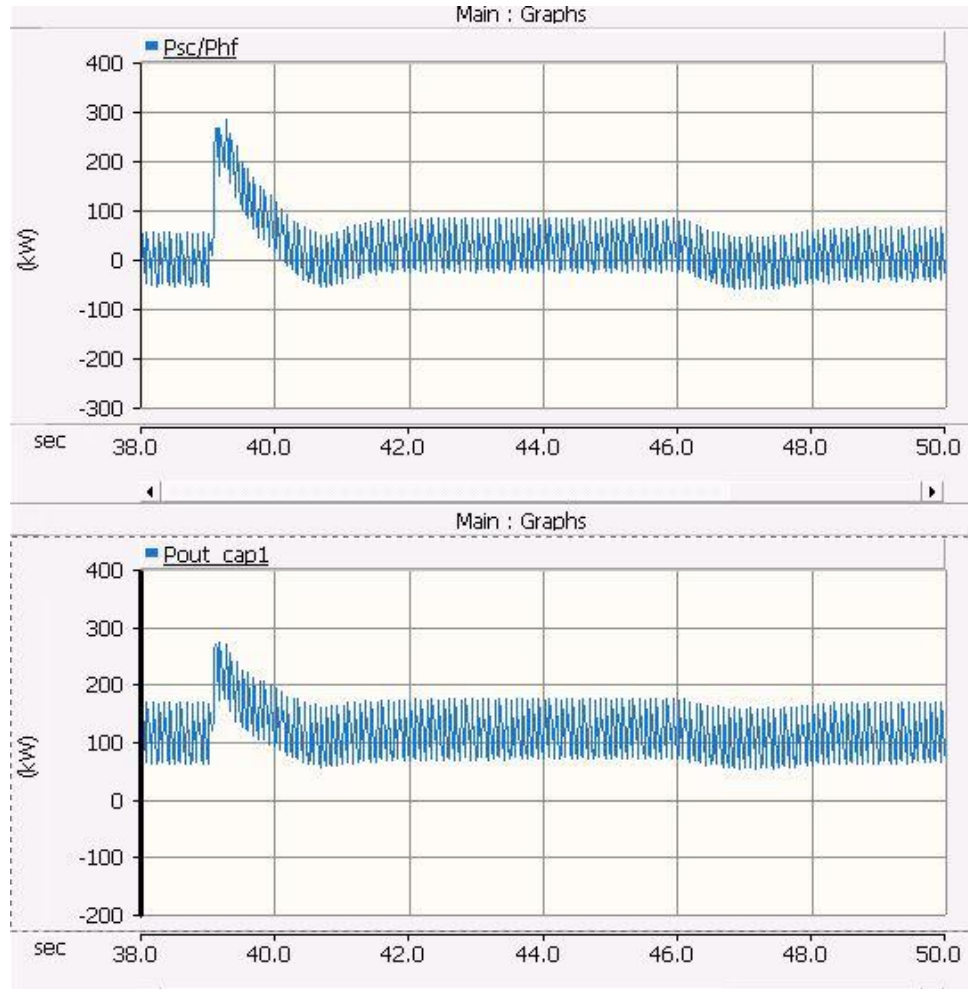


Figure 5.20 High frequency power demand and the UC response after irradiance change

Figure 5.20 shows the UC response to intermittence in PV. We can see that the UC power output is around 150 kW for intermittence condition. This compared to Figure 5.19 proves that the UC only operates in case of intermittence when the PV cannot supply the demanded power.

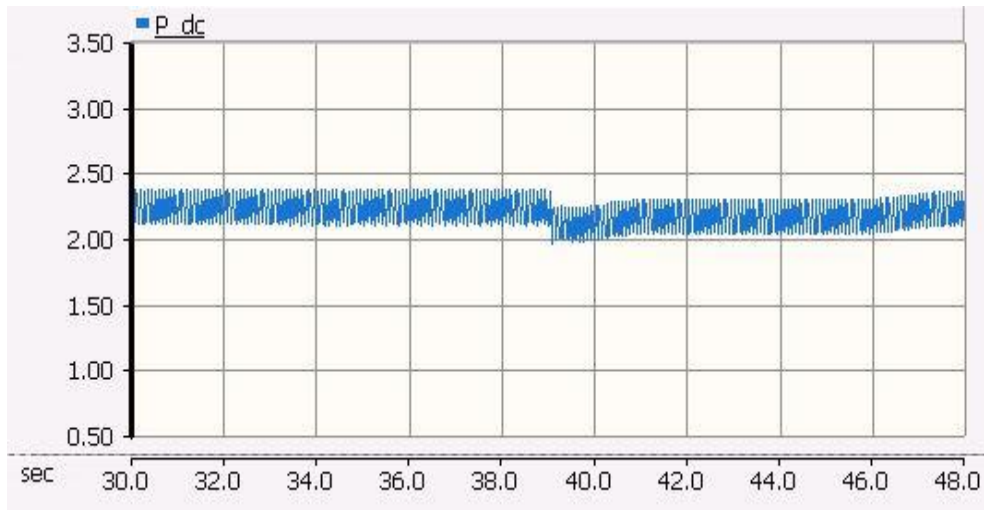


Figure 5.21 DC power transferred to AC side before and after the irradiance change

The above set of graphs validate the PV and HESS connected to the Inverter in off-grid mode of operation. In Figure 5.21 we can observe that the P<sub>dc</sub> demand is constant at 2.2 MW of power it remains the same irrespective of the intermittence since that is the load demand.

In the next chapter we will discuss the hypothesis of supervisory control and prove it using a corresponding simulation.

## CHAPTER 6: SUPERVISORY CONTROL ON PV FARM AND HESS

In this chapter we propose the hypothesis that Active and Reactive power can be commanded in addition to the give AC load, thus making total power equal to 2 MW. This would optimize the PV farm and provide the full capacity of 2 MW as dis-patchable power with the support of HESS. In addition to the mismatch power seen by HESS, the commanded power will also be seen as a reference for HESS.

In an attempt to achieve this we add the Q and S control loops to the existing inverter controls. The Q and S loops can be seen in the figures below.

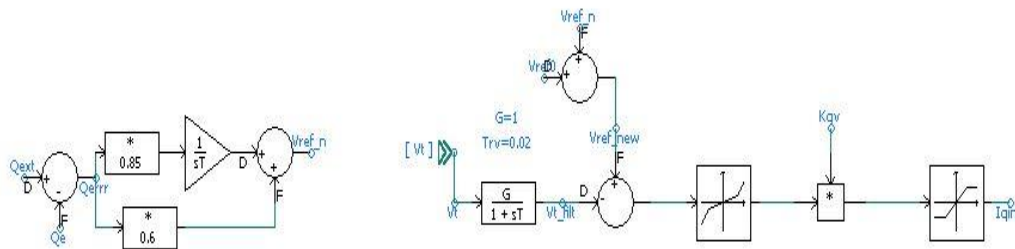


Figure 6.1 Q loop addition to the existing reactive power control on Inverter

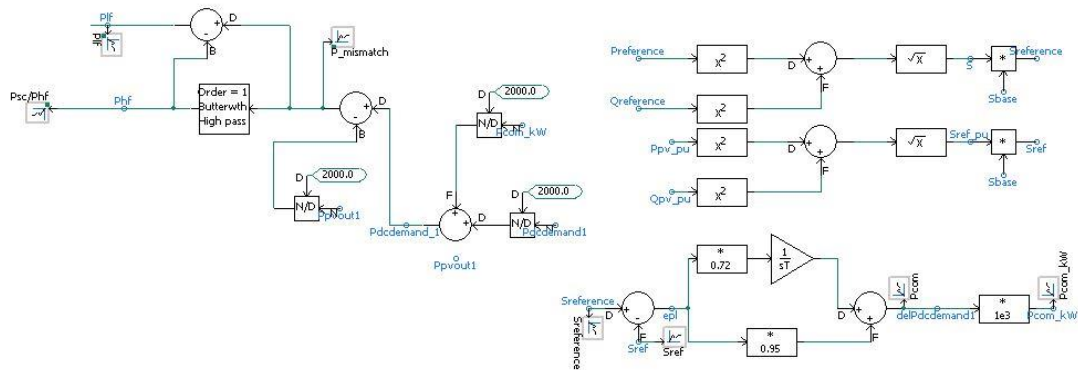


Figure 6.2 S loop addition to the existing control structure on Inverter

The Q loop would compare the commanded Q with actual Q at the inverter output and generate a Voltage reference signal which was previously static and set to a constant 1 p.u. This would take care of the Voltage support on the micro-grid.

Whereas the S loop would compare commanded apparent power and actual power on the AC side of the inverter and generate a DC equivalent of power which would be added to the power mismatch of the HESS. This loop would ensure load following characteristics of the system for total load up to 2 MW

To test this hypothesis PV farm was subjected to irradiance change after 6 seconds and the reduced PV power was taken up by battery.

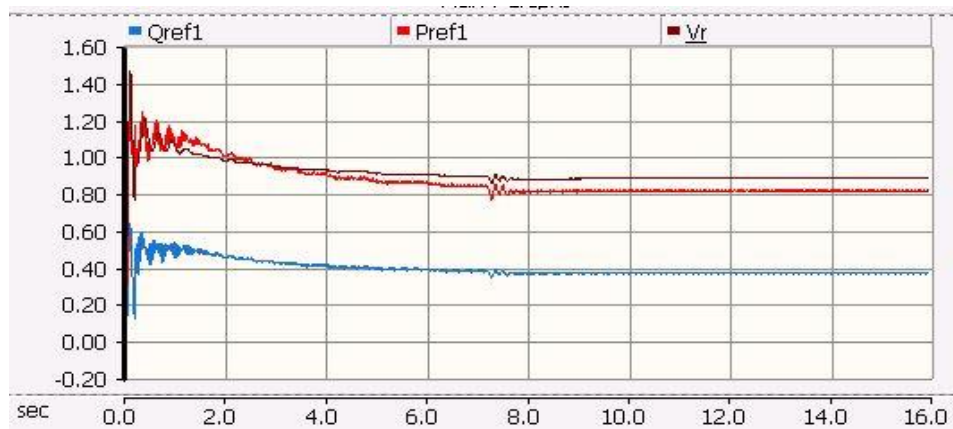


Figure 6.3 Pref1 and Qref1 is the active and reactive power commanded from the inverter

Figures 6.3 shows the AC side active and reactive power commanded from the inverter. The commanded  $P = 0.8$  p.u. which comes to 1.6 MW of active power and  $Q = 0.4$  p.u. which calculates to be 0.8 MW of reactive power.

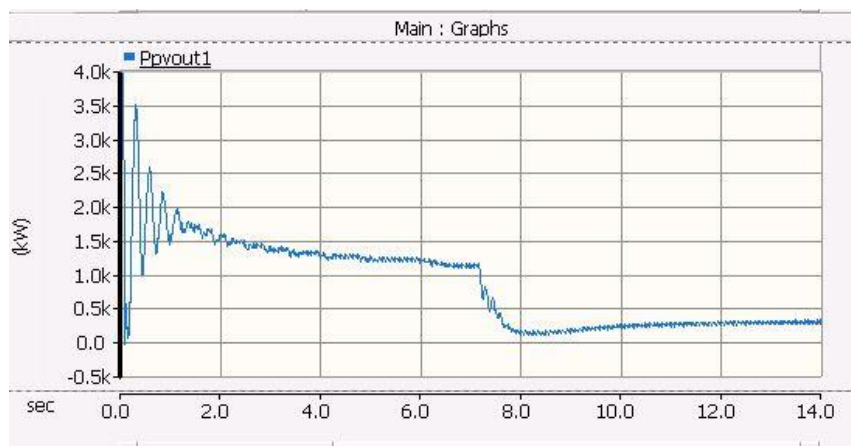


Figure 6.4 PV power before and after irradiance change

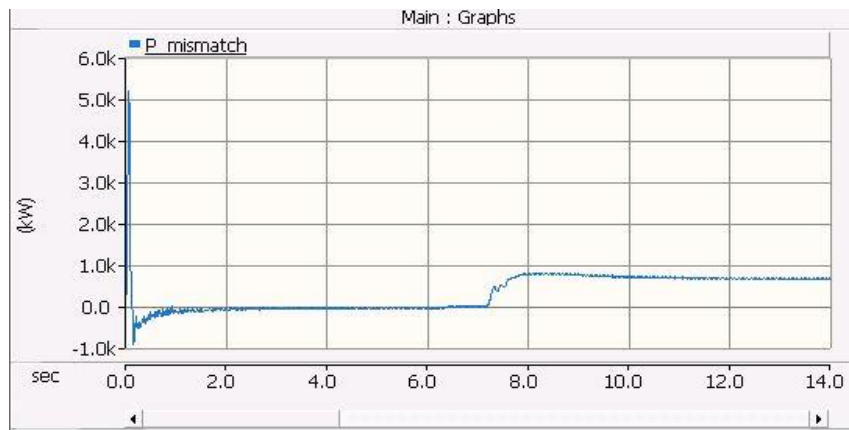


Figure 6.5 Power mismatch before and after irradiance change

To simulate intermittence condition we perturb the PV farm with a step change in the irradiance from to  $1000 \text{ W/m}^2$  to  $250 \text{ W/m}^2$ . The result of this perturbation can be seen in Figure 6.4 where the PV output power  $P_{pvout1}$  drops from  $1.2 \text{ MW}$  of steady state value to  $400 \text{ kW}$  value after the end of transients caused by irradiance change. Similarly figure 6.5 shows the increase in  $P_{mismatch}$  as the PV output drops along with drop in irradiance.

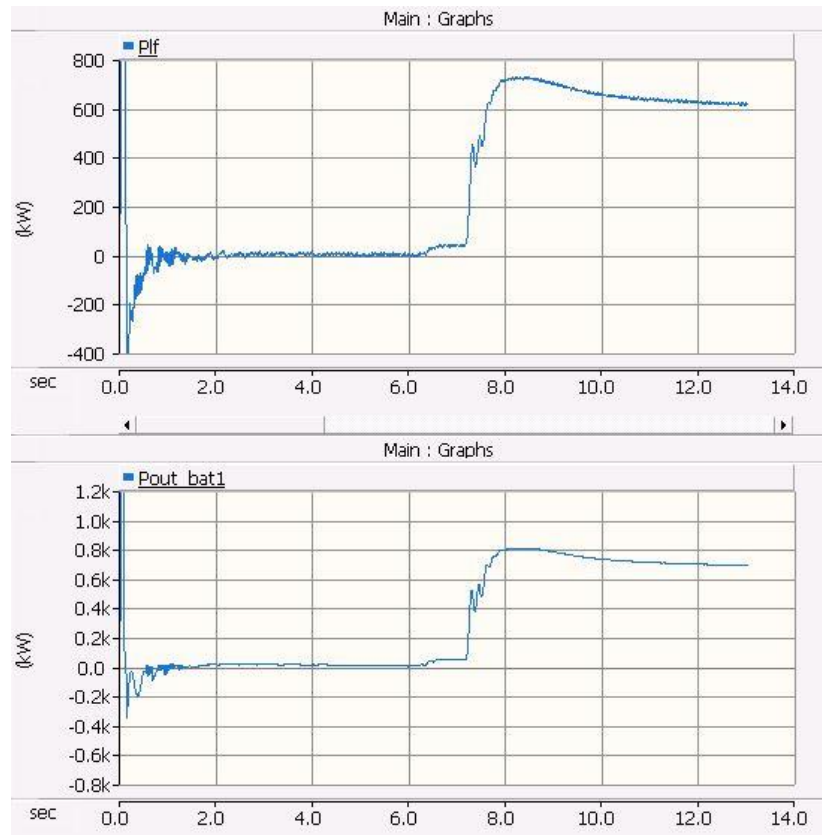


Figure 6.6 Low frequency power demand and Battery response before and after changing irradiance

Based on the Pmismatch graph the Plf (low frequency power reference) is set for the battery system. Figure 6.6 shows the full profile of Plf and Pout\_bat1 (battery output) through the irradiance change occurring at 7 second of simulation time. We can see Plf reference and Pout\_bat1 rise from 0 W to 650 kW of steady state power.

The Phf (high frequency power reference) is not discussed here because we have simulated this condition of PV intermittence with a constant AC power demand. This means that we will not see any high frequency power demand for this particular simulation and hence the UC system output would be 0 W (following its 0 W reference).

The above set of graphs also show that the battery power matches the low frequency power demand which now has the commanded power component added to it. This validates our S loop that we added to the PV system for adjusting the commanded power into the total DC demand at the input of the Inverter.

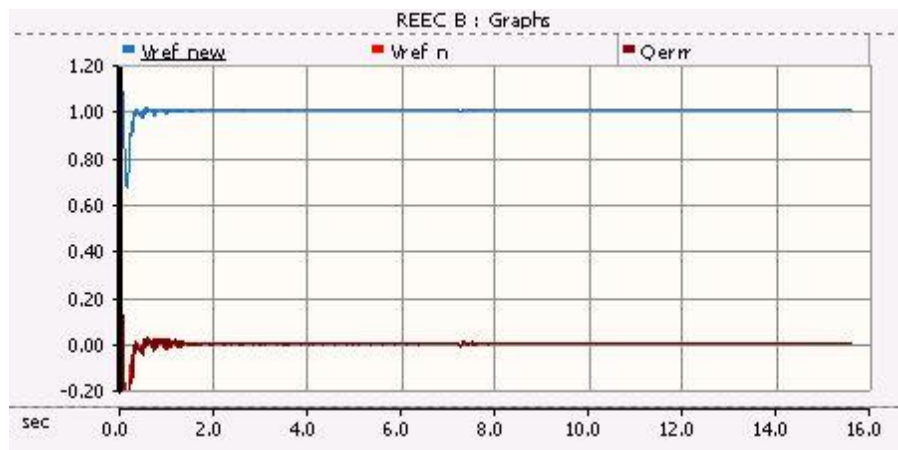


Figure 6.7 Graphs of reference Inverter side voltage and actual voltage and the error in the Q loop (reactive power loop)

Figure 6.7 shows that the actual AC side voltage matches the reference value with the Q loop error showing a zero. This validates our control on the Q loop.

Thus the validation of the S loop and Q loop which are responsible for apparent and reactive power control on the AC side depending on the commanded power proves our hypothesis.

## CHAPTER 7: CONCLUSION AND FUTURE WORKS

Based on the simulation results presented from chapter 2 through chapter 6 the following can be concluded:

- Implementation of cascade control on battery and ultra-capacitor system based on inner loop current control and outer loop power control proves to be an accurate and optimal solution as far as HESS integration is concerned. The load following graphs for various cases such as slow and fast varying load, sunny and cloudy irradiance curve and step changes in both the load and irradiance validates the robustness of the cascade control structure employed on the HESS.
- Battery and ultra-capacitor based HESS is efficient and capable of offsetting the intermittence brought in PV farm by variable irradiance which is tested by simulating for an irradiance curve taken from actual solar irradiance value for sunny and a cloudy day.
- Using HESS with the PV farm in an integrated model explained and validated the advantages of entrusting the battery and ultra-capacitor combination for ancillary services like load following and voltage support considering the possible real life intermittence in the PV.

- Employing a d-q based inverter architecture for the micro-grid bring in optimally controlled active and reactive power loops by the virtue of decoupling offered by the architecture. This architecture improves the ability of scheduling the power dispatch algorithm of the HESS.
- The scheduling of the power dispatch of the HESS is accomplished by supervisory control. This approach uses the DC equivalent reference of the AC power demand seen at the inverter side along with control on the inverter voltage. Both these loops are instrumental in providing an accurate set point for the HESS as well as maintaining the reactive power balance at the inverter. Thus the implementation of this architecture enhances the overall micro-grid efficiency and makes it dispatch-able for loads up to 2 MW.

More improvements can be done on this structure in the future with implementation and validation in on-grid environment with the involvement of complex systems. Controller logic and system topologies can be made more flexible. Adaptive controllers can be implemented on the outer loops to optimize the system performance. Real time analysis of the system with Hardware-In-Loop test bed can give more realistic insight to the system characteristic and response. Power scheduling priority and development of related algorithm can enable detailed testing cases to the same system.

## REFERENCES

- [1] P.L. Robert H Lasseter, Paolo Piagi, “Control and Design of Microgrid Components,” University of Wisconsin-Madison 2006.
- [2] U.S.D.O.E. Dan Ton, “Solar Energy Grid Integration Systems – Energy Storage (SEGIS – ES),” Program Concept Paper May 2008.
- [3] M.J. Erickson and R H Lasseter, “Integration of battery energy storage element in CERTS microgrid”, Energy Conversion Congress and Exposition (ECCE), 2010 IEEE, 2010, pp. . 2570-2577.
- [4] M.J. Erickson, et al.,” Comparison of PV inverter controller configurations for CERTS microgrid”, Energy Conversion Congress and Exposition (ECCE), 2011 IEEE 2011, pp. 659-666.
- [5] G.C. Jin Eyer, “Energy Storage for the Electricity Grid: Benefits and Market Potential Assessment Guide”, Sandia National Laboratories February 2012.
- [6] C. Abbey ana G. Joos, “Short-term energy storage for wind energy applications”, Industry Applications Conference, 2005. Fortieth IAS Annual Meeting Conference Record of the 2005, 2005, pp. 2035-2042 Vol. 3
- [7] H. Fakham, et al., “Power Control Design of a Battery Charger in Hybrid Active PV Generator for Load-Following Applications”, Industrial Electronics, IEEE Transactions on, vol.58, 85-94, 2011.
- [8] Z. Haihua et al, “Composite Energy Storage system Involving Battery and Ultra capacitor with Dynamic Energy Management in Microgrid Applications”, Power Electronics, IEEE Transactions on vol. 26, pp. 923-930, 2011.
- [9] N. Mendis, et al.,”Application of a Hybrid energy storage in a remote area power supply system”, Energy Conference and Exhibition (EnergyCon), 2010 IEEE International, 2010, pp. 576-681.
- [10] L. Wei, et al., “Real-Time simulation of a Wind Turbine Generator Coupled with a Battery Super capacitor Energy storage system”, Industrial Electronics, IEEE Transactions on, vol. 57, pp. 1137-1145, 2010.
- [11] Z. Tao and B. Francois, “Energy Management and Power Control of a Hybrid Active Wind generator for Distributed Power Generation and Grid Integration”, Industrial Electronics, IEEE Transactions on, vol. 58, pp. 95-104, 2011.
- [12] Z. Yu, et al., “Control Strategies for Battery/Super capacitor Hybrid Energy Storage Systems”, in Energy 2030 Conference, 2008, ENEREGY 2008. IEEE, 2008, pp.1-6.

- [13] A. Etxeberria, et al., "Comparison of Sliding Mode and PI Control of a Hybrid Energy Storage System in a Microgrid Application", *Energy Procedia*, vol 12. Pp. 966-973,2011.
- [14] A. Etxeberria, et al., "Comparison of three topologies and controls of a hybrid energy storage system for microgrids", *Energy conversion and management*, vol. 54 pp. 113-121, 2012.
- [15] F.S Garcia et al. , "Control strategy for Battery-Ultra capacitor Hybrid Energy Storage System", in *Applied Power Electronics Conference and Exposition*, 2009
- [16] M.I. Lijun Gao, Roget A. Dougal, Senior Member, IEEE, and Shenygyi Liu, Senior Member, IEEE. (2005, *Power Enhancement of an Actively Controlled Battery/Ultra capacitor Hybrid*. Volume 20 (*IEEE Transactions on Power Electronics*))
- [17] H. Babazadeh, et al., "Sizing of battery and super capacitor in a hybrid energy storage system for wind turbines," in *Transmission and Distribution Conference and Exposition (T&D)*, 2012 IEEE PES, 2012, pp.1-7
- [18] L. Di, et al. "Design of a power management system for an active PV station including various storage technologies", in *Power electronics and Motion control conference*, 2008. *EPE-PEMC 2008*. 13<sup>th</sup>, 2008, pp 2142-2149.
- [19] H. Fakhm, et. al, "Control system and power management for a PV based generation unit including batteries", in *Electrical Machines and Power Electronics*, 2007. *ACEMP '07*. International Aegean conference on, 2007,pp. 141-146.
- [20] D. Lu. And B. Francois. "Strategic framework of an energy management of a microgrid with a photovoltaic-based active generator", in *Advanced Electromechanical Motion systems and Electric drives joint Symposium*, 2009, *ELECTROMOTION 2009*. 8<sup>th</sup> International Symposium on 2009., pp1-6.
- [21] S. B. Kjaer, "Design and control of an Inverter for photovoltaic Applications", *Phd Dissertation*, Aalborg University, 2005.
- [22] G. Boyle, *Renewable Energy: Power for Sustainable future*,: Oxford University Press, 1996.
- [23] pveducation.edu
- [24] A. D. Rajapaksen and D. Muthumuni, "Simulation tools for System grid integration studies", in *Electrical Power & Energy Conference (EPEC)*, 2009, pp. 1-5.

- [25] S. A. Rahman and R K Varma, "PSCAD/EMTDC model of a 3-phase grid connected photovoltaic solar system," in North American Power symposium.
- [26] [yinglisolar.com](http://yinglisolar.com)
- [27] M. Veerachary, "Power tracking for nonlinear PV sources with coupled inductor SEPIC converter", AES IEEE transaction pp. 1019-1029, 2005.
- [28] G. M. S. Azevedo, et al., "Evaluation of maximum power point tracking methods for grid connected photovoltaic systems," in Power Electronics Specialist Conference, 2008. PESC 2008. IEEE 2008. Pp. 1456-1462.
- [29] D. M. Robert. W. Erickson, "Fundamentals of Power Electronics (Second Edition)," ed Boulder, Colorado.
- [30] M. F. S. John G. Kassakian, George. C. Verghese, Principles of Power Electronics
- [31] T.M.U. Ned Mohan, William P. Robbins, Power Electronics, Third ed. Wiley – India, 2009.
- [32] L. Poh. Chiang and D.G. Holmes,"Analysis of multi loop control strategies for LC/CL/LCL-filtered voltage-source and current-source inverters", Industry Applications, IEEE Transaction on pp. 644-654, 2005
- [33] M. F. Schlecht "Harmonic-Free Utility/DC Power Conditioning Interfaces," Power Electronics, IEEE Transactions on, vol. PE-1, pp.231-239, 1986.
- [34] N. Mendis, et al. "Active power management of a super capacitor-battery hybrid energy storage system for standalone operation of DFIG based wind turbines", in Industry Society Annual Meeting (IAS), 2012, IEEE 2012 pp.1-8
- [35] A. Vezzini., "Lithium ion battery system and their application", June 2009
- [36] K. Taesic and Q. Wei, "A Hybrid Battery Model Capable of Capturing Dynamic Circuit Characteristics and Nonlinear Capacity Effects", Energy Conversion, IEEE Transaction on, pp. 1172-1180, 2011.
- [37] O. Tremblay et al., "A Generic Battery Model for the Dynamic Simulation of Hybrid Electric Vehicles," in Vehicle Power and Propulsion Conference, 2007. VPPC 2007. IEEE 20007, pp. 284-289
- [38] B. Yann Liaw, et al., "Modeling of lithium ion cells – A simple equivalent circuit model approach", Solid State Ionics, vol. 835-839, 2004
- [39] G. Lijun, et al. "Dynamic lithium-ion battery model for system simulation", Components and Packaging Technologies, IEEE Transaction on. 25, pp. 495-505, 2002

- [40] L.D. Olivier Tremblay, “Experimental Validation of a battery Dynamic Model for EV Applications”, *World Electric Vehicle Journal*, vol.3. May 2009.
- [41] C.M. Shephred, “Theoretical Design of Primary and Secondary Cells”, U.S. Naval Laboratory, Washington, D.C. 1963.
- [42] D. A. New, “Double and Layer Capacitors: Automotive Applications and Modeling”, MS, Department of Electrical Engineering and Computer Science, Massachusetts Institutes of Technology, Massachusetts, 2002.
- [43] S. Lisheng and M.L. Crow, “Comparison of ultra-capacitor electric circuit models,” in *Power and Energy Society General Meeting – Conversion and Delivery of Electrical Energy in the 21<sup>st</sup> Century*, 2008, pp. 1-6.
- [44] P.J. M. John H. Miller, Mark Cohen, “Ultra capacitors for Energy Buffers in Multiple Zone Electrical Distribution System”, Maxwell Technologies.
- [45] A.M. Van Voorden, et al. “The Application of Super Capacitors to relieve Battery-Storage systems in Autonomous Renewable Energy Systems,” in *Power Tec, 2007 IEEE Lausanne*, 2007. Pp. 479-484
- [46] J.C. Basilio and S.R. Matos, “Design of PI and PID controllers with transient performance specification”, *Education, IEEE Transactions on*, vol 45. Pp. 364-370, 2002.
- [47] a. N. B. N. J. G. Ziegler, “Optimal Settings for automatic controllers”, *Trans. ASME*, vol. 64. Pp. 759-768, 1942.
- [48] Gayatri A. Deshpande, Sukumar Kamalasadana, “An approach for micro grid management with hybrid energy storage system using batteries and ultra-capacitors”, *IEEE conference publication, 2014 IEEE PES General Meeting*, 2014.
- [49] E. Muljadi, M. Singh, V. Gevorgian , “PSCAD Modules representing PV Generators”, NREL, TP-5500-58189

## APPENDIX: MATLAB CODE

Design of DC-DC Boost converter for PV farm is explained here,

The MATLAB code for the boost converter design and its PI controller can be seen

below:

```
%PI compensator code of boost converters in my thesis
clc
clear all
close all

Vin=550;
Vout=1200;
Dprime=Vin/Vout;
D=1-Dprime
Pin=2e6;
Iin=Pin/Vin;
Iind=Iin;
Fsw=1000;
T=1/Fsw;
P=Vin*Iin;
Pout=2e6;
R=Vout^2/Pout
I2=Pout/Vout
ripple=0.02;
I_ripple=ripple*I2
V_ripple=ripple*Vout

%Element design
Ldesign=D*T*Vin/(2*I_ripple)
L=1.25*Ldesign
Cdesign=Vout*D*T/(2*R*V_ripple)
H=1; %unity gain feedback

num1=[(-Iind/Cdesign) (Dprime*Vout/(Ldesign*Cdesign))];
den1=[1 1/(R*Cdesign) Dprime^2/(Ldesign*Cdesign)];
sys1=tf(num1,den1)
figure(1);
margin(sys1);
hleg1=legend('Uncompensated boost converter bode plot')
set(hleg1, 'Location', 'Best')

sys2=feedback(sys1,H)
figure(2);
```

```

step(sys2);
hleg2=legend('Step response of Uncompensated system');
set(hleg2, 'Location', 'Best')

wc=1; %crossover frequency
a=-wc*Iind*Ldesign/(Dprime*Vout);
b=(wc/(R*Cdesign))/(Dprime^2/(Ldesign*Cdesign)-wc^2);
Phase_Margin=90*pi/180; %PM=-(-180-angleL(s))
c=-Phase_Margin-(90*pi/180)-atan(a)+atan(b); %c=atan(wc*Tz)
Tz=tan(c)/wc %Tz for 90 degree PM design, fix the Tz in the
compensator design

%Finding Kp:

d=((Dprime^2/(Ldesign*Cdesign)-wc^2)^2)+(wc/(R*Cdesign))^2);
e=(1+(wc*Tz)^2);
f=((Dprime*Vout/(Ldesign*Cdesign))^2)+(wc*Iind/Cdesign)^2);
Kp=sqrt(wc^2*d/(e*f))

%Compensator design PI controller: K(1+Tzs)/s

K=Kp;
num3=K*[Tz*1 1];
den3=[1 0];
sys3=tf(num3,den3)
figure(3)
margin(sys3);
hleg3=legend('PI controller bode plot');
set(hleg3, 'Location', 'Best')

%overall system transfer function

num4=conv(num1,num3);
den4=conv(den1,den3);
sys4=tf(num4,den4)
figure(4);
margin(sys4);
hleg4=legend('Compensated system bode plot');
set(hleg4, 'Location', 'Best')

%Closed loop tf:

sys5=feedback(sys4,H);
%step response:
figure(5);
step(sys5);
hleg5=legend('Step response of compensated system');
set(hleg5, 'Location', 'Best')

```

The output window of MATLAB gives the following PI controller transfer function:

sys3 =

$$\frac{2.255e-05 s + 0.000381}{s}$$

Continuous-time transfer function.

Bode plots have already been discussed in the corresponding chapters. It can be noted that the same boost converter code was used for the battery and the ultra-capacitor controller designs and hence is not repeated here.